Process studies of the ReShift™ technology for CO-rich syngas production

Fanny Hagström

Tove Olsson

Master Thesis

Chemical Engineering

Department of Process and Life Science Engineering

Lund University

Sweden

June 9, 2026

Supervisors:

Christian Hulteberg, Lund University

Martin Østberg, Topsoe A/S

Peter Mølgaard Mortensen, Topsoe A/S

Thomas Norup From, Topsoe A/S

Examiner:

Sara Blomberg, Lund University

Abstract

Producing syngas with a low H_2/CO ratio remains challenging in current industrial practice, primarily due to process limitations related to feedstock composition, reaction thermodynamics and restricted flexibility in conventional reforming technologies. This report investigates the potential of the Topsoe ReShift^{TM} technology as a revamp option for syngas production with a lower H_2/CO ratio, lower steam-to-carbon (S/C) ratio and improved CO_2 utilization. By using Topsoe's internal software GIPS, a simulation was developed based on a running industrial steam methane reforming (SMR) plant and an existing base-case simulation, and sensitivity analyses were carried out for both a conventional SMR process and the integrated ReShift^{TM} process. The effects of reformer operating conditions, CO_2 addition to the APOC reactor, CO_2 preheat temperature and CO_2 addition upstream of the tubular reformer were evaluated with focus on achieving increased CO production at a low S/C ratio while avoiding carbon formation. Based on the sensitivity analyses, selected cases, with the objective to achieve a H_2/CO ratio of 1, were further assessed with respect to duty demand, CO_2 emissions and a rough estimate of revamp investment cost. The results show that the ReShift^{TM} technology enables operation at lower S/C ratios than conventional SMR while maintaining carbon-free operation and achieving significant net CO_2 consumption in all the investigated ReShift cases. However, these benefits come at the expense of higher energy demand and additional equipment. Among the evaluated cases, no single configuration was optimal for all criteria, and the preferred revamp solution depends on the relative importance of syngas composition, energy demand, CO_2 utilization and investment cost.

Acknowledgements

We would like to express our gratitude to our university supervisor Christian Hulteberg for his guidance and support throughout this work. We also wish to thank our supervisors at Topsoe, especially Martin Østberg, as well as Thomas Norup From and Peter Mølgaard Mortensen, for their valuable input and support during the project. In addition, we would like to thank Jonas Ishøj for his help with questions related to GIPS simulations. Their support and expertise have been appreciated and have contributed significantly to this study. Finally, we are grateful for the opportunity to conduct this project in collaboration with Topsoe and to everyone in the Topsoe R&D who met with us, shared their knowledge and inspired us throughout this project.

Table of contents

List of abbreviations and symbols

Abbreviation	Description
APOC	adiabatic post converter
ATR	autothermal reforming
CCS	carbon capture and storage
CL	chemical looping
DMR	dry methane reforming
HDS	hydrodesulfurization
LHHW	Langmuir-Hinshelwood-Hougen-Watson
OC	oxygen carrier
PFD	process flow diagram
PFR	plug-flow reactor
POX	partial oxidation
PSA	pressure swing adsorption
RWGS	reverse water-gas shift
S/C ratio	steam-to-carbon ratio
SPARG	sulfur passivated reforming
SMR	steam methane reforming
WHB	waste heat boiler
WGS	water-gas shift

Symbol	Description	Unit
$a_{c,eq}$	carbon activity at equilibrium	dimensionless
$a_{c,s}$	steady-state carbon activity	dimensionless
DEN	fraction of free sites in the reactions	dimensionless

$F_{i,in}$	inlet volumetric flow of component *i*	Nm^3/h
$F_{i,out}$	outlet volumetric flow of component *i*	Nm^3/h
$F_{i,SMR}$	volumetric flow rate of component *i* from the tubular reformer	Nm^3/h
$F_{CO2,External}$	volumetric flow rate of external CO_2	Nm^3/h
$F_{CO2,recycle}$	volumetric flow rate of the CO_2 recycle stream	Nm^3/h
ΔG_C	Gibbs energy deviation from graphite	kJ/mol
$\Delta H^{\circ}_{298\,K}$	heat of reaction at 25°C	kJ/mol
K_{eq}	chemical equilibrium constant	-
k_{SMR}	rate constant of SMR reaction	$mol/(kg_{cat}\ s)\ bar^{0.5}$
k_{WGS}	rate constant of WGS reaction	$mol/(kg_{cat}\ s)\ bar^{-1}$
K_{SMR}	chemical equilibrium constants of SMR	bar^2
K_{WGS}	chemical equilibrium constants of WGS	dimensionless
K_{CO}, K_{H_2}, K_{CH_4}	adsorption constants of CO, H_2 and CH_4	bar^{-1}
K_{H_2O}	adsorption constant of water	dimensionless
k_g	rate of gasification	-
k_{-c}	rate constant for carbon removal	-
K'_W	steam adsorption constant	dimensionless
p_i	partial pressure of reactant *i*	bar
P_i	particle pressure of component *i* inside the catalyst pellet	bar
$p_{i,s}$	partial pressure of component *i* on the pellet surface	bar
P_{tot}	total pressure	bar
$Q_{r,eq}$	equilibrium reaction quotient	-
Q_{E231}	heat duty of heat exchanger E231	MW

r_j	reaction rate of reaction *j*	mol/(kg_{cat} s)
R	gas constant	J/mol/K
S_i	selectivity of component *i*	%
T	temperature	°C or K
ΔT_{app}	temperature approach to equilibrium	°C
T_{exit}	actual outlet temperature	°C
T_{eq}	equilibrium temperature	°C
T_s	temperature on the pellet surface	°C
V_p	catalytic pellet volume	m^3
X_i	conversion of component *i*	%
y_i	mole fraction of component *i*	mole/mole
Y_i	yield of component *i*	%
$\widehat{y_{CH_4}}$	normalized gas composition of CH_4	dimensionless
$\widehat{y_{H_2O}}$	normalized gas composition of H_2O	dimensionless
$\widehat{y_{CO_2}}$	normalized gas composition of CO_2	dimensionless
α	describes kinetic order	dimensionless
η_j	effectiveness factor for reaction *j*	dimensionless

1. Introduction

Synthesis gas, commonly known as syngas, is a gas mixture consisting mainly of hydrogen (H_2), carbon monoxide (CO), carbon dioxide (CO_2), steam, and methane (CH_4), formed during the conversion of hydrocarbons (Rostrup-Nielsen et al., 2011). Among these components, CO is a key intermediate in the chemical industry and serves as a precursor for a wide range of value-added products (Kang et al., 2025). In particular, CO-rich syngas play an important role in the production of higher alcohols, synthetic fuels, acetic acid and polymers such as polycarbonates and polyurethane (Daza et al., 2016; Kang et al., 2025; Mortensen et al., 2020). Steam reforming is a widely used process for syngas production, in which hydrocarbons react with steam. A promising approach for CO_2 utilization is to partially replace steam with CO_2 as reactant in the reforming process (hereafter referred to as CO_2 reforming), as it enables the production of CO-rich syngas while simultaneously incorporating CO_2 into the process (Mortensen et al., 2023). The CO_2 reforming process has the potential to achieve net negative CO_2 emissions if it is designed to consume more CO_2 than is generated by the energy supply required for operation (e.g. fuel used for heating) (Mortensen et al., 2020). However, the addition of CO_2 to conventional steam methane reforming increases the risk of carbon formation, which may limit catalyst lifetime and operational stability (Mortensen et al., 2023).

An alternative approach to adjusting syngas composition is the Topsoe ReShift™ technology, which enables production of syngas at low H_2/CO ratios. The process is centered around an adiabatic post converter (APOC) reactor installed downstream of the tubular reformer after introduction of preheated CO_2. This technology is particularly attractive for revamp projects in existing reforming units, where there is an interest in reaching lower H_2/CO ratios and operating at lower steam-to-carbon (S/C) ratios, while avoiding the risk of carbon formation. A lower S/C ratio reduces the overall plant flowrate, which can increase unit capacity by allowing a higher carbon feed rate (Mortensen et al., 2023).

1.1. Aim

The aim of this study is to simulate and optimize a revamp configuration based on the ReShift™ technology, using conventional steam reforming as the reference case for production of CO-rich syngas. The study focuses on improving CO_2 utilization and achieving lower H_2/CO and S/C ratios, while maintaining a safe operation margin with respect to carbon formation limits to avoid the risk of catalyst deactivation. Process performance is evaluated through simulation-based optimization of syngas composition, energy demand, and CO_2 emissions. In addition, the competitiveness of the ReShift™ revamp configuration is assessed in comparison with industrial syngas production technologies, and a preliminary economic feasibility analysis will also be included.

1.2. Methodology

The project started with a literature survey of technologies for producing CO-rich syngas. This underlain the basis for the project study and provided relevant industrial processes for

comparison with the ReShift™ technology. A running industrial plant referred to as *Reference Industrial Unit* (Appendix B.1) served as the base, and the steam reforming process and revamp case were simulated using Topsoe's internal software GIPS. Multiple sensitivity analyses were carried out to study the effect of operating conditions including tubular reformer outlet temperature and pressure, S/C ratio of the tubular reformer, CO_2 preheat temperature and external addition of CO_2 to the APOC reactor. Further evaluations were performed on the CO_2 flow and distribution with the addition of CO_2 upstream of the tubular reformer to improve CO_2 utilization and achieve lower H_2/CO ratio, without risking carbon formation. Based on the results, a few cases were selected with the aim of achieving a H_2/CO ratio of 1.0. These cases were compared in terms of product flow and duty demand. Following that, a CO_2 emission analysis and a simple cost estimation were carried out for two of the selected revamp cases.

1.3. Disposition

Following this introduction, Section 2 presents the theoretical background relevant to the study. Section 3 describes the methodology, including process modelling, assumptions and simulation approach. Section 4 presents and discusses the results of the simulations, sensitivity analyses and the selected case evaluations. Finally, Section 5 discusses areas that could be interesting to investigate further, and Section 6 summarizes the main conclusions of the study and provides recommendations based on the results obtained. Appendix A provides supporting data and graphs, while Appendix B includes confidential Topsoe information.

2. Theoretical background

This section presents the theoretical background relevant to the study by briefly introducing different methods for syngas manufacturing, followed by a more detailed description of a steam methane reforming plant. Carbon formation in reforming processes is also discussed, and the section concludes with CO_2 reforming via the reverse water-gas shift reaction.

2.1. Syngas manufacturing

The required composition of syngas depends on its intended downstream application. Different processes require specific H_2/CO ratios to achieve optimal performance. For instance, the Fischer-Tropsch process, which converts syngas into transportation fuels, typically requires a H_2/CO ratio in the range of 2.0-2.2 (Aasberg-Petersen et al., 2004; Ross, 2012). Similarly, methanol synthesis generally operates with a H_2/CO ratio around 2.0, while synthesis of dimethyl ether (DME) and oxo-alcohols requires CO-rich syngas (Kang et al., 2025; Ross, 2012). The final syngas composition is influenced by several process variables, including the feed composition as well as the operating temperature and pressure (Rostrup-Nielsen et al., 2011).

2.1.1. Steam methane reforming

Typical feedstock used in conventional steam methane reforming (SMR) today are natural gas and naphtha. In the SMR process, the feedstock is converted by reaction with steam to produce syngas over a catalytic bed at elevated temperatures (800–950 °C) and pressures of around 20-30 bar (Ghoneim et al., 2016; Gangadharan et al., 2012; Rostrup-Nielsen et al., 2011). This process will be further discussed in Section 2.2. The CO-content in the syngas can be increased by decreasing the H/C ratio in the feed gas. This can be achieved by using a low S/C ratio, use of naphtha instead of natural gas as feed, partial oxidation, and addition of CO_2 to the feed. However, most of these approaches increase the risk of carbon formation (Rostrup-Nielsen et al., 2011).

2.1.2. Partial oxidation

An alternative to SMR is partial oxidation, where oxygen is added to the feed, causing internal combustion that provides the heat required for reforming. The overall reaction is highly exothermic, eliminating the need for external heat input. Two common methods are non-catalytic partial oxidation (POX) and autothermal reforming (ATR). POX removes the need for the large heat transfer surfaces used in SMR but requires an oxygen plant. Additionally, it is generally operated at pressures around 20-30 bars and typically achieves a H_2/CO ratio of 2 (Singh et al., 2025). ATR combines partial oxidation with steam reforming using a burner and a fixed catalyst bed, allowing lower operating temperature (800-1000°C) compared to POX, while offering advantages such as shorter residence times and improved energy efficiency (Rostrup-Nielsen et al., 2011; Singh et al., 2025; Speight, 2014).

2.1.3. Dry methane reforming

As previously mentioned in the introduction, CO_2 can partially replace steam in the feed to a SMR plant to obtain lower H_2/CO ratios in the produced syngas (Rostrup-Nielsen., 2011; Dybkjær, 1995). When steam is completely replaced by CO_2 in SMR, the process is referred to as dry methane reforming (DMR). The stoichiometric DMR reaction produces syngas with a H_2/CO ratio of 1, which is lower than what is typically obtained from conventional processes such as SMR and partial oxidation. However, in practice the SMR reaction will occur simultaneously with the DMR reaction due to the reverse water-gas shift (RWGS) reaction, which generates steam that can react in the SMR reaction (Salahi et al., 2023). As the DMR reaction is highly endothermic, high operating temperatures (around 800-900°C) are required to achieve effective methane conversion (de Dios Garcia et al., 2021; Singh et al., 2025). Furthermore, lower pressures increase conversion rates of CO_2 and CH_4, reduce formation of byproducts, reduce the risk of carbon formation, as well as decrease the H_2/CO ratio. At pressures in the range of 12-25 atm, a H_2/CO ratio around 1.6-1.7 can be achieved (Singh et al., 2025).

As in the SMR process, carbon formation can lead to severe catalyst deactivation, thereby limiting the broader application of DMR (Kang et al., 2025). Considerable research efforts have therefore focused on the development of catalysts for the DMR reaction to enhance conversion, improve selectivity, and mitigate carbon deposition. Sharifnattaj et al. (2025) investigate this in their review article on catalysts for DMR. Despite these advances, the current industrial feasibility of such catalysts remains limited and will not be further addressed in this work.

2.1.4. Chemical looping

Chemical looping (CL) technology is an alternative method to revamp conventional processes for converting CO_2 to CO or syngas. In CL, one reaction is divided into multiple sub-reactions that proceed in separate steps and at distinct sites. The process includes repeated cycles of reduction and oxidation where oxygen carriers (OCs) act as intermediates that transfer oxygen continuously. For the RWGS-CL process, these redox cycles introduce a way to circumvent the equilibrium barrier. Furthermore, the reactant and product are separated, thereby avoiding unwanted side reactions. The RWGS-CL process also simplifies gas separation of produced CO, and allows lower operating temperatures (Kang et al., 2025).

The DMR-CL technology offers a way of producing CO in oxidation steps and syngas in reduction steps using CH_4 and CO_2. The advantage of the DMR-CL process is that carbon formation can be eliminated as CO_2 reacts with carbon (C) in the oxidation step, resulting in production of CO. For RWGS-CL and DMR-CL, the separation of reactants and products between the redox steps allows unwanted side reactions to be effectively suppressed. The challenges remain in developing OCs for DMR-CL with high selectivity to syngas, efficient conversion of CO_2, and well-maintained redox properties (Kang et al., 2025).

2.2. Steam reforming plant

An example of the process flow diagram (PFD) of a conventional steam reforming process is shown in Figure 2.1, commonly using natural gas as feedstock in a SMR process. The steam reforming reactions take place in the fired tubular reformer which is centered on the PFD. Before the tubular reformer, feed stream purification and preparation steps such as hydrogenation and sulfur removal are included. Downstream the tubular reformer steam generation followed by separation and purification steps are illustrated. This includes water (H_2O) and CO_2 removal, as well as cryogenic separation in a cold box. If CO_2 addition is wanted upstream of the tubular reformer, the separated CO_2 can be recycled and added together with external CO_2, which is also seen in this figure.

This section provides a brief description of the unit operations in the process design, starting with the reaction fundamentals.

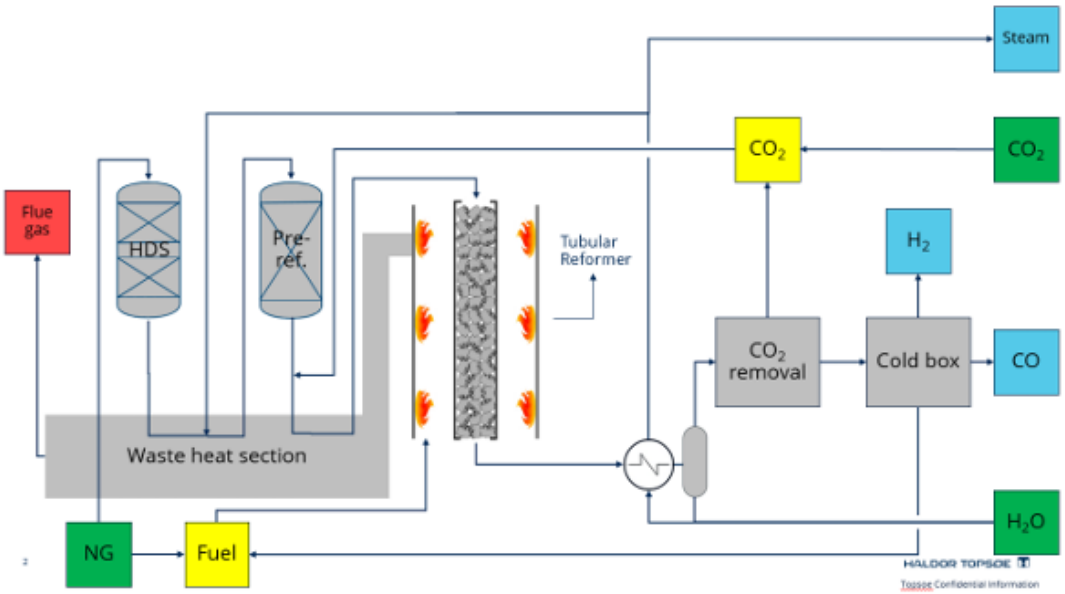

Figure 2.1. A simple overall PFD for a SMR plant, illustrating the processes upstream and downstream of the tubular reformer. The figure is taken from an internal Topsoe presentation.

2.2.1. Thermodynamics in SMR

The reactions taking place in the SMR process are explained below with thermodynamic data from Barin (1989). There are two primary reactions taking place, with the first one being the endothermic SMR reaction (1) according to (Mortensen et al., 2020):

$$CH_4\ (g) + H_2O\ (g) \leftrightarrow CO\ (g) + 3H_2\ (g)\ \left(\Delta H^{\circ}_{298\ K} = 206\ kJmol^{-1}\right) \qquad (1)$$

In addition to reaction (1), the second main reaction that occurs is the water gas shift (WGS) reaction (2):

$$CO\ (g) + H_2O\ (g) \leftrightarrow CO_2\ (g) + H_2\ (g)\ \left(\Delta H^{\circ}_{298\,K} = -41\ kJmol^{-1}\right) \quad (2)$$

Reaction (1) and (2) are independent, but there are other steam reforming reactions which can be drawn from these. For instance, steam and CH_4 also react according to:

$$CH_4\ (g) + 2H_2O\ (g) \leftrightarrow CO_2\ (g) + 4H_2\ (g)\ \left(\Delta H^{\circ}_{298\,K} = 165\ kJmol^{-1}\right) \quad (3)$$

Furthermore, the DMR reaction is the reaction between CH_4 and CO_2:

$$CH_4\ (g) + CO_2\ (g) \leftrightarrow 2CO(g) + 2H_2\ (g)\ \left(\Delta H^{\circ}_{298\,K} = 247\ kJmol^{-1}\right) \quad (4)$$

Since the reforming reactions (1), (3) and (4) are endothermic, high temperatures are required to achieve a high CH_4 conversion. The reactions (1)-(4) are reversible, meaning that at a specified temperature the reaction will not have complete conversion. Because the reforming reactions proceed rapidly due to the high operating temperature and the presence of a catalyst, the achieved conversion is close to equilibrium conversion (Rostrup-Nielsen et al., 2011).

According to Le Chatelier's principle, higher temperatures shift the equilibrium toward CO formation. Furthermore, the CH_4 content increases with pressure (Dybkjær, 1995). This is evident when looking at the equilibrium constant in equation (5) where it is seen that higher pressure will shift the reaction towards the reactant side.

$$K_{eq,SMR} = \frac{p_{CO} * (p_{H_2})^3}{p_{CH_4} * p_{H_2O}} = \frac{y_{CO} * y_{H_2}^3}{y_{CH_4} * y_{H_2O}} * P_{tot}^2 \quad (5)$$

where p_i represents the partial pressure of the reactants and products in the SMR reaction (1), y_i is the mole fraction of component *i* and P_{tot} is the total pressure (Rostrup-Nielsen et al., 2011).

Steam content is an important operating parameter in the SMR process because it affects the reaction equilibrium, product composition, and catalyst stability. The steam content is typically expressed in S/C ratio, which describes the amount of steam relative to the amount of carbon in the feedstock. In a SMR process with a prereformer, the S/C ratio or H_2O/CH_4 ratio (if all C is CH_4) typically corresponds closely to the overall steam-to-hydrocarbon-carbon ratio at the prereformer inlet (Mortensen et al., 2023).

As can be seen in reaction (1) and (3), higher steam content favors methane conversion in accordance with Le Chatelier's principle. A high S/C ratio is also necessary to reduce the risk of carbon formation (Grossmann et al., 2016). Furthermore, the S/C ratio influences the energy economy of the process, as higher ratios result in larger volumes of gases that must be heated (Rostrup-Nielsen et al., 2011).

2.2.2. Hydrogenation and sulfur removal

Hydrocarbons used as feedstocks in steam reforming, such as natural gas and naphtha, often contain varying amounts of sulfur compounds (Lloyd, 2011). Natural gas typically contains 5–20 ppm sulfur, whereas liquid hydrocarbon fractions may contain up to 500 ppm (Christensen, 1996). Most of the metal catalysts used in steam reforming are sensitive to poisoning, particularly by sulfur. This is because sulfur compounds are strongly chemisorbed on the metal surface, resulting in deactivation of the catalyst (Hulteberg, 2012; Rostrup-Nielsen, 1982). The dissociative absorption of hydrogen sulfide (H_2S) on a nickel catalyst at temperature levels of common industrial processes is described by reaction (6) (Rostrup-Nielsen, 1982):

$$Ni + H_2S \leftrightarrow Ni - S + H_2 \tag{6}$$

Even small coverage of sulfur on nickel results in strong deactivation of the catalyst, while full coverage results in complete deactivation. Purification of the feedstock for the reforming process is therefore necessary to avoid catalyst deactivation. The feed purification is typically done by catalytic hydrotreating followed by absorption desulfurization, where the two steps are included in the hydrodesulfurization (HDS) operation shown in Figure 2.1.

During catalytic hydrotreating, organic sulfur compounds in the feedstock, such as mercaptans and thiophenes, are converted to H_2S through reaction with H_2 (Lloyd, 2011; Rostrup-Nielsen et al., 2011). This step is typically done over a Co(Ni)Mo/Al_2O_3 catalyst with reaction temperatures from 350°C to 400°C. In the absorption desulfurization step, H_2S is removed by absorption on zinc oxide shown in reaction (7) at the same operating temperature interval used in the catalytic hydrotreating step (Rostrup-Nielsen et al., 2011; Rostrup-Nielsen, 1982).

$$H_2S + ZnO \leftrightarrow ZnS + H_2O \tag{7}$$

2.2.3. Prereformer

An adiabatic prereformer is used to convert higher hydrocarbons to C_1-components, i.e. CH_4 and carbon oxides, through reforming reactions (1), (4) and (8) (Aasberg-Petersen et al., 2004; Chen et al., 2004; Christensen, 1996). Steam reforming of higher hydrocarbons can be described by the following reaction (8):

$$C_nH_m\ (g) + nH_2O\ (g) \rightarrow nCO\ (g) + (n + 0.5m)H_2\ (g)\ \left(\Delta H^{\circ}_{298\,K} < 0\ kJmol^{-1}\right) \tag{8}$$

For production of syngas using natural gas as feed, the prereformer has a low operating temperature range from 350-550°C, and it is typical to have a S/C ratio of 0.3-2.0 (Christensen, 1996; Rostrup-Nielsen et al., 2011). For higher hydrocarbons (n >1), the steam reforming reaction (8) can be considered irreversible resulting in full conversion if the catalyst activity is sufficient (Dybkjær, 1995). After this initial reaction, the system approaches equilibrium controlled by the exothermic methanation reaction (reversed reaction (1)) and the WGS reaction (2) (Aasberg-Petersen et al., 2004; Christensen, 1996).

Typically, a highly active nickel catalyst is used in an adiabatic prereformer. In addition, the catalyst removes any residual sulfur compounds remaining after the desulfurization step, preventing it from entering the tubular reformer and downstream catalysts (Rostrup-Nielsen et al., 2011). The reactor is rather simple due to adiabatic operating conditions and moderate process temperatures, but understanding of process kinetics, influence of catalyst poisons and limits for carbon formation are still needed (Christensen, 1996).

Integrating a prereformer upstream of the tubular reformer enables further optimization of tubular reformer operation and allows the feed to be preheated to approximately 650°C, thereby reducing the required size of the tubular reformer. Without a prereformer, the preheater risks causing steam cracking, which produces olefins from higher hydrocarbons in the feed. This constitutes a problem since olefins easily form carbon in the reformer (Rostrup-Nielsen et al., 2011). Furthermore, a prereformer has been shown to improve feedstock flexibility, increase production capacity, increase catalyst and tube lifetime, and eliminate problems of carbon formation and hot banding in tubular reformers (Christensen, 1996).

2.2.4. Tubular reformer

Tubular reforming is the primary process step for producing syngas by steam reforming. In the tubular reformer, illustrated in the center of Figure 2.1, high-alloy reforming tubes are installed in a furnace, where normally nickel-based catalysts are placed in the tubes. The tubular reformer typically consists of up to 1000 vertical tubes with lengths ranging from 10 to 13 m and outer diameters of 100 to 200 mm (Rostrup-Nielsen et al., 2011). The hydrocarbons and steam pass through the reactor tubes where the reforming reactions take place. Since steam reforming reactions are strongly endothermic, high operating temperatures are required (Lloyd, 2011). Typical operating conditions in a tubular reformer include inlet temperatures of 450-650°C and outlet temperatures of 700-950°C, although the exact values depend on the process application. Operation at elevated temperatures can lead to catalyst sintering, resulting in a reduction in active surface area and catalytic activity. In addition, high temperatures and mechanical stress promote creep of the reformer tube material. Consequently, the design of tubular reformers is primarily constrained by the mechanical properties of the tube materials (Rostrup-Nielsen et al., 2011).

The reforming process is normally operated at pressures of 20–30 bar, as the feedstock is supplied within this range and elevated pressures are required for downstream processes. However, as discussed in Section 2.2.1, CH_4 conversion increases at lower pressures. This creates a trade-off, since higher pressures are needed in downstream processing but operating

at lower pressures requires compression of the process gas, which is both costly and energy intensive (Singh et al., 2025).

In steam reforming processes, S/C ratios of around 2.5-4 are usually common. As already mentioned, a higher S/C ratio enhances the conversion of CH_4 and is necessary to avoid carbon formation (Grossmann et al., 2016). However, higher S/C ratios result in increased mass flow through the plant, which demands more energy for steam production and raises both investment and operating costs (Rostrup-Nielsen et al., 2002). Lowering the S/C ratio in steam reforming plants is of particular interest, as it enhances the economic feasibility of the process and results in reduced H_2/CO ratios in the syngas (Grossmann et al., 2016). The higher amount of unconverted CH_4 resulting from a low S/C ratio can be compensated for by increasing the outlet temperature of the tubular reformer (Rostrup-Nielsen et al., 2011).

The furnace in a tubular reformer consists of a radiant box with burners and a convection section to recover waste heat from the flue gases exiting the radiant section. Different reformer furnace arrangements exist where the burners are placed on the bottom, on the top, on the walls or a mixture of these (Rostrup-Nielsen et al., 2011). The furnace operates at temperatures of approximately 1000°C (Lloyd, 2011). The difference in enthalpy between the exit and the inlet gas corresponds to the reformer heat duty. The duty includes both the heat of reaction and the heat required to reach the reformer outlet temperature (Dybkjær, 1995). In a tubular reformer furnace, about 50% of the combustion heat from the burners are transferred to the process gas through the reformer tube walls. The rest is recovered from the hot flue gas in the waste heat section (Figure 2.1) where it is used for preheating reformer feed and combustion air as well as producing steam. As a result, the overall thermal efficiency of the reformer can reach up to 95% (Dybkjær, 1995; Rostrup-Nielsen et al., 2011).

2.2.5. Downstream processes

Downstream of the tubular reformer, several purification and conditioning steps are generally used to obtain the gas composition required for its intended use. One common step is WGS, which is used to increase the H_2/CO ratio in the syngas according to reaction (2). This is particularly important in industrial processes to produce hydrogen, ammonia and other bulk chemicals. Since the WGS reaction is exothermic, high conversion is favored at lower temperatures than those used for the SMR reaction (Ertl et al., 1997; Rostrup-Nielsen et al., 2011). The product gas can be dried either directly downstream of the reformer or after the WGS step, if WGS is included. Drying is achieved by cooling the gas in a series of heat exchangers, for example using cooling water, typically with simultaneous steam generation, as shown in Figure 2.1. When the gas is cooled below its dew point, water condenses and is removed from the stream, resulting in a dry product gas (Mortensen et al., 2023).

Furthermore, the composition of the syngas can be modified by CO_2 removal. The removal of CO_2 from the gas stream is important not only because it leads to improved process performance and economic efficiency, but also due to its negative environmental impact. Following purification, captured CO_2 can be recycled as a high-purity carbon source in industrial chemical processes. The selection of CO_2 removal processes for a syngas stream

depends on technical and economic factors including gas composition, removal objectives, operating conditions, cost, desired CO_2 purity and process operability (Samipour et al., 2020). In large plants, CO_2 and other acid gases are commonly removed by absorption processes based on either chemical or physical absorption (Rostrup-Nielsen et al., 2011). In physical absorption processes, gases are physically dissolved in liquid solvents. Physical absorption typically exhibits a lower absorption capacity than chemical absorption at low CO_2 partial pressures. Consequently, chemical absorption is better suited for low CO_2 partial pressures, whereas physical absorption is more effective at high CO_2 partial pressures. Chemical absorption involves absorption of a component in the gas stream which reacts with an absorbent dissolved in a liquid solvent. Amine-based absorption is the most notable chemical absorption technology for carbon capture and storage (CCS), particularly at the industrial scale (Samipour et al., 2020). Moreover, the ReShift™ technology offers a solution for CO_2 utilization and complements CO_2 capture technologies (Mortensen et al., 2023).

Other common processes for separation and purification of the syngas mixture include pressure swing adsorption (PSA) and cryogenic separation (cold box). PSA is now a well-established technology where some of the key industrial applications include gas drying, air separation, H_2 purification, and CO_2 recovery. H_2 purities above 99.9% can be achieved, while CO_2, unreacted CH_4, and CO are effectively captured (Li et al., 2019; Oh et al., 2024). In the PSA process, gases are separated by selectively adsorbing components from a gas mixture onto a solid adsorbent at a relatively high pressure. This is done by passing the gas through a packed column containing the adsorbent, producing a gas stream enriched in the less strongly adsorbed components. The adsorbed components are then desorbed by reducing their partial pressures in the gas phase within the column (Sircar, 2002).

The cold box separation method utilizes the difference in boiling temperatures and pressures to separate the components in the gas, typically for purification of H_2 and CO, while removing impurities such as CH_4, CO_2 and nitrogen (N_2). H_2 has relatively high volatility compared to the other components, so the temperature is decreased to condensate CO, CH_4, CO_2, N_2 and other gases. Therefore, the product stream needs to be cooled to low temperatures prior to the cold box. Furthermore, there will be some impurities that will remain as saturated vapor, making it difficult to achieve H_2 purity standards required for fuel cell vehicles (Kim et al., 2022). The purified H_2 gas stream will contain around 98% H_2 and thus further purification of the H_2 stream may be required, which can be done by adding a PSA unit after the cold box (Dutta et al., 1995; Song et al., 2015). The liquid CO-rich stream is instead flashed and distilled to produce a CO-stream of high purity (Dutta et al., 1995). Furthermore, it is important to remove CO_2 and H_2O from the feed gas upstream of the cold box to avoid clogging of the equipment (Kim et al., 2022).

2.3. Carbon formation

There are three types of carbon that can form: filamentous carbon (whisker), polymerization deposits (gum) and pyrolytic carbon (coke). Whisker carbon can form at a low S/C ratio, high temperature and in presence of olefins or aromatics. The whisker carbon occurs specifically on

nickel-based catalysts and results in the formation of nanotubes (whisker) which may cause a breakdown of the catalyst pellet. Gum carbon blocks the nickel surface and is formed by a low S/C ratio, in absence of H_2, low temperature, and in presence of aromatics. Lastly, pyrolytic coke encapsulates the catalyst pellet and can form deposits on the tube wall. This can occur at high temperatures, long residence time, in the presence of olefins or by sulfur poisoning (Rostrup-Nielsen et al., 2011; Sehested, 2006). Both gum formation and pyrolytic carbon are associated with the presence of higher hydrocarbons, which is why it can be of advantage to remove these upstream of the process in a prereformer (Mortensen et al., 2020). Whisker carbon is formed through dissociation of hydrocarbons or CO on the nickel catalyst surface, according to reactions (9)-(12):

$$CH_4 \leftrightarrow C + 2H_2 \ (\Delta H^{\circ}_{298\,K} = 75\ kJmol^{-1}) \tag{9}$$

$$2CO \leftrightarrow C + CO_2 \ (\Delta H^{\circ}_{298\,K} = -173\ kJmol^{-1}) \tag{10}$$

$$CO + H_2 \leftrightarrow C + H_2O \ \left(\Delta H^{\circ}_{298\,K} = -131\ kJmol^{-1}\right) \tag{11}$$

$$C_nH_m \rightarrow nC + 0.5mH_2 \ \left(\Delta H^{\circ}_{298\,K} > 0\ kJmol^{-1}\right) \tag{12}$$

The Boudouard reaction (10) is significantly (3-10 times) faster than the CH_4 decomposition reaction (9) (Christensen, 1996; Ertl et al., 1997; Rostrup-Nielsen et al., 2011). For a specified catalyst, there are certain operating conditions where the risk of carbon formation can be eliminated. Thus, there are operation limits regarding catalyst temperature, S/C ratio and H_2 content in the feed (Christensen, 1996).

In steam reforming, there are two types of limits that need to be considered. One is controlled by thermodynamics and the other by kinetics. The principle of equilibrated gas can be used to evaluate the thermodynamic potential of carbon formation (Christensen, 1996; Sehested, 2006). It states that carbon formation can be expected on a nickel catalyst if the gas shows affinity for carbon after the gas has been equilibrated. Thus, the carbon potential is calculated for the equilibrated gas, since most of the gas inside the catalyst particle will be near the thermodynamic equilibrium (Christensen, 1996; Holt et al., 2019; Rostrup-Nielsen et al., 2011). Only one of the carbon forming reactions (9)-(11) is needed to be considered since the gas is at equilibrium (Christensen, 1996; Rostrup-Nielsen et al., 2011). Based on reaction (9), the potential of carbon formation from the CH_4 decomposition reaction can be calculated with equation (13):

$$-\Delta G_C = RT\ ln\left[\frac{K_{eq}}{Q_{r,eq}}\right] = RT\ ln\, K_{eq}\left[\frac{p_{CH_4}}{p^2_{H_2}}\right]_{equilibrated\ gas} \tag{13}$$

$$-\Delta G_C > 0 \Longrightarrow Carbon$$

where K_{eq} denotes the CH_4 decomposition reaction (9), R is the gas constant, T is the temperature, $Q_{r,eq}$ represents the equilibrium reaction quotient, and p_{CH_4} and p_{H_2} are the partial pressures of CH_4 and H_2, respectively (Rostrup-Nielsen et al., 2011).

However, it is possible to circumvent the thermodynamic limit by, for instance, using a noble metal catalyst, which has low affinity for carbon, or a sulfur passivated catalyst, which means the principle is no law of nature (Rostrup-Nielsen et al., 2011). In sulfur passivated reforming (SPARG), a controlled level of sulfur partially blocks the catalyst surface, inhibiting the rate of carbon formation more than the rate of methane reforming. This enables operation at conditions that would otherwise lead to carbon formation (Bengaard et al., 2002; Rostrup-Nielsen, 1984). Thus, addition of CO_2 in SPARG can achieve a H_2/CO ratio of below 1, while circumventing carbon formation (Ertl et al., 1997; Mortensen et al., 2015).

Carbon formation cannot be predicted by thermodynamics alone, so a kinetic model is also needed for accurate prediction. Though it should be noted that the kinetics are dependent on the catalyst and the type of higher hydrocarbons present (Christensen, 1996; Holt et al., 2019). One way to evaluate the kinetic potential of carbon formation is with the actual gas principle. However, when using a prereformer, the potential for whisker carbon formation at the inlet is eliminated. Since the actual gas principle predicts carbon at inlet conditions of a conventional steam reformer (450-650°C), a more detailed approach is therefore needed. Instead, it can be based on the kinetic analysis of the steady-state activity of carbon on the catalyst (14) (Rostrup-Nielsen et al., 2011):

$$a_{c,s} = \frac{a_{c,eq}}{1 + \frac{k_g}{k_{-c}} K'_W \left(\frac{p_{H_2O}}{p_{H_2}}\right)^{\alpha} p_{H_2}^{1.5}} \tag{14}$$

where k_g is the rate of gasification, k_{-c} is the rate constant for carbon removal, K'_W is the steam adsorption constant, α describes the kinetic order, and p_{H_2O} is the partial pressure of steam. $a_{c,eq}$ is the carbon activity at equilibrium with a given composition in the gas phase (not necessarily an equilibrated gas), defined as (15) (Rostrup-Nielsen et al., 2011):

$$a_{c,eq} = K_{eq} \frac{p_{CH_4}}{p_{H_2}^2} \tag{15}$$

The equilibrium constant, K_{eq}, is once again related to the CH_4 decomposition reaction (9). There is potential for carbon formation when the saturation value $a_{c,s} > 1$ (Holt et al., 2019; Rostrup-Nielsen et al., 2011).

From the molar O/C and H/C ratios in the feed stream and the temperature and pressure at the tubular reformer outlet, the H_2/CO ratios of the outlet gas and the thermodynamic carbon limit can be calculated (Song et al., 2006). The molar O/C and H/C ratios can be calculated using equations (16) and (17):

$$O/C = \frac{\left(y_{H_2O,in} + y_{CO,in} + 2 * y_{CO_2,in}\right)}{\left(y_{CO,in} + y_{CO_2,in} + y_{CH_4,in}\right)} \tag{16}$$

$$H/C = \frac{\left(2 * y_{H_2,in} + 2 * y_{H_2O,in} + 4 * y_{CH_4,in}\right)}{\left(y_{CO,in} + y_{CO_2,in} + y_{CH_4,in}\right)} \tag{17}$$

Where, $y_{i,in}$ is the molar fraction of component *i* at the reactor inlet.

The results can be presented in a Tøttrup diagram, which illustrates the thermodynamic carbon formation limit under the specified operating conditions. By plotting the relationship between the feed gas compositions, the diagram shows whether an operating point lies within a carbon-safe region or in a region where carbon formation is thermodynamically favored in the equilibrated gas (Song et al., 2006). Hence, the Tøttrup diagram is a useful tool for evaluating the margin to carbon formation and for comparing the effect of different operating conditions on carbon formation risk.

Figure 2.2 shows a Tøttrup diagram for a tubular reformer outlet pressure of 28 barg and an outlet temperature of 930°C. The green line represents the graphitic carbon limit, while the blue line represents an experimentally determined carbon limit for a standard Topsoe nickel catalyst with a particle size of 250 nm.

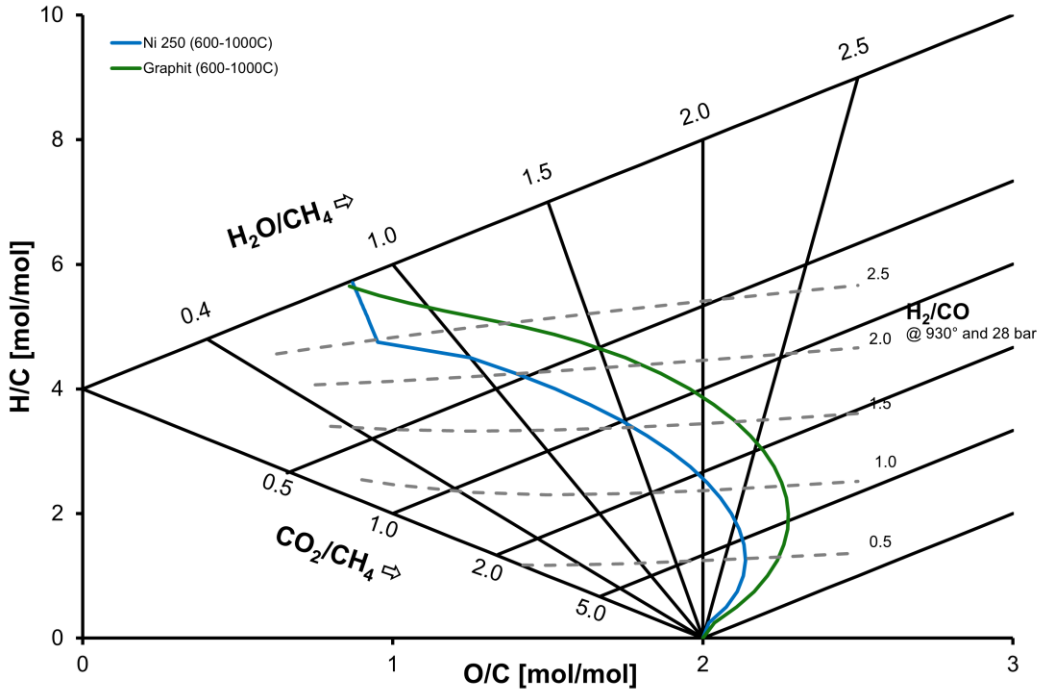

Figure 2.2. Carbon limit diagram for the tubular reformer at a pressure of 28 barg and an outlet temperature of 930°C. Operation to the left of the carbon limit curves indicates a thermodynamic potential for carbon formation in the equilibrated gas. The dotted lines indicate the operating points corresponding to the respective H_2/CO ratios.

These carbon limit curves are calculated under conditions where the SMR reaction (1) and WGS reaction (2) are at equilibrium, and the carbon activity of the methane decomposition reaction (9) is equal to 1. For the graphitic carbon limit, the coefficients used to calculate the carbon formation equilibrium are taken from Rostrup-Nielsen et al. (2011) and are listed in Appendix A (Table A.1). For the nickel catalyst carbon limit, experimentally determined coefficients are used, which are listed in Appendix B.4 (Table B.1).

Operation to the right of the carbon limit curves corresponds to the carbon-free region, where carbon formation is not thermodynamically favored. The diagram can therefore be used to identify feasible operating conditions that avoid the risk of carbon formation.

Carbon formation in the tubular reformer can have serious operational consequences. Formation of whisker carbon can lead to breakdown of the catalyst, which increases the pressure drop across the catalyst bed and leads to uneven flow distribution. These effects can promote the development of hot spots, reduce catalyst performance, and shorten catalyst lifetime (Rostrup-Nielsen, 1982). In addition, removing deposited carbon or replacing deactivated catalyst results in production downtime, which can be costly for plant operation.

2.4. CO_2 reforming and reversed water-gas shift

The utilization of CO_2 in reforming technologies is a promising approach for producing syngas with a low H_2/CO ratio. Moreover, increasing the CO_2/CH_4 ratio has been shown to enhance the CH_4 conversion (Jensen et al., 2021). However, because CO_2 reforming decreases the

atomic H/C ratio, it also increases the risk of carbon formation (Rostrup-Nielsen et al., 2011). An alternative pathway involves converting the captured CO_2 to CO via the RWGS reaction through the addition of H_2. By operating the reactor with initially high H_2/CO_2 ratio, syngas can be produced through the RWGS reaction, offering greater control of the final gas composition (Bown et al., 2021). An industrial example of this approach is Johnson Matthey's HyCOgen™ technology, which applies the RWGS concept to enable CO_2 valorization for syngas and sustainable fuel production in commercial applications (HyCOgen™ technology, n.d.). Similarly, Shell and MAN Energy Solutions have previously in 2023 partnered up for a pilot plant to develop the RWGS technology (Shell, 2023). Both cases highlight the growing industrial commitment to scalable CO_2 solutions.

As mentioned, another promising technology utilizing the RWGS is the ReShift™ technology, which involves adding an APOC reactor with a nickel catalyst, directly downstream of the tubular reformer after introduction of preheated CO_2. It can be used for both new plants and the revamping of existing ones, e.g. SMR or ATR processes. This technique allows the reformer to work at a minimum S/C ratio while circumventing the problem of carbon formation (Mortensen et al., 2020).

2.4.1. ReShift™ process integration

In Figure 2.3, a flowsheet of a revamp configuration of the ReShift™ technology is shown, using steam reforming as the base case. A more detailed description of the process steps for the SMR can be found in Section 2.2. The outlet stream from the tubular reformer in the SMR has a temperature up to 950°C and is mixed with preheated CO_2 before entering as feed in the APOC reactor. The CO_2 can be supplied either from the downstream CO_2 removal section or from an external CO_2 source and should be preheated to above 600°C to avoid excessive cooling of the mixed gas entering the APOC (Mortensen et al., 2020). It is of interest to preheat the CO_2 feed to a temperature as high as possible to achieve improved conversion to CO and avoid the carbon limit in the APOC with a safety margin. The product stream from the APOC is cooled in a waste heat boiler (WHB) to generate steam which is used in previous process steps. Additional cooling steps usually follow to reach a temperature below the condensation point of the stream, which separates the water from the gas resulting in a dry syngas (Mortensen et al., 2023). There are many areas of application for the dry syngas, but one example seen in Figure 2.3 is purification of the stream to pure CO by CO_2 removal and cryogenic separation in a cold box (Section 2.2.5) (Mortensen et al., 2020; Samipour et al., 2020).

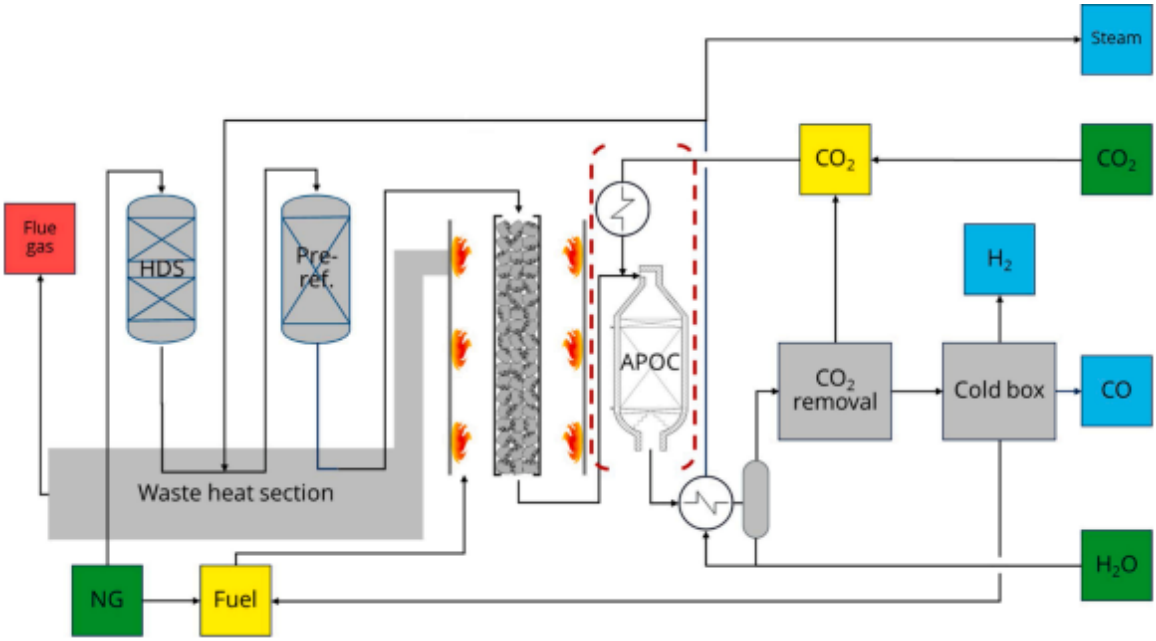

Figure 2.3. A simple overall PFD of a SMR process combined with an APOC reactor, as an example of a revamp configuration using the ReShift™ technology. Figure taken from (Mortensen et al., 2020) with permission.

2.4.2. Thermodynamics in ReShift™

The same reforming reactions (1)-(4) take place in the ReShift™ technology as in the conventional SMR. Since CO_2 is added to the feed, the overall reaction, combining reaction (1) and (4), can be written as reaction (18):

$$CH_4(g) + xH_2O(g) + (1-x)CO_2(g) \leftrightarrow (2-x)CO(g) + (2+x)H_2(g) \qquad (18)$$

where *x=1* equals the SMR reaction (1) and *x=0* equals the DMR reaction (4) (Mortensen et al., 2023). Addition of CO_2 pushes the WGS reaction (2) towards RWGS reaction (19) due to Le Chatelier's principle, resulting in production of CO (Bown et al., 2021; Mortensen et al., 2023):

$$CO_2(g) + H_2(g) \leftrightarrow CO(g) + H_2O(g) \left(\Delta H^{\circ}_{298\,K} = 41\ kJmol^{-1}\right) \qquad (19)$$

The RWGS reaction is reversible and therefore limited by thermodynamic equilibrium. As an endothermic reaction, it is favored at higher temperatures, while the equilibrium is independent of pressure (Bown et al., 2021; Chen et al., 2020; Su et al., 2017). This can be explained by the equal stoichiometric coefficients on the reactant and product sides, as also reflected by the equilibrium constant (20) for the RWGS reaction (19) (Rostrup-Nielsen et al., 2011):

$$K_{eq,RWGS} = \frac{p_{CO} * p_{H_2O}}{p_{CO_2} * p_{H_2}} = \frac{p_{CO} * p_{H_2O}}{p_{CO_2} * p_{H_2}} \quad (20)$$

where p_i and y_i represents the partial pressure and mole fraction, respectively, of the reactants and products. In contrast, the competing CO_2 methanation reaction (reversed reaction (3)) is exothermic and thus favored at lower temperatures (typically 200-500°C), and higher pressures according to Le Chatelier's principle. Consequently, CO selectivity increases with temperature, whereas CH_4 selectivity increases at lower temperatures and elevated pressures (Bown et al., 2021).

From a kinetic perspective, reaction rates differ depending on the process configuration. In SMR, the exothermic WGS reaction (2) proceeds rapidly, reaching equilibrium quickly, while the reforming reactions (1), (3) and (4) are comparatively slower (Chen et al., 2020; Kang et al., 2025). In contrast, when integrating an APOC reactor, the RWGS reaction (19) is instead the slower reaction, whereas the exothermic methanation reactions (reversed reaction (1) & (3)) are faster at lower temperatures (Christensen, 1996; Kang et al., 2025). These differences in reaction kinetics influence how closely the system approaches equilibrium under given operating conditions. Thus, the temperature approach can be used to estimate the product gas composition, which indicates the deviation from equilibrium. It is defined as the difference between the actual outlet temperature and the equilibrium temperature corresponding to the outlet composition, as can be seen in equation (21):

$$\Delta T_{app} = T_{exit} - T_{eq} \quad (21)$$

where T_{exit} is the actual outlet temperature and T_{eq} is the equilibrium temperature. With this definition in equation (21), the temperature approach remains positive as long as the process operates below the equilibrium curve. If the process instead lies above the equilibrium curve, the terms can be reversed to maintain a positive value of the temperature approach (Rostrup-Nielsen et al., 2011).

2.4.3. Circumventing the carbon limit

An illustration of how the carbon limit can be circumvented with the ReShift™ technology can be seen in Figure 2.4, at a S/C ratio of 1.0. The outlet temperature from the tubular reformer is above 900°C, which then enters the APOC (Mortensen et al. 2020). During the reforming in the APOC, the temperature will decrease since the RWGS reaction (19) is endothermic (Bown et al., 2021). As can be seen in Figure 2.4, the outlet temperature of the APOC is still well above the carbon formation limit while being able to achieve a H_2/CO ratio below 1.0. This

would not be possible to achieve in one step in a SMR process at the same S/C ratio (Mortensen et al. 2020).

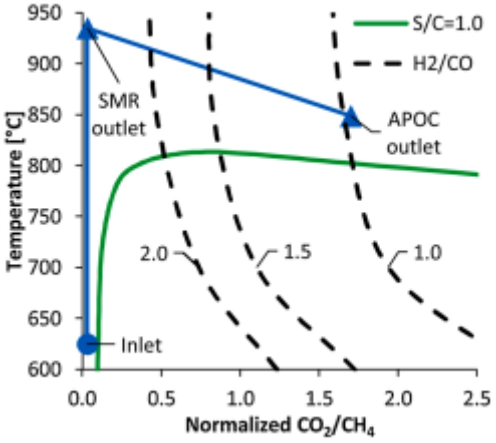

Figure 2.4. An example illustrating how the carbon formation limit can be avoided at a normalized S/C ratio of 1.0. Figure is taken from (Mortensen et al., 2020).

It should be noted that the introduction of pure CO_2 into the process gas does not significantly affect the normalized S/C ratio. Consequently, the corresponding curve is valid for all process conditions at a given S/C ratio (Mortensen et al. 2020).

For a gas mixture in thermodynamic equilibrium, the normalized CO_2/CH_4 and H_2O/CH_4 can be determined from the normalized compositions of CH_4, H_2O and CO_2 when the H/C and O/C ratios are known, according to equations (22)-(24):

$$\widehat{y_{CH_4}} = \frac{H/C - 2 * O/C + 4}{2 * H/C + 4 * O/C} \tag{22}$$

$$\widehat{y_{H_2O}} = \frac{2 * H/C + 4 * O/C - 8}{2 * H/C + 4 * O/C} \tag{23}$$

$$\widehat{y_{CO_2}} = \frac{2 * O/C - H/C + 4}{2 * H/C + 4 * O/C} \tag{24}$$

Here, $\widehat{y_{CH_4}}$, $\widehat{y_{H_2O}}$ and $\widehat{y_{CO_2}}$ are the normalized gas compositions of CH_4, H_2O and CO_2, respectively. The normalized gas is defined as the hypothetical gas mixture containing only CH_4, H_2O and CO_2 for a given O/C and H/C ratio. However, this system of equations is only

applicable when all solutions are positive, which requires the following conditions to be satisfied:

$$\begin{gathered} H/C > 2 * O/C - 4 \\ H/C < 2 * O/C + 4 \\ H/C > 0 \\ O/C > 0 \end{gathered} \tag{25}$$

The normalized H_2O/CH_4 ratio can be used as an approximation of the overall S/C ratio at the reformer inlet when the feed contains a high CH_4 concentration, as is the case for natural gas (Mortensen et al. 2020).

3. Development of the GIPS simulation

This section describes the development of the GIPS simulation, including PFDs, modelling and assumptions, process evaluation, and optimization. A running industrial plant, referred to as *Reference Industrial Unit* (Appendix B.1) and an existing base case GIPS simulation of the ReShift^{TM} process with a S/C ratio of 1.76 (calculation number provided in Appendix B.2), served as the basis for this study. Based on this *Reference Industrial Unit* and base case GIPS simulation, a new GIPS simulation (calculation number in Appendix B.3) was developed and used in a revamp study to optimize the process for a lower H_2/CO ratio while maintaining a low S/C ratio and low energy demand using the ReShift^{TM} technology.

3.1. Process flow diagram

Figure 3.1 shows the PFD of the conventional SMR process, with CO_2 recycling to the tubular reformer. However, the stream data in the figure is shown for a case without recycling the CO_2 stream. The natural gas feed first passes through a control valve, adjusting the flow to 40 barg. It should be noted that the actual feed conditions are not considered in this simulation. In practice, the feedstock is typically imported at a much lower pressure and would therefore need to be compressed. H_2 is added to the natural gas feed, and the mixture is heated stepwise in heat exchangers E217 and E214 to 375°C before entering the adiabatic hydrogenation reactor for sulfur removal.

Steam is added to stream 2030 to obtain the specified S/C ratio, after which the mixture is preheated to 520°C before entering the prereformer. In the prereformer, higher hydrocarbons are converted to C_1 components. If desirable, additional CO_2 can then be added to stream 2061. The stream is subsequently preheated in heat exchanger E211 to 640°C before entering the tubular reformer. The ILOS and OLOS unit operations located before and after the tubular reformer are included only for simulation purposes, representing additional pressure drops and heat losses. Downstream of the tubular reformer, the outlet stream is cooled stepwise in three heat exchangers to separate water in the next unit operation V221. CO_2 is then removed, and the remaining gas is separated in a cold box into H_2 and CO product streams, as well as an off-gas stream. The removed CO_2 is mixed with external CO_2 (stream 5000) and subsequently cooled to 40°C and then compressed to 33.2 barg in compressor K231 to facilitate recycling (if used).

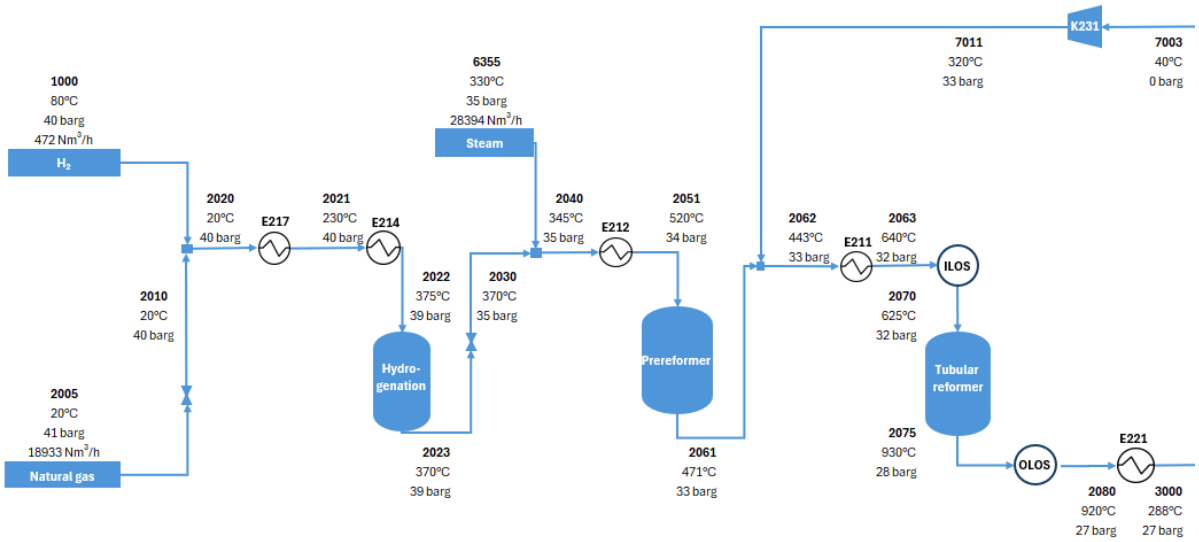

Calc. No.:

Composition [mole%] Stream	2005	2020	2023	2051	2061	2070	2075	3070	3030	3032	3040	3050	3060	7001	7011
Oxygen	0,0	0,0	0,0	0,0	0,0	0,0	0,0	0,0	0,0	0,0	0,0	0,0	0,0	0,0	0,0
Hydrogen	0,0	2,4	2,4	1,0	8,1	6,8	47,7	0,0	57,4	62,0	0,0	98,2	22,2	1,1	0,6
Water	0,0	0,0	0,0	59,4	49,1	40,6	17,3	99,9	0,5	0,5	0,0	0,0	5,5	0,4	0,2
Nitrogen	0,4	0,4	0,4	0,2	0,1	0,1	0,1	0,0	0,1	0,1	0,1	0,0	0,8	0,0	0,0
Carbon Monoxide	0,0	0,0	0,0	0,0	0,1	0,1	23,9	0,0	28,8	31,1	99,9	0,4	5,5	0,0	0,0
Carbon Dioxide	0,0	0,0	0,0	0,0	3,2	19,9	6,1	0,1	7,4	0,0	0,0	0,0	0,1	98,4	99,2
Methane	89,3	87,2	87,2	35,4	39,4	32,6	4,9	0,0	5,9	6,4	0,0	1,4	66,0	0,0	0,0
Flow [Nm³/h]	18933	19405	19405	47799	51137	61934	93167	15780	77388	71591	21805	43794	5993	5796	10796

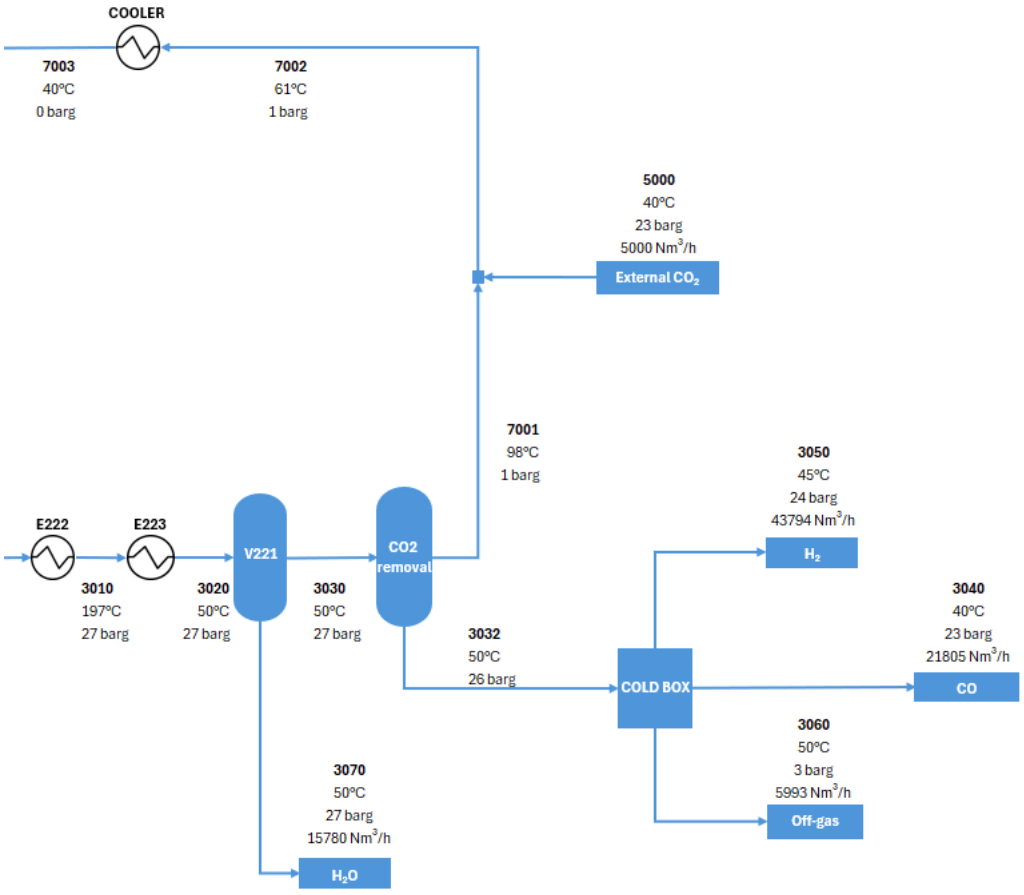

Figure 3.1. PFD of the SMR base case with CO_2 recycling. The figure is divided in two parts, with the upper one corresponding to the left side of the PFD and the bottom one the right side of the PFD. Stream data shown for a case with S/C ratio 1.3 and no CO_2 recycling to the tubular reformer.

Figure 3.2 shows the PFD of the integrated process, consisting of a conventional SMR section followed by the APOC unit. The unit operations upstream of the tubular reformer are the same as those shown in Figure 3.1. The outlet stream from the tubular reformer (stream 2080) is mixed with CO_2 before entering the APOC reactor, where the RWGS reaction is the main reaction. The REILOS and REOLOS unit operations placed before and after the APOC serve the same simulation purpose as ILOS and OLOS. The downstream process of the APOC reactor looks the same as in Figure 3.1, except for the CO_2 recycling section where the recycle stream 7001 first is cooled to 40°C (COOLER1) and then compressed to 33.2 barg in compressor K221. If recycling to both the SMR inlet and the APOC inlet is desired, the compressed CO_2 stream is split. Otherwise, the entire recycle stream (stream 7004) is returned to the APOC, where it is mixed with external CO_2, cooled to 40°C (COOLER2), compressed to 27.7 barg in compressor K222 and preheated to the specified preheat temperature in heat exchanger E231.

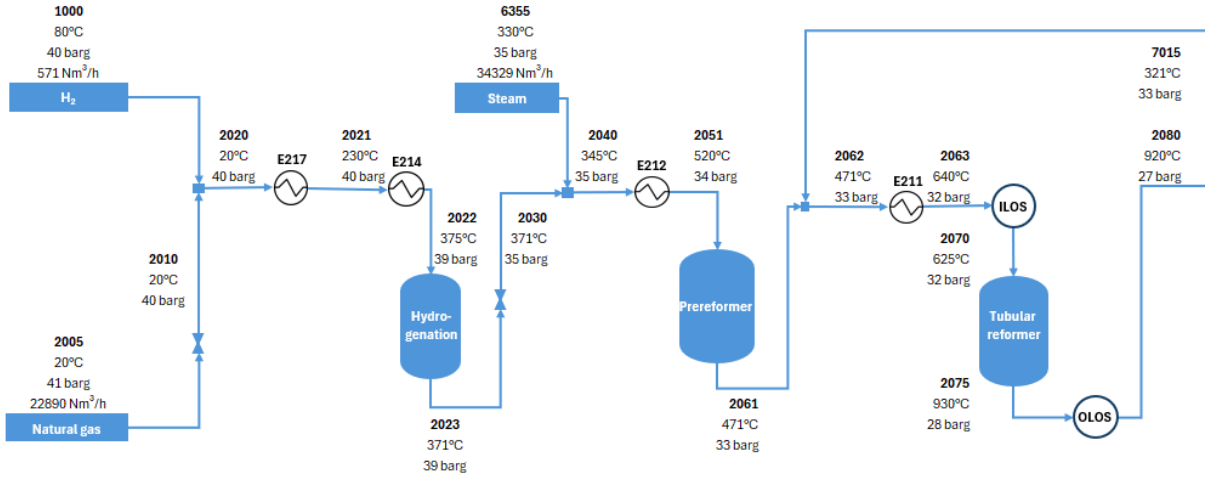

Calc. No.:

Composition [mole%]															
Stream	2005	2020	2023	2051	2061	2070	2075	2086	2090	3070	3030	3032	3040	3050	3060
Oxygen	0,0	0,0	0,0	0,0	0,0	0,0	0,0	0,0	0,0	0,0	0,0	0,0	0,0	0,0	0,0
Hydrogen	0,0	2,4	2,4	1,0	8,1	8,1	58,5	50,7	41,8	0,0	52,0	58,6	0,0	98,2	13,2
Water	0,0	0,0	0,0	59,4	49,1	49,1	13,6	11,8	20,1	99,9	0,5	0,5	0,0	0,0	3,6
Nitrogen	0,4	0,4	0,4	0,2	0,1	0,1	0,1	0,1	0,1	0,0	0,1	0,1	0,1	0,0	0,6
Carbon Monoxide	0,0	0,0	0,0	0,0	0,1	0,1	16,9	14,6	21,0	0,0	26,1	29,5	99,9	0,4	3,3
Carbon Dioxide	0,0	0,0	0,0	0,0	3,2	3,2	2,8	15,8	9,1	0,1	11,3	0,0	0,0	0,0	0,0
Methane	89,3	87,2	87,2	35,4	39,4	39,4	8,1	7,0	8,1	0,0	10,1	11,4	0,0	1,4	79,3
Flow [Nm³/h]	22890	23460	23460	57789	61833	61833	95192	110134	108088	21284	86804	76863	22180	44446	10236

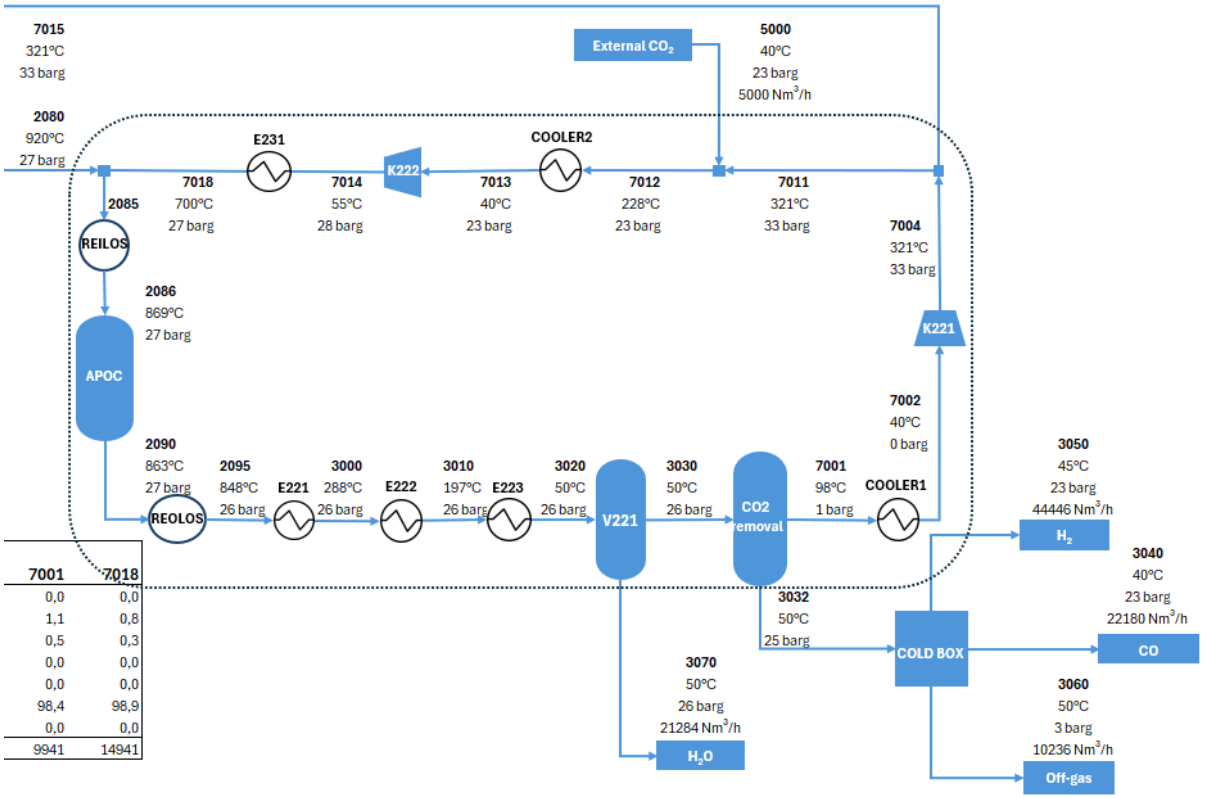

7001	7018
0,0	0,0
1,1	0,8
0,5	0,3
0,0	0,0
0,0	0,0
98,4	98,9
0,0	0,0
9941	14941

Figure 3.2. PFD of the overall revamp process, including feed pretreatment, the SMR section and the integrated APOC reactor with CO_2 recycling. The figure is divided in two parts, with the upper one corresponding to the left side of the PFD and the bottom one the right side of the PFD. Stream numbers are shown, and the system boundary around the ReShift™ process is indicated with a dashed line. Shown for a case with 5000 Nm³/h external CO_2 addition and 700°C CO_2 preheat temperature.

A system boundary is defined as a dashed line around the APOC section, including the recycling loop. In the evaluation of CO_2 flow to the APOC reactor, the external CO_2 addition is used as the operating variable. However, because CO_2 entering the system boundary also includes CO_2 from the tubular reformer outlet stream, these contributions are considered together and referred to as the fresh CO_2 flow, as defined in equation (36).

3.2. Modelling and assumptions

Steady-state process simulations were performed using Topsoe's internal software, GIPS. The reactors were represented using plug-flow reactor (PFR) models, and the APOC reactor was additionally described as a fixed-bed reactor using a one-dimensional heterogenous model. The one-dimensional assumption can be justified by the adiabatic reactor configuration, for which radial temperature and concentration gradients are typically negligible (Christensen, 1996). In the tubular reformer, both axial and radial temperature gradients will develop, and therefore the two-dimensional model is used. The radial gradients in the reformer are required to predict the risk of carbon formation (Rostrup-Nielsen et al., 2011). A homogenous model is used for the tubular reformer which only considers pellet kinetics, while the heterogenous model is based on intrinsic reaction kinetics, considering temperature and concentration profiles inside the catalyst particle (Christensen, 1996). Thermodynamic properties were calculated using a property method appropriate for syngas, capable of representing polar, non-ideal mixtures. The method combines the UNIQUAC activity coefficient model for the liquid phase and the Soave-Redlich-Kwong equation of state for the vapor phase.

The following input conditions and assumptions were considered in the simulation model:

- The reactors operate at constant temperatures predetermined from sensitivity analysis.
- The compressors operate with an isentropic efficiency of 100% and with 11.1% loss of compression work.
- Heat exchanger E231, which preheats the CO_2 stream, is an electric heat exchanger.
- Pressure drops and heat losses are constant.
- Cooling duties (E221, E222, E223, COOLER in SMR base case and COOLER1 and COOLER2 in ReShift case) are assumed to be integrated with simultaneous steam generation and are therefore excluded in the duty calculations.
- The S/C ratio corresponds to the amount of steam relative to the amount of hydrocarbon in stream 2030 (Figure 3.1 and 3.2)
- The temperature approach to equilibrium for the SMR reaction is 4.3°C in the tubular reformer.
- The temperature approach to equilibrium for the RWGS reaction is 15°C in the APOC reactor.
- The effectiveness factor for the SMR reaction is calculated in GIPS and the value varies with the axial distance from the tubular reformer inlet.

3.3. Intrinsic kinetic model and effectiveness factor

There are several ways to describe the kinetics of steam reforming, and the specific kinetic models used in this study are not explicitly stated, due to confidentiality. However, to gain insight into the possible kinetic behavior of the process, reaction rate expressions based on the Langmuir-Hinshelwood-Hougen-Watson (LHHW) model are presented. The kinetic model considered is based on Xu and Froment (1989) for a Ni/$MgAl_2O_4$-spinel catalyst at 3-10 bar and 573-848 K. The model is well-established, although extrapolation beyond the validated range should be treated with caution. The chemical reactions in this process can be represented by the two independent reactions; SMR reaction (1) and WGS reaction (2), for which the reaction rate expressions by this model are given by (26)-(28):

$$r_{SMR} = \frac{k_{SMR}}{p_{H_2}^{2.5}}\left(p_{CH_4}p_{H_2O} - \frac{p_{H_2}^3 p_{CO}}{K_{SMR}}\right)(DEN)^{-2} \tag{26}$$

$$r_{WGS} = \frac{k_{WGS}}{p_{H_2}}\left(p_{CO}p_{H_2O} - \frac{p_{H_2}p_{CO_2}}{K_{WGS}}\right)(DEN)^{-2} \tag{27}$$

$$DEN = 1 + K_{CO}p_{CO} + K_{H_2}p_{H_2} + K_{CH_4}p_{CH_4} + \frac{K_{H_2O}p_{H_2O}}{p_{H_2}} \tag{28}$$

where k_{SMR} and k_{WGS} are the rate constants of SMR and WGS, and p_i is the partial pressure of component *i*. Furthermore, K_{SMR} and K_{WGS} are the chemical equilibrium constants of SMR and WGS, K_{CO}, K_{H_2}, $K_{CH_4}$and K_{H_2O} are the adsorption constants of CO, H_2, CH_4 and water, and DEN is the fraction of free sites in the reactions (Santos et al., 2023).

It is widely accepted that the same kinetic descriptions used for steam reforming can be applied to CO_2 reforming over a nickel catalyst (Rostrup-Nielsen et al., 2011).

Effectiveness factors are often used in heterogenous models to simplify kinetic expressions, by considering transport restrictions. The effectiveness factor is the ratio between the actual reaction rate with pore diffusion and the intrinsic reaction rate without transport restrictions (Christensen, 1996; Santos et al., 2023). It is useful because it shows how efficiently the catalyst is utilized and helps simulations to better represent industrial conditions. An expression for the effectiveness factor for a reaction *j* is given by equation (29):

$$\eta_j = \frac{\int_0^{V_P} r_j(P_i, T_P)dV}{r_j(p_{i,s}, T_s)V_p} \tag{29}$$

Where V_p is the catalytic pellet volume, r_j is the reaction rate, P_i is the particle pressure of component *i* inside the catalyst pellet, *T* is the temperature inside the catalyst pellet, $p_{i,s}$ is the

partial pressure of component i on the pellet surface and T_s is the temperature on the pellet surface (Santos et al., 2023).

3.4. Process evaluation

The reaction performance was evaluated by conversion, selectivity and yield for different components which are calculated as follows:

$$X_{CH_4} = \frac{F_{CH_4,in} - F_{CH_4,out}}{F_{CH_4,in}} * 100\% \quad (30)$$

$$X_{CO_2} = \frac{F_{CO_2,in} - F_{CO_2,out}}{F_{CO_2,in}} * 100\% \quad (31)$$

$$S_{CO} = \frac{F_{CO,out} - F_{CO,in}}{F_{CO_2,in} - F_{CO_2,out}} * 100\% \quad (32)$$

$$S_{CH_4} = \frac{F_{CH_4,out} - F_{CH_4,in}}{F_{CO_2,in} - F_{CO_2,out}} * 100\% \quad (33)$$

$$Y_{CO} = \frac{F_{CO,out} - F_{CO,in}}{F_{CO_2,in}} * 100\% \quad (34)$$

$$Y_{CH_4} = \frac{F_{CH_4,out} - F_{CH_4,in}}{F_{CO_2,in}} * 100\% \quad (35)$$

where $F_{i,in}$ is the inlet volumetric flow of component i, $F_{i,out}$ is the outlet volumetric flow of component i, X_{CH_4} is the CH_4 conversion, X_{CO_2} is the CO_2 conversion, S_{CO} is the CO selectivity, S_{CH_4} is the CH_4 selectivity, Y_{CO} is the CO yield and Y_{CH_4} is the CH_4 yield (Santos et al., 2023).

Fresh CO_2 inlet flow was used to express the CO_2 flow that enters the APOC reactor excluding the recycle stream, and is defined as:

$$F_{CO_2,Fresh} = F_{CO_2,SMR} + F_{CO_2,External} \quad (36)$$

where $F_{CO_2,SMR}$ is the volumetric flow of CO_2 from the tubular reactor and $F_{CO_2,External}$ is the volumetric flow of external CO_2 addition.

The relative change or delta change in E231 heat duty and CO product flow compared to a reference case is calculated according to equation (37) and (38):

$$\Delta CO = \frac{F_{CO,out} - F_{CO,ref}}{F_{CO,ref}} * 100\% \quad (37)$$

$$\Delta Duty = \frac{Q_{E231} - Q_{E231,ref}}{Q_{E231,ref}} * 100\% \quad (38)$$

where $F_{CO,ref}$ is the volumetric product flow of CO out of the APOC for the reference case, and Q_{E231} is the heat duty of heat exchanger E231, with $Q_{E231,ref}$ as the heat duty of the reference case.

The CO_2 recycling ratio and total C_1 recycling ratio, described by equations (39) and (40), respectively, were used to evaluate the effectiveness of the recycling loop and to determine the optimum level of CO_2 recycling to the APOC reactor.

$$CO_2\ recycling\ ratio = \frac{F_{CO_2,recycling}}{F_{CO_2,SMR} + F_{CO_2,External}} \quad (39)$$

$$Total\ C_1\ recycling\ ratio = \frac{F_{CO_2,recycling}}{F_{CO,SMR} + F_{CO_2,SMR} + F_{CH_4,SMR} + F_{CO_2,External}} \quad (40)$$

where $F_{CO_2,recycling}$ is the CO_2 recycling flow to the APOC, $F_{i,SMR}$ is the flow of component i from the tubular reformer, and $F_{CO_2,External}$ is the flow of external CO_2 addition. All flows are expressed as volumetric flows. The CO_2 recycling ratio tells how big the CO_2 recycling is relative to the fresh CO_2 feed, while total C_1 recycling ratio tells how big the CO_2 recycling is relative to all fresh C_1 -compounds entering the APOC.

3.5. Process optimization

At first, a conventional SMR process based on the *Reference Industrial Unit* and the GIPS base case was simulated, and a sensitivity analysis of the tubular reformer was carried out by varying the reformer outlet temperature, pressure and S/C ratio. The objective of this step was to identify operating conditions suitable for subsequent APOC integration, with focus on achieving a low S/C ratio while maintaining sufficiently high conversion and, secondarily, a low H_2/CO ratio. The duty of the tubular reformer was fixed throughout the study at a value corresponding to the base case.

The ReShift^{TM} section was then integrated into this process, and a sensitivity analysis was performed to evaluate the effects of CO_2 addition and CO_2 preheat temperature in heat exchanger E231 (Figure 3.2). The objective of this step was to increase product flows, especially CO, while maintaining sufficiently high H_2 flow and limiting the associated energy demand. Additional sensitivity analyses were carried out to investigate the effect of adding

CO_2 upstream of the tubular reformer in the ReShift^{TM} process and which S/C ratios were required for carbon free operation. In several parts of the study, root functions were applied to determine process variables that fulfilled specified constraints, for example to maintain a fixed tubular reformer duty or to identify the CO_2 inlet flow required to meet a target condition. All simulations were conducted using parameter ranges that ensured operation outside carbon formation conditions.

Based on the results of the sensitivity analyses, a limited number of cases were selected for further evaluation, including cases aimed at achieving a H_2/CO ratio of 1.0 as well as comparison cases. These cases were subsequently evaluated with respect to CO_2 emissions and a rough estimate of the revamp investment cost.

4. Results & Discussion

This section is divided into subsections in which the results of the SMR and ReShift™ simulations are presented and discussed. Based on these results, selected cases are compared further, followed by a CO_2 emission analysis, an economic analysis and a short simulation software discussion.

4.1. Analysis of the SMR process

In the first part of the project, a conventional SMR process was simulated according to the PFD shown in Figure 3.1, but without recycling or adding external CO_2. CH_4 conversion and H_2/CO ratio were evaluated at different tubular reformer outlet temperatures, S/C ratios, and tubular reformer outlet pressures. To analyze each parameter individually, the other parameters were set at default values shown in Table 4.1. The duty of the tubular reformer was set to a fixed value corresponding to operation at a S/C ratio of 1.76 according to the base case. This was done since a fixed duty is often used in revamp projects because the existing equipment and utility systems impose limitations on the amount of heat that can be supplied to the process. The natural gas flow rate was adjusted using a root function to keep the duty constant. The S/C ratio was set to 1.1 as default value, which with the current feed ratios and operating conditions lies outside the carbon formation region, shown in Figure A.1 in Appendix A.2. This lower ratio was selected in the present study to better reflect the intended operating conditions.

The objective of this sensitivity analysis was to evaluate the influence of parameter variations on the SMR reaction and to provide insight into operating conditions that favor low H_2/CO ratios, low S/C ratios, and high CH_4 conversion.

Table 4.1. Default values for the analysis of the SMR process.

Parameter	Value
Tubular reformer outlet temperature	930°C
Tubular reformer outlet pressure	27.7 barg
S/C ratio	1.1
Duty tubular reformer	59.45 MW

Figure 4.1 illustrates the dependence of CH_4 conversion and H_2/CO ratio on the tubular reformer outlet temperature. At an outlet temperature of 800°C, the CH_4 conversion is 35.7%. The CH_4 conversion increases with increasing tubular reformer temperature, reaching a value of 75.7% at an outlet temperature of 1000°C. For a corresponding system at equilibrium, i.e. the temperature approach to equilibrium for the SMR reaction (1) equals zero, the CH_4 conversion is 36.6% at 800°C and 76.3% at 1000°C. The H_2/CO ratio decreases with increasing tubular reformer temperature, starting at a value of 4.52 at an outlet temperature of 800°C and ending at a value of 3.13 at 1000°C. As shown in Figure 4.1, operation at higher temperatures

results in both higher CH_4 conversion and lower H_2/CO ratios. The lower H_2/CO ratio can be explained by the endothermic SMR reaction (1) being more favored at higher temperatures than the exothermic WGS reaction (2). However, catalyst stability and mechanical properties of the tube material impose practical limits on the operating temperature.

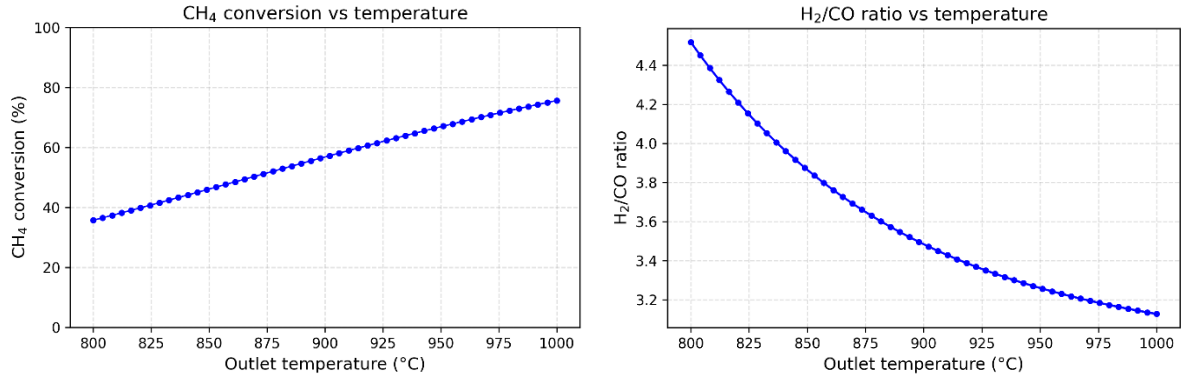

Figure 4.1. CH_4 conversion and H_2/CO ratio at varying outlet temperatures of the tubular reformer. With default values from Table 4.1.

Figure 4.2 shows the dependence of CH_4 conversion and H_2/CO ratio on the tubular reformer outlet pressure. At an outlet pressure of 18.2 barg, the CH_4 conversion is 71.0%. The CH_4 conversion decreases with increasing tubular reformer pressure, reaching a value of 63.0% at an outlet pressure of 27.7 barg. This can be explained by that an increase in pressure shifts the SMR reaction (1) toward the reactant side, resulting in a lower CH_4 conversion. The H_2/CO ratio increases slightly with increasing tubular reformer pressure, starting at a value of 3.22 at an outlet pressure of 18.2 barg and ending at a value of 3.34 at 27.7 barg. Increasing pressure suppresses SMR reaction (1), while enhancing the relative contribution of the WGS reaction (2) since a larger amount of H_2O is available to drive the reaction, which reduces CO more strongly than H_2, and thereby increasing the H_2/CO ratio.

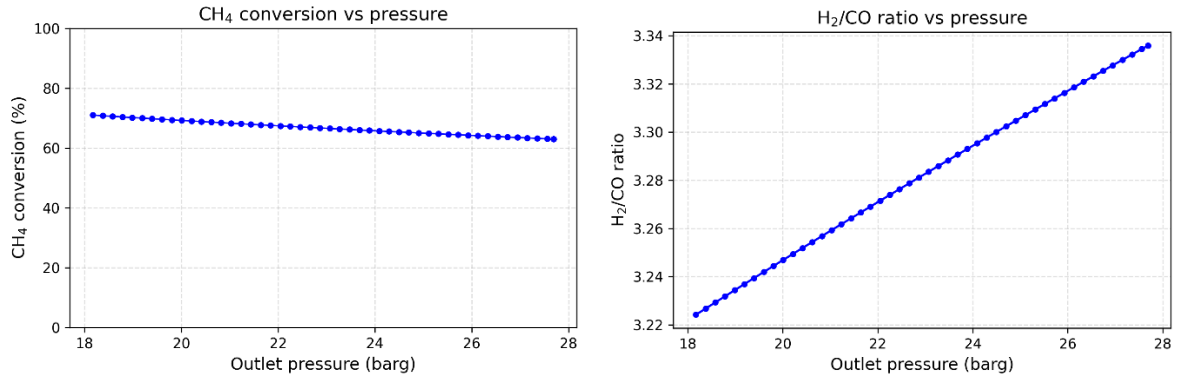

Figure 4.2. CH_4 conversion and H_2/CO ratio at varying outlet pressures of the tubular reformer.

As the previous results indicates that high temperature and low pressure are favorable, the reformer outlet temperature and pressure were set to 930°C and 27.7 barg, respectively. These values were chosen considering the material temperature limits and the high-pressure requirements of downstream processes. Under these conditions, the S/C ratio was varied, and the results are presented in Table 4.2.

Table 4.2. H_2/CO ratio, CH_4 conversion, and product flow rates at varying S/C ratios. At an outlet pressure of 27.7 barg, an outlet temperature of 930°C and a fixed duty in the tubular reformer.

S/C ratio	H_2/CO ratio	CH_4 conversion (%)	CO product flow rate (Nm^3/h)	H_2 product flow rate (Nm^3/h)	CH_4 product flow rate (Nm^3/h)	CH_4 slip (%)
1.0	3.27	59.9	16,659	54,432	11,067	13.1
1.2	3.40	65.8	16,262	55,344	8639	10.4
1.4	3.54	70.7	15,850	56,036	6906	8.5
1.6	3.67	74.8	15,435	56,578	5617	6.9

To better visualize the results in Table 4.2, the effect of varying the S/C ratio on CH_4 conversion and H_2/CO ratio is shown in Figure 4.3. These results can be explained with Le Chatelier's principle since increasing the S/C ratio shifts the SMR reaction (1) toward the products, thereby increasing the CH_4 conversion, while simultaneously promoting the WGS reaction (2), which increases the H_2/CO ratio.

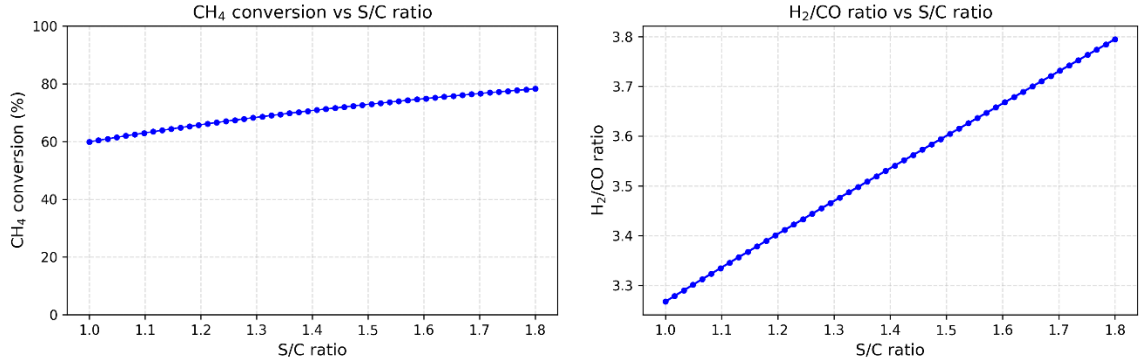

Figure 4.3. CH_4 conversion and H_2/CO ratio at varying S/C ratios.

As mentioned in Section 2.2.4, industrial SMR plants usually operate at S/C ratios above 2.5 to achieve high CH_4 conversion, which is consistent with the results in Table 4.2, where relatively low CH_4 conversions of around 60-75% are achieved at S/C ratios in the range of 1.0-1.6. On the other hand, the product flow rate of CO increases by 7.9% when decreasing S/C ratio from 1.6 to 1.0, while the H_2 product flow rate decreases by 3.8%. Furthermore, only decreasing the S/C ratio from 1.4 to 1.2 gave a 2.6% increase in CO product flow rate and 1.2% decrease in H_2 product flow rate. It can also be seen that a lower S/C ratio results in lower

H_2/CO ratios, but it comes at a cost of lower CH_4 conversion. Since the duty is kept constant, a decreased S/C ratio results in a larger carbon (natural gas) feed flow rate, but the lower conversion still results in a slightly lower total product flow rate of H_2 and CO.

Considering only the stoichiometry of the SMR reaction (1), the minimum theoretical H_2/CO ratio is 3. However, in practice other reactions such as the WGS reaction (2) also occur, producing additional H_2 and consuming CO. As a result, the actual H_2/CO ratio is expected to be higher than 3. This is consistent with the results in Table 4.2 where a S/C ratio of 1 gives a H_2/CO ratio of approximately 3.27.

4.2. First analysis of the ReShift™ process

The ReShift™ technology was simulated by integrating an APOC unit, CO_2 recycle and external CO_2 feed streams, as well as the associated compressors (K221 and K222) and a heat exchanger (E231) for the CO_2 streams, into the conventional SMR process based on the *Reference Industrial Unit* (Figure 3.2). To evaluate the effects of external CO_2 addition and CO_2 preheating temperature in E231, the default operating conditions obtained from the SMR analysis were used as baseline (Table 4.3). Considering the results from varying the S/C ratio in Section 4.1, a ratio of 1.3 was chosen as the default value for this analysis. The CO_2 recycle split to the tubular reformer was set to 0, meaning that the entire CO_2 recycle stream entered the APOC reactor inlet.

Table 4.3. Default operating conditions for the ReShift™ process.

Variable	Value
Tubular reformer outlet temperature	930°C
S/C ratio	1.3
Tubular reformer outlet pressure	27.7 barg
APOC inlet pressure	27.1 barg
CO_2 recycled to tubular reformer (split)	0
External CO_2 addition to APOC	1000-10,000 Nm^3/h
Preheating temperature of CO_2 in E231	700-900°C
Duty tubular reformer	59.45 MW

As described in Section 3.1, the fresh CO_2 inlet flow rate was applied as the basis for evaluating process performance. The corresponding values of external CO_2 addition expressed as fresh CO_2 inlet flow rate are summarized in Table 4.4.

Table 4.4. External CO_2 inlet flow rate to the APOC reactor and the corresponding fresh CO_2 inlet flow rate.

External CO_2 addition to APOC (Nm^3/h)	Approximate fresh CO_2 inlet flow rate (Nm^3/h)
1000	3600
5000	7600
10000	12,600

To illustrate the carbon distribution and recycling within the process, a carbon flow diagram was created, as shown in Figure 4.4. It is shown for a representative case with a CO_2 preheat temperature of 800°C and an external CO_2 flow rate of 5000 Nm^3/h. The carbon flow diagram includes the inlet and outlet streams of the tubular reformer, the APOC and CO_2 removal section, as well as the CO_2 recycle stream. Each arrow represents the flow of a carbon-containing component (CO_2, CO or CH_4), with the corresponding flow rates presented in Table A.2 in Appendix A.3. The recycled CO_2 stream leaving the CO_2 removal section has a purity of 98.40 dry mole% and is fully recirculated to the APOC reactor.

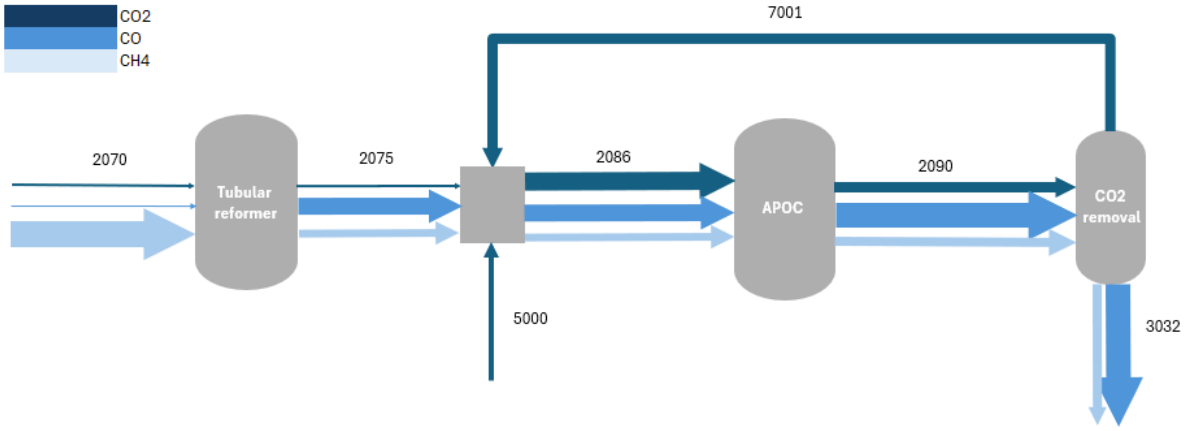

Figure 4.4. Carbon flow diagram of the overall process, including the inlet and outlet streams of the tubular reformer, APOC and CO_2 removal section, as well as the CO_2 recycle stream. Arrow widths reflect the relative flow rates of CO_2, CO, and CH_4. The case shown has an external CO_2 flow rate of 5000 Nm^3/h and a CO_2 preheat temperature of 800°C. Stream numbers are also shown for each stream.

The CO_2 conversion in the APOC when varying the fresh CO_2 addition flow (equation (36)), ranging from 3600 to 12,600 Nm^3/h, at three different CO_2 preheat temperatures, is illustrated in Figure 4.5. For all three cases, the CO_2 conversion exhibits an initial increase with an increasing fresh CO_2 inlet flow rate, followed by a maximum and a subsequent decrease.

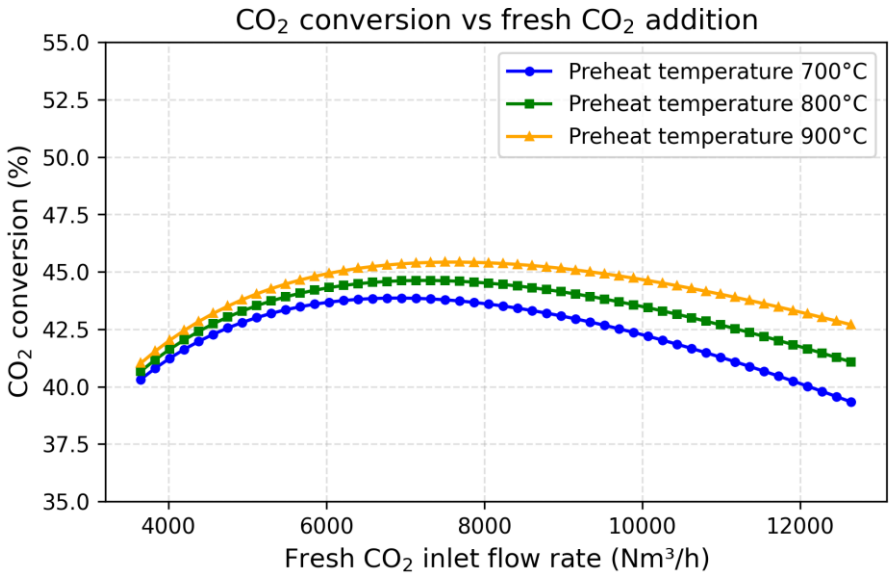

Figure 4.5. Effect of fresh CO_2 addition flow rate (3600–12,600 Nm^3/h) on CO_2 conversion in the APOC reactor at preheating temperatures of 700, 800 and 900°C.

The maximum CO_2 conversions are reached at a fresh CO_2 inlet flow rate between around 7000 to 7700 Nm^3/h, which corresponds to an external CO_2 addition of approximately 4300 to 5040 Nm^3/h. This result indicates that there is an optimal CO_2 addition level for the RWGS reaction (19), beyond which further increases in CO_2 feed leads to a decrease in CO_2 conversion due to equilibrium limitations. With a CO_2 preheat temperature of 800°C, the maximum CO_2 conversion is 44.6% at a 15°C approach to equilibrium and 45.8% at a 0°C approach, indicating that the equilibrium temperature approach has only a minor effect in this case.

The higher CO_2 conversion that is observed at elevated temperature is mainly due to the endothermic nature of the RWGS reaction, for which higher temperature shifts the equilibrium toward product formation. In addition, increasing the temperature enhances reaction kinetics, allowing the system to approach equilibrium more rapidly. Increasing the external CO_2 flow lowers the mixed-stream temperature upstream of the APOC, whereas a higher CO_2 preheat temperature helps maintain a higher APOC inlet temperature. As shown in Figure 4.5, the influence of preheat temperature becomes more pronounced at higher external CO_2 flow rates, because larger CO_2 additions have a greater effect on the mixed-stream temperature at the APOC inlet.

In the following section, process performance is evaluated using product flow rates rather than the H_2/CO ratio. It can be observed that the H_2/CO ratio decreases from approximately 2.6 to 1.5 when increasing the fresh CO_2 inlet flow (Figure A.2 in Appendix A.4). At different preheat temperatures, the H_2/CO ratio shows only minor changes, which can be explained by the observation that H_2 and CO product flows are changed in the same direction when changing the preheat temperature. Product flow rates therefore provide a clearer basis for comparing the effects of these parameters.

The effect of external CO_2 addition and CO_2 preheat temperature on the product flows is illustrated in Figure 4.6, which shows the outlet flow rates of CO, H_2, CO_2 and CH_4 as functions of the fresh CO_2 inlet flow at three different preheat temperatures. These results complement the CO_2 conversion trends discussed in a previous paragraph. Although the CO_2 conversion in the APOC reactor reaches a maximum and then decreases with higher inlet CO_2 flow rates, the CO outlet flow increases continuously with increasing external CO_2 addition for all three temperatures. This indicates that, despite a lower fractional conversion at high CO_2 addition, the larger CO_2 supply in the reactor results in increased CO production. The effect of temperature is comparatively weaker, with higher preheat temperatures giving slightly higher CO product flows. This is consistent with the higher CO_2 conversions observed at elevated temperatures, particularly at larger CO_2 inlet flows where preheating has a greater impact on the APOC inlet temperature.

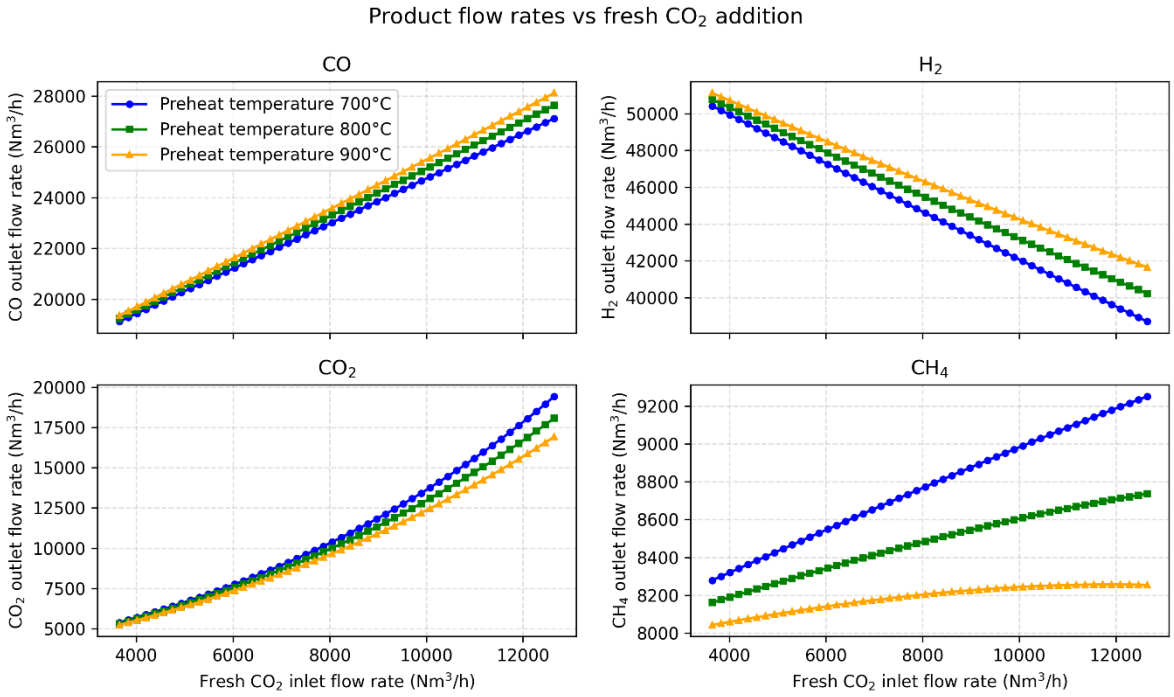

Figure 4.6. Four subplots showing product flow rates of CO, H_2, CO_2 and CH_4 as functions of the fresh CO_2 inlet flow, at three different preheat temperatures (700, 800 and 900°C).

The sensitivity of CO production to changes in operating conditions is quantified by step-response calculations, summarized in Appendix A.5 (Table A.3-A.5). Increasing the fresh CO_2 addition from 3600 to 12,600 Nm^3/h at a preheat temperature of 700°C resulted in a 41.8% relative increase in CO production. In comparison, increasing the CO_2 preheat temperature from 700 to 900°C at a fresh CO_2 addition of 7600 Nm^3/h increases the CO production by only 2.4%, and by 3.7% at a fresh CO_2 addition of 12,600 Nm^3/h. Thus, increasing the fresh CO_2 flow has a stronger effect on the amount of CO produced, while increasing the temperature mainly improves how selectively carbon is converted.

The CO_2 outlet flow also increases with increasing fresh CO_2 inlet flow, in agreement with the CO_2 conversion results which showed a declining CO_2 conversion at higher inlet flow rates as previously discussed. This explains the larger incremental increase in CO_2 outlet flow at higher CO_2 inlet flows, which can be seen in Figure 4.6.

The CH_4 flow subplot in Figure 4.6 is especially useful for illustrating how the methanation (reversed reaction (3)) tendency changes with operating conditions. At higher CO_2 addition, the CH_4 flow rate increases, indicating that methanation becomes more pronounced. In contrast, increasing the CO_2 preheat temperature reduces the CH_4 flow rate, demonstrating that higher temperature inhibits methanation. This highlights an important trade-off; while higher CO_2 addition increases CO production, it also increases the tendency for methane formation unless sufficiently high preheat temperatures are applied. Furthermore, other methanation reactions also occur like reversed reaction (1), which is enhanced when more CO product is formed.

The H_2 product flow decreases with increasing fresh CO_2 inlet flow, which is consistent with greater H_2 consumption in the RWGS reaction and the methanation reaction as more CO_2 is introduced. In addition, lower CO_2 preheat temperature gives lower H_2 outlet flow, which is likely related to the stronger methanation tendency at lower temperatures.

These product flow trends are reflected in the yield and selectivity results shown in Figure 4.7. Although the CH_4 flow increases with increasing fresh CO_2 inlet flow, indicating enhanced methanation, the CO flow increases even more strongly compared to the amount of CO_2 added. As a result, the CO selectivity increases while the CH_4 selectivity decreases at higher fresh CO_2 inlet flow rates, showing that the additional CO_2 is converted preferentially to CO rather than CH_4.

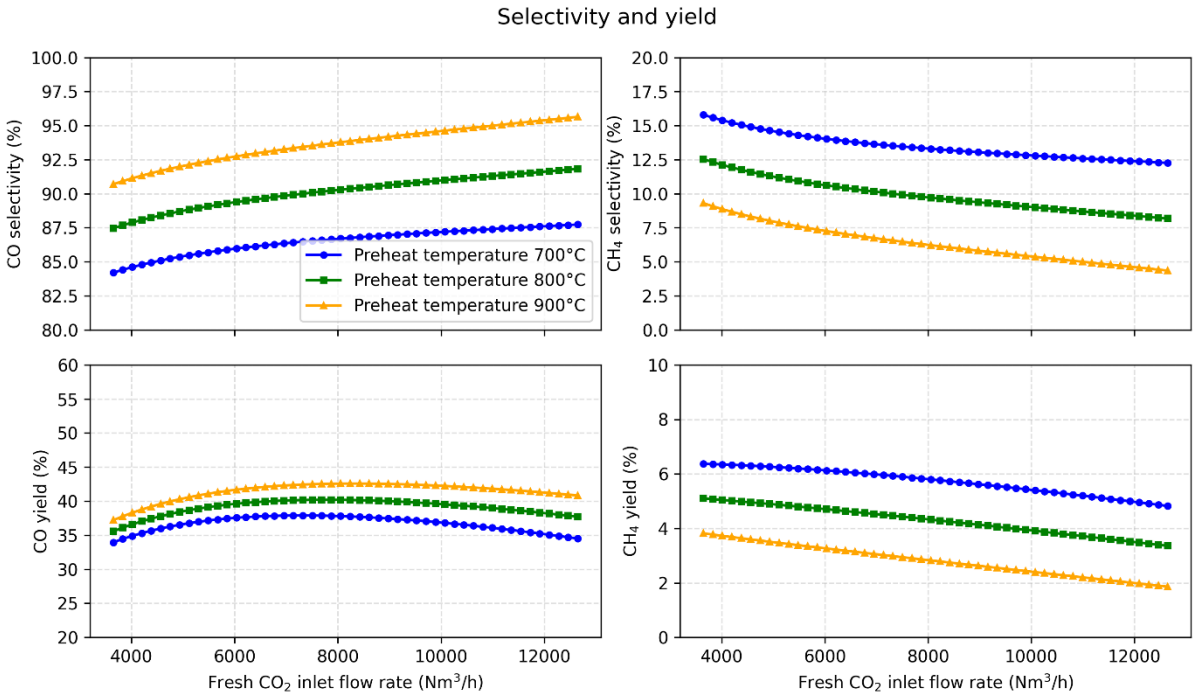

Figure 4.7. Selectivity and yield of CO and CH_4 as a function of fresh CO_2 inlet flow rate. The three curves in each subplot correspond to one CO_2 preheat temperature each (700, 800 or 900°C).

Furthermore, increasing the CO_2 preheat temperature had the desired effect of increasing both CO selectivity and yield, while decreasing CH_4 selectivity and yield. This is consistent with the suppression of methanation observed in the product flow Figure 4.6.

A maximum is observed in the CO yield curve. At a CO_2 preheat temperature of 700°C, the maximum CO yield is 37.9%. At 900°C, the corresponding maximum is 42.6%. This result confirms that higher preheat temperature improves the process performance by increasing the yield of the desired CO product, while simultaneously reducing the yield of undesired CH_4.

Figure 4.8 shows the temperature change across the APOC and the corresponding outlet temperature for different fresh CO_2 inlet flows, and CO_2 preheat temperatures. Since the RWGS reaction is endothermic, a temperature decrease across the APOC reactor is expected, and this behavior is observed for all investigated cases except the one with the lowest preheat temperature and CO_2 addition. The magnitude of the temperature drops increases with both increasing fresh CO_2 inlet flow and increasing CO_2 preheat temperature. At a fresh CO_2 inlet flow rate of 3600 Nm^3/h and a preheat temperature of 700°C, the temperature in the APOC reactor increases by 1.5°C, likely due to the exothermic methanation reaction. At the same fresh CO_2 inlet flow rate but with a preheat temperature of 900°C, the temperature instead decreases by 12.0°C, indicating that methanation is suppressed at the higher temperature. At a fresh CO_2 inlet flow rate of 7600 Nm^3/h, increasing the preheat temperature from 700 to 900°C causes the temperature drop to increase from 5.9°C to 33.4°C. This indicates a greater extent of endothermic reaction at higher CO_2 flow and higher temperatures.

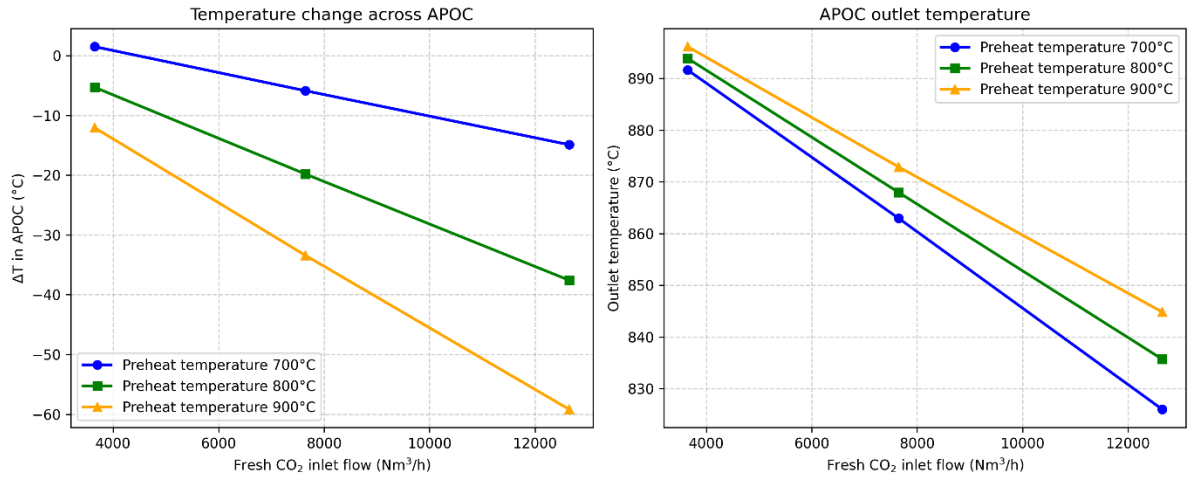

Figure 4.8. Temperature change across the APOC reactor and APOC outlet temperature as functions of fresh CO_2 inlet flows for three different CO_2 preheat temperatures.

The APOC outlet temperature is particularly important from an operational perspective, since excessively low temperatures may increase the risk of carbon formation. Despite the larger temperature drop at higher preheat temperature, the outlet temperature increases slightly with increasing preheat temperature for all CO_2 flows. In contrast, increasing fresh CO_2 inlet flow significantly lowers the outlet temperature. For example, at 700°C preheat, increasing the fresh CO_2 inlet flow from 3600 to 12,600 Nm^3/h reduces the outlet temperature from 891.6 to 826.0°C. Thus, higher CO_2 addition reduces the thermal margin, while increased preheating helps to compensate for this effect.

In Figure 4.9, the carbon limit curve at a S/C ratio of 1.3 is shown together with the temperature change across the APOC reactor for four different fresh CO_2 inlet flow rates at a preheat temperature of 800°C. As seen from the figure, the APOC reactor operates well above the carbon formation region when the fresh CO_2 inlet flow rate varies between 3600 and 12,600 Nm^3/h, whereas a flow rate of 19,000 Nm^3/h brings operation closer to the carbon limit, reaching a H_2/CO ratio of 1. From a carbon formation perspective, these results indicate that a higher fresh CO_2 inlet flow rate could be applied than what has been investigated previously in this report to achieve a lower H_2/CO ratio.

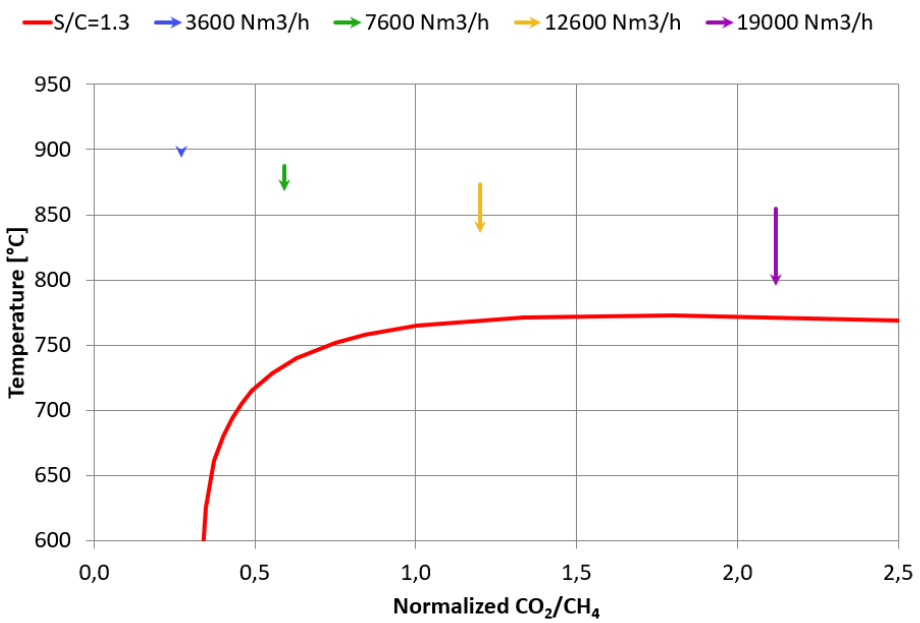

Figure 4.9. Carbon limit curve at 27.1 barg and S/C ratio=1.3, with four cases illustrating the temperature change across the APOC reactor for different fresh CO_2 inlet flows at a CO_2 preheat temperature of 800°C.

Figure 4.10 illustrates the trade-off between increased CO product flow and the required heat duty in heat exchanger E231 when varying the fresh CO_2 addition at different CO_2 preheat temperatures. The delta changes of CO outlet flow and E231 duty are calculated relative to the reference case with a fresh CO_2 inlet flow rate of 3600 Nm^3/h and a CO_2 preheat temperature of 700°C. The relative increase in CO product is similar for all three preheat temperatures, whereas the increase in heat duty is much more dependent on the preheat temperature. Thus, increasing the CO_2 preheat temperature mainly increases the energy penalty rather than the CO gain. Furthermore, changing the fresh CO_2 inlet flow rate from 3600 to 12,600 Nm^3/h at a preheat temperature of 700°C increases the CO product flow by 41.8%, while the heat exchanger duty increases by 360%. This shows that the gain in CO production is accompanied by a disproportionately large increase in energy demand.

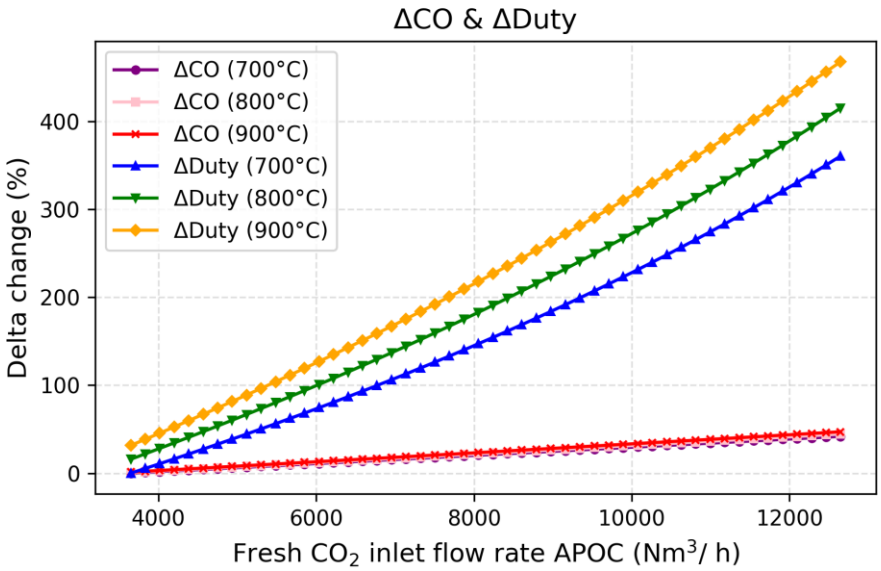

Figure 4.10. Relative increase in CO product flow and E231 heat duty as functions of fresh CO_2 addition at different CO_2 preheat temperatures. Delta changes are calculated relative to the reference case with 3600 Nm^3/h fresh CO_2 addition and 700°C CO_2 preheat temperature (first data point in the blue and purple curves).

The impact of operating conditions on reactor sizing is shown in Table 4.5, which presents the required APOC catalyst volume for different external CO_2 inlet flows and CO_2 preheat temperatures. The catalyst volume calculation is shown in Appendix A.6. The catalyst volume increases clearly with increasing fresh CO_2 addition, from about 6.5-6.6 m^3 at 3600 Nm^3/h fresh CO_2 to about 10.7-11.2 m^3 at 12,600 Nm^3/h fresh CO_2. In contrast, the effect of the preheat temperature is small, with only a slight decrease in required catalyst volume as the preheat temperature increases from 700 to 900°C. This shows that the required catalyst volume is affected mainly by the CO_2 flow rate rather than the preheat temperature.

Table 4.5. Required catalyst volume (m^3) at different fresh CO_2 inlet flows and CO_2 preheat temperatures.

Fresh CO_2 inlet flow \ CO_2 preheat temperature	Catalyst volume (m^3)		
	700°C	800°C	900°C
3600 Nm^3/h	6.56	6.54	6.52
7600 Nm^3/h	8.24	8.17	8.11
12,600 Nm^3/h	11.16	10.89	10.66

Considering catalyst volume and delta changes together, these results highlight a trade-off. Increasing the fresh CO_2 addition increases the CO product flow but also increases both the heat duty in E231 and the required catalyst volume. Increasing the preheat temperature results in a larger E231 duty requirement, while having only a minor effect on the relative CO increase and catalyst volume. From a process design perspective, fresh CO_2 addition is therefore the

main driver for increased production and reactor size, whereas preheat temperature mainly influences the energy demand and product distribution as previously discussed. An appropriate operating point should therefore balance the benefit of higher CO production against the penalty of increased heating duty and catalyst requirement.

Figure 4.11 illustrates the CO_2 and total C_1 recycling ratio as functions of the CO_2 flow rate to the APOC for external CO_2 additions of 1000 to 10,000 Nm^3/h at preheat temperatures of 700, 800 and 900°C. The CO_2 and total C_1 recycling ratio are calculated according to equation (39) and (40), respectively. The CO_2 recycling ratio is above 1 across the entire range, showing that the APOC operation is dominated by internal CO_2 recycling. It decreases initially with increasing external CO_2 addition, reaches a minimum at the CO_2 flow corresponding to maximum CO_2 conversion, and then increases slightly. This indicates the most efficient loop operation with respect to CO_2 recycling at the point of maximum conversion. The total C_1 recycling ratio increases approximately linearly with CO_2 inlet flow, from about 0.20 to 0.50, with only minor temperature effects. While higher recycling can improve CO yield, it also increases internal circulation, heat duty, compressor work and equipment size.

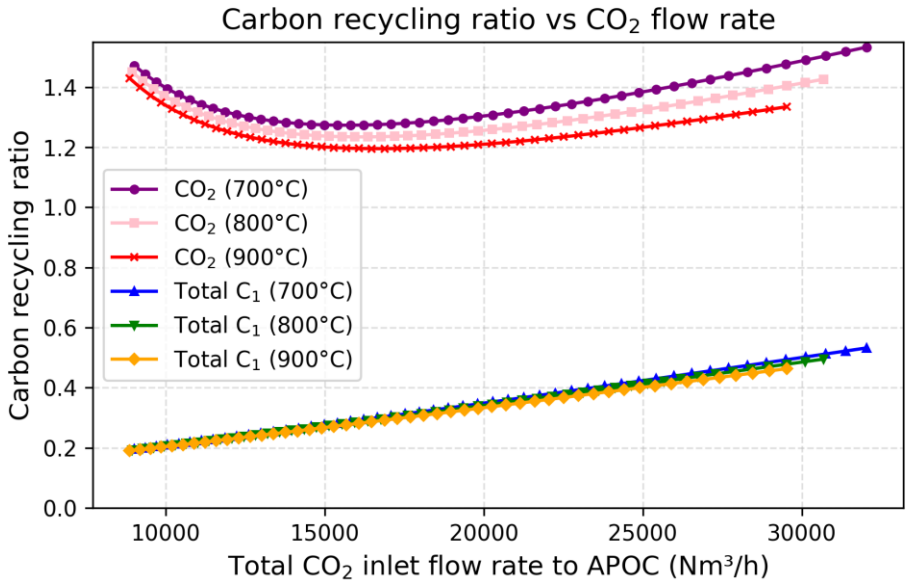

Figure 4.11. The total CO_2 inlet flow rate to the APOC versus the total C_1 recycling ratio and CO_2 recycling ratio at preheated temperatures of 700, 800 and 900°C.

4.3. Second analysis of the ReShift™ process

In this section, the ReShift™ technology was examined further by varying the CO_2 recycle split to assess the impact of CO_2 addition to the tubular reformer. The default values used are listed in Table 4.6. The total CO_2 inlet flow rate to the APOC reactor was fixed to 16357.6 Nm^3/h, which corresponds to an external CO_2 addition of 4700 Nm^3/h and CO_2 preheat

temperature of 800°C with complete CO_2 recycling to the APOC. This flow rate was chosen based on the maximum CO_2 conversion observed at these conditions as previously discussed in Section 4.2. The CO_2 preheat temperature of 800°C was selected based on previous results showing that higher temperatures are beneficial in terms of methanation suppression and increased temperature drop across the APOC reactor (Figure 4.8), but they also require higher heat duty.

Table 4.6. Default operating conditions for the ReShift™ process.

Variable	Value
Tubular reformer outlet temperature	930°C
S/C ratio	1.3
Tubular reformer outlet pressure	27.7 barg
APOC inlet pressure	27.1 barg
Total CO_2 inlet flow rate to the APOC	16,358 Nm^3/h
Preheating temperature of CO_2 in E231	800°C
Duty tubular reformer	59.45 MW

Figure 4.12 shows the changes in product and natural gas feed flow rates as the CO_2 inlet flow rate to the tubular reformer was varied. The CO_2 flow to the tubular reformer inlet was controlled by adjusting the split of the CO_2 recycle stream. At this S/C ratio, the split to the tubular reformer could not be increased above 0.6 without causing carbon formation, which corresponds to a total CO_2 inlet flow rate of 8270 Nm^3/h to the tubular reformer. The external CO_2 addition was adjusted to maintain the total CO_2 inlet flow rate to the APOC at the specified value mentioned previously. As expected, the natural gas feed flow rate decreases with increasing CO_2 inlet flow, since the tubular reformer duty was kept constant by adjusting the natural gas feed to compensate for the change in CO_2 inlet flow.

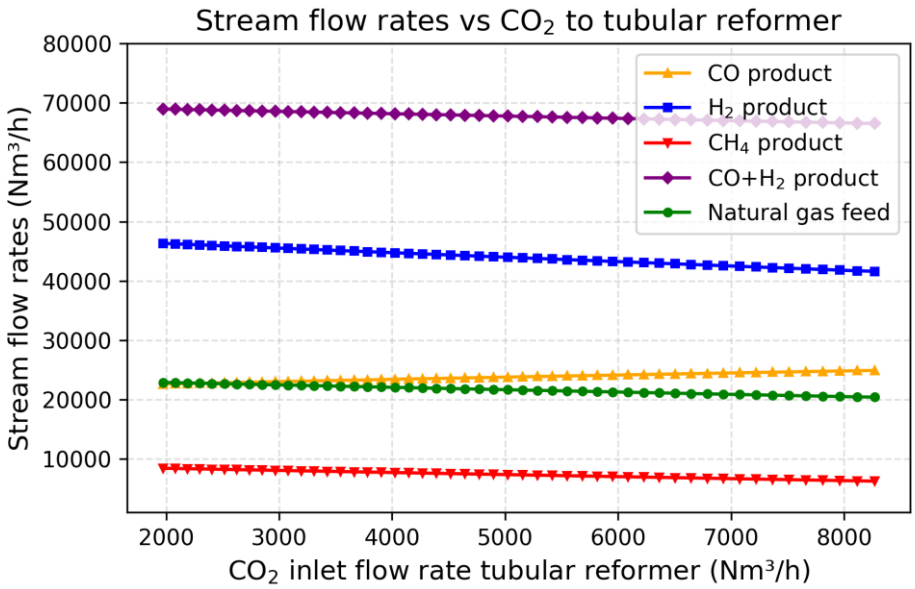

Figure 4.12. Product flow rates of CO, H_2, CH_4 and total syngas (H_2+CO), together with the natural gas feed, as functions of CO_2 inlet flow rate to the tubular reformer. The S/C ratio is 1.3, and the tubular reformer is operated at fixed duty.

The CO product flow increases slightly, from 22,627 to 24,922 Nm^3/h, as the total CO_2 inlet flow rate increases from 1972 to 8270 Nm^3/h. In contrast, the H_2 product flow decreases from 46,327 to 41,612 Nm^3/h over the same range of CO_2 inlet flow rates. These results indicate an increased contribution from the DMR reaction (4) which produces equimolar amounts of H_2 and CO, and a reduced contribution from the SMR reaction (1), which produces more H_2 than CO. However, the combined H_2 and CO product flow is also seen to decrease with increasing CO_2 inlet flow, which is likely because of both a lower natural gas feed and a higher CO_2 inlet flow rate.

The slight decrease in CH_4 product flow at higher inlet CO_2 flows can also be explained by the lower natural gas feed flow, as mentioned earlier, and the higher CH_4 conversion shown in Figure 4.13 (left). The CH_4 conversion in the tubular reformer increased from 68.4% to 73.7%, as the CO_2 inlet flow rate increased from 1972 to 8270 Nm^3/h.

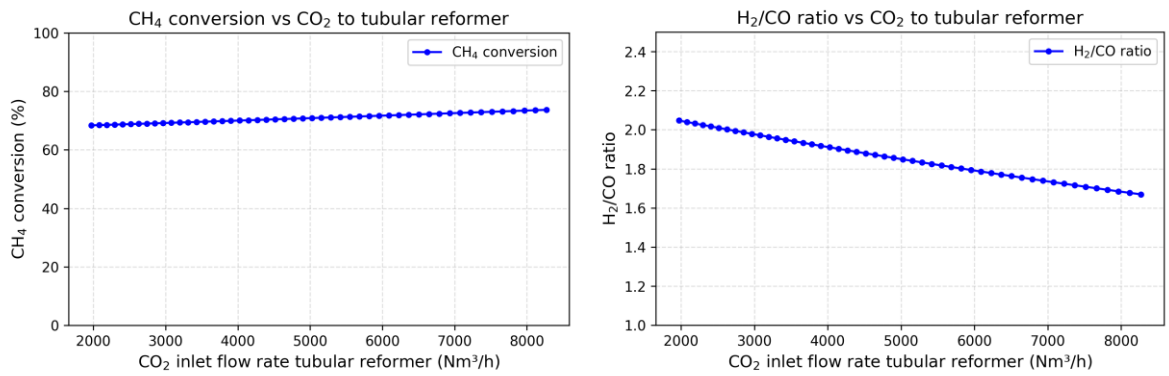

Figure 4.13. CH_4 conversion (to the left) in the tubular reformer and H_2/CO ratio (to the right) in the APOC outlet, as a function of CO_2 inlet flow rate to the tubular reformer. The S/C ratio is 1.3, and the tubular reformer is operated at fixed duty.

Figure 4.13 (right) confirms the previous results, which showed an increase in CO product flow and a decrease in H_2 product flow, when the H_2/CO ratio is evaluated at increasing CO_2 inlet flow rates to the tubular reformer. Over the range investigated, the H_2/CO ratio at the APOC outlet decreases from 2.05 to 1.67.

The minimum S/C ratio required to avoid carbon formation in the tubular reformer was evaluated for different CO_2 inlet flow rates. The results are shown in Figure 4.14 together with the S/C ratio including a 10% steam margin, representing a more realistic operating condition for safe operation. The corresponding data are presented in Appendix A.7 in Table A.6. As expected, increasing the CO_2 inlet flow to the tubular reformer requires a higher S/C ratio. With the 10% margin included, the required S/C ratio increases from 0.98 at a CO_2 inlet flow rate of 2041 Nm^3/h to 1.96 at a CO_2 inlet flow rate of 15,395 Nm^3/h.

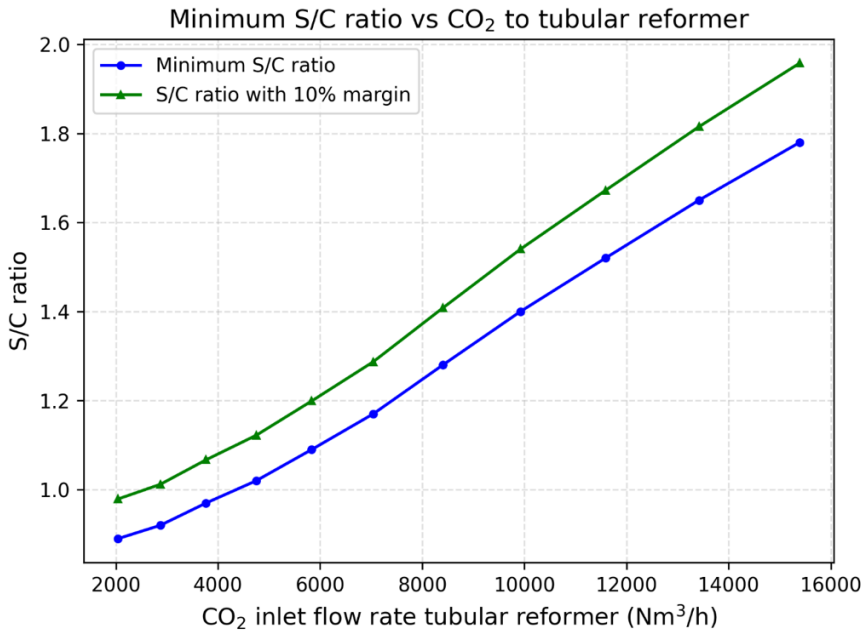

Figure 4.14. Minimum S/C ratio required to avoid carbon formation in the tubular reformer as a function of CO_2 inlet flow rate. The green curve shows the corresponding S/C ratio including a 10% margin. The tubular reformer is operated at fixed duty.

Using these S/C ratios with a 10% margin, the effect of CO_2 inlet flow on the feed and product streams was further evaluated. As shown in Figure 4.15, the natural gas feed flow decreases from 26,002 to 16,512 Nm^3/h. This is a consequence of the fixed reformer duty, since higher CO_2 and steam addition reduce the allowable natural gas throughput. In contrast, the total carbon feed to the reformer remains relatively constant, as part of the reduced CH_4 input is replaced by added CO_2.

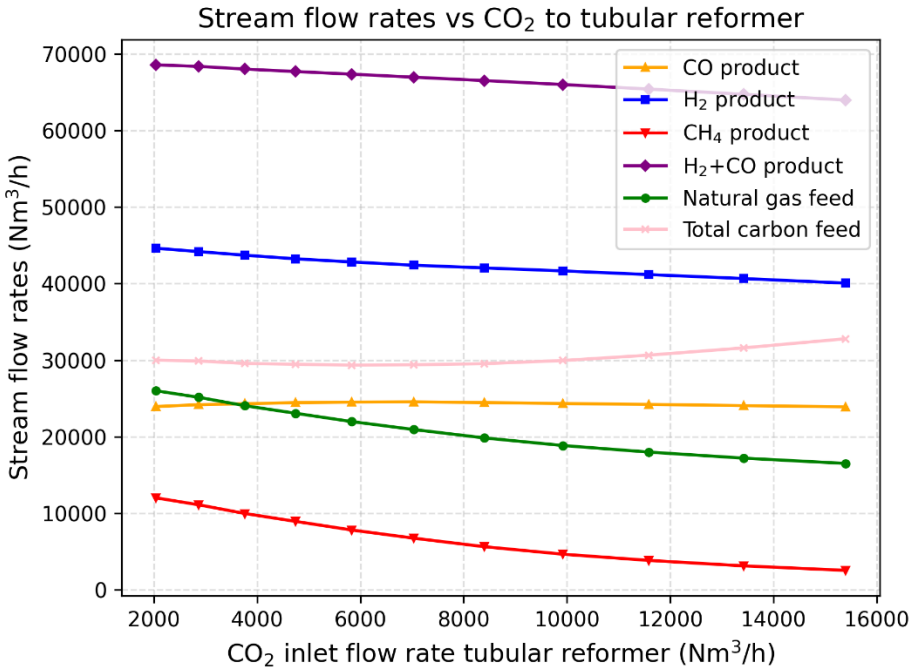

Figure 4.15. Product flow rates of CO, H_2, CH_4 and total syngas (H_2+CO), together with the natural gas feed and total carbon feed, as functions of CO_2 inlet flow rate to the tubular reformer. The tubular reformer is operated at fixed duty.

A strong decrease in CH_4 product flow is observed with increasing CO_2 inlet flow. This is consistent with the substantial increase in CH_4 conversion, which rises from 59.2% to 87.2% over the investigated range. The higher CH_4 conversion is mainly attributed to the increased steam content required to avoid carbon formation at higher CO_2 inlet flows. The higher S/C ratio promotes reforming of CH_4, which explains the strong decrease in CH_4 in the product stream.

The CO product flow increases slightly with increasing CO_2 inlet flow. However, the increase remains limited because the fixed reformer duty reduces the natural gas throughput, while the higher steam content shifts the SMR and WGS equilibria in a way that counteracts a larger increase in CO. A small maximum is observed in the CO product flow, reaching 24,554 Nm^3/h at a CO_2 inlet flow of 7038 Nm^3/h, after which the negative effects of reduced natural gas throughput and higher steam content outweigh the benefit of further CO_2 addition.

Figure 4.16 shows the normalized performance of the tubular reformer expressed as CO product/natural gas feed and H_2 product/natural gas feed, as functions of CO_2 inlet flow rate. Both ratios increase with increasing CO_2 inlet flow, indicating improved natural gas utilization. This means that although the absolute H_2 product flow decreases and the absolute CO product flow increases only slightly, the natural gas that is fed to the reformer is converted more efficiently into the desired products. The increase in CO/natural gas feed is particularly clear, showing that CO production per unit of natural gas is enhanced at higher CO_2 inlet flow. Similarly, the increase in H_2/natural gas feed shows that the decrease in H_2 production is

smaller than the decrease in natural gas feed. Overall, these results show that adding CO_2 to the tubular reformer improves the utilization of the natural gas feed, even though the total syngas production decreases under fixed duty operation.

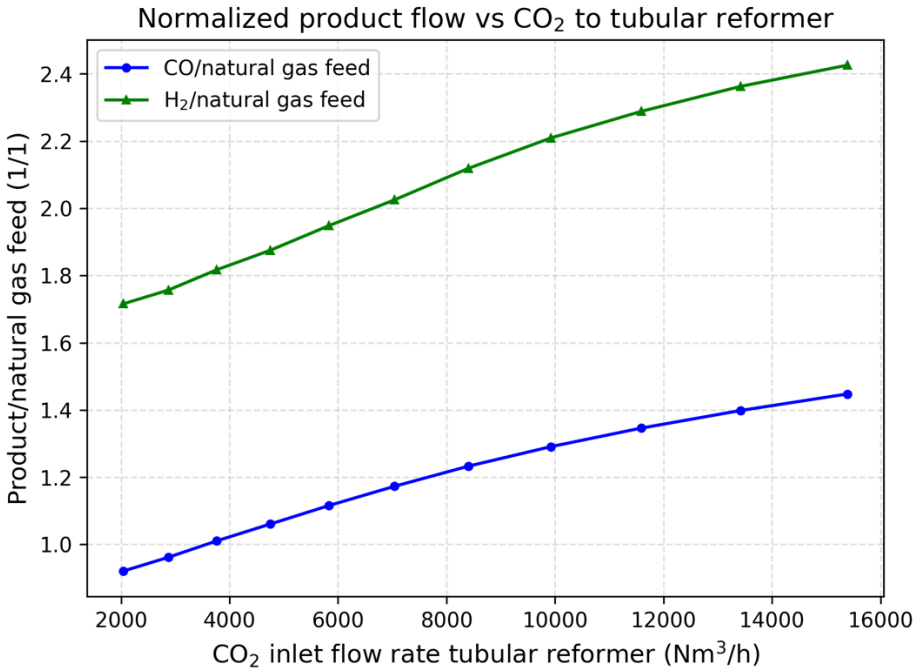

Figure 4.16. Normalized performance of the tubular reformer expressed as CO product/natural gas feed and H_2 product/natural gas feed, as functions of CO_2 inlet flow rate. The tubular reformer is operated at fixed duty.

4.4. Third analysis of the ReShift™ process

This section evaluates different cases derived from the *Reference Industrial Unit* and the revamp study using ReShift technology, targeting a fixed H_2/CO ratio of 1.0, which may be required by customers seeking CO-rich syngas. For some cases, a higher H_2/CO ratio was necessary to ensure feasibility or to match the operating conditions used in previous results.

The cases are listed in Table 4.7, which presents the S/C ratio, H_2/CO ratio, carbon risk in the tubular reformer and APOC, pressure drop in the tubular reformer, feasibility status, as well as the main strengths and weaknesses. Operating points in the tubular reformer for the different cases are presented in Figure A.3 (Appendix A.8). SMR cases 1, 2, and 3 were simulated according to the PFD shown in Figure 3.1. The results for SMR 1 indicate that a S/C ratio of 3.64 is required to achieve a H_2/CO ratio of 1.0 through the addition of external CO_2, while avoiding carbon formation with a 10% safety margin. However, this results in a high pressure drop in the tubular reformer, making the case infeasible. In SMR 2, the S/C ratio was set to 1.76, and the maximum allowable pressure drop was set to 5 bar to ensure feasibility. In this case, the maximum allowable pressure drop limits the amount of external CO_2 that can be added, as these operating conditions do not present a risk of carbon formation (more than 10% safety margin). The resulting H_2/CO in this case is 2.20. In SMR 3, a S/C ratio of 1.287 was

applied. This value was based on the results presented in Section 4.3, where the maximum amount of CO_2 that could be added to the tubular reformer at this S/C ratio without risking carbon formation was determined. Under these conditions, the resulting H_2/CO ratio is 2.59. Like SMR 2, the case is feasible and does not present a risk of carbon formation, however, the H_2/CO ratio remains relatively high. These results confirm that the SMR cases are not suitable when the objective is to achieve a low H_2/CO ratio.

Table 4.7. Selected SMR and ReShift cases with different S/C ratios and H_2/CO ratios, showing for each case the risk of carbon formation, overall feasibility and main strengths and weaknesses.

Case	S/C ratio	H_2/CO ratio	Carbon risk SMR/APOC	Pressure drop tubular reformer (bar)	Status	Strengths/weaknesses
SMR 1	3.641	1.0	No	20.28	Infeasible	Too high pressure drop
SMR 2	1.76	2.2	No	4.99	Feasible	High H_2/CO
SMR 3	1.287	2.59	No	3.74	Feasible	High H_2/CO
ReShift 1	1.3	1.0	No	3.33	Feasible	Highest CO production Highest duty /compressor work
ReShift 2	1.17	1.0	No	3.37	Feasible	Lowest S/C Highest CO/duty
ReShift 3	1.287	1.0	No	3.74	Feasible	Lower duty than Reshift 2 but higher S/C
ReShift 4	1.287	1.56	No	3.74	Feasible	Lowest duty among ReShift cases

ReShift cases 1, 2, 3, and 4 are based on the revamp study, and the corresponding PFD is shown in Figure 3.2. In all cases, the CO_2 preheat temperature was set to 800°C, while the CO_2 split to the APOC and tubular reformer was varied. As shown in Table 4.7, none of the cases present a risk of carbon formation. This is further illustrated in Figure 4.17, which shows the carbon formation limits for different S/C ratios, including the four ReShift cases.

ReShift 1 was evaluated with a CO_2 split of 0 to the tubular reformer and a S/C ratio of 1.3. For all cases targeting a H_2/CO ratio of 1, the external CO_2 addition was adjusted accordingly to achieve the desired syngas composition.

SMR 3, ReShift 3 and ReShift 4 were evaluated at the same S/C ratio and with the same CO_2 addition to the tubular reformer, corresponding to a 10% safety margin against carbon formation. These cases are therefore directly comparable. The main difference between ReShift 3 and 4 is the resulting H_2/CO ratio. ReShift 3 was adjusted to achieve a H_2/CO ratio of 1, whereas ReShift 4 was evaluated at the maximum CO_2 conversion observed in Section 4.2, resulting in a H_2/CO ratio of 1.56.

ReShift 2 was also intended to be based on the minimum S/C ratio results presented in Section 4.3. However, the initially investigated S/C ratio of 1.067 resulted in an operation too close to the carbon limit in the APOC reactor. To maintain an acceptable safety margin, steam addition was therefore increased by 10%, corresponding to a final S/C ratio of 1.17.

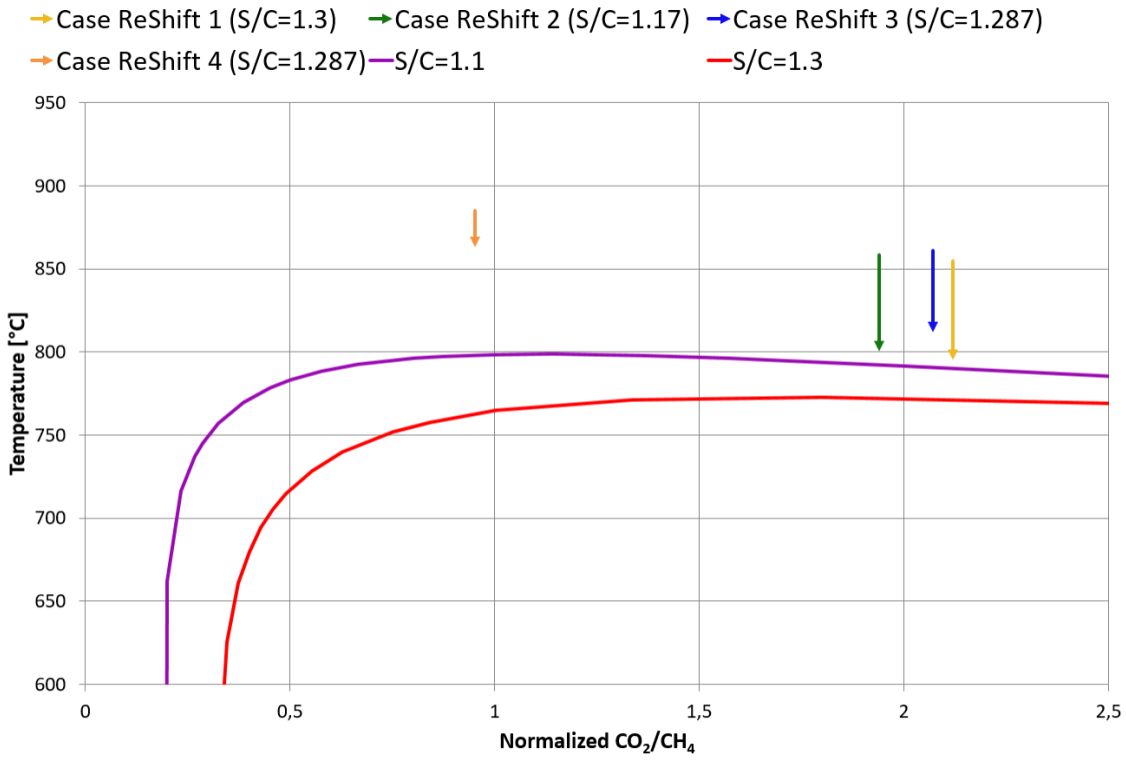

Figure 4.17. Carbon limit curves in the APOC reactor for two different S/C ratios of 1.1 and 1.3, and a pressure of 27.1 barg. The four selected ReShift cases are shown with arrows representing the temperature drop in the reactor, and the end of the arrow representing the point at the outlet of the APOC reactor. Operation above the carbon limit corresponds to carbon-free region.

Figure 4.18 presents the cases SMR 3, ReShift 3 and ReShift 4 to compare the effect of increasing CO_2 addition to the APOC reactor on the resulting syngas composition. As shown in the figure, the H_2/CO ratio decreases with increasing CO_2 addition, while the APOC outlet conditions approach the carbon limit as more CO_2 is introduced. The H_2/CO curves were calculated assuming equilibrium conditions, whereas the simulation cases were performed with a temperature approach to equilibrium of 15°C for the RWGS reaction. This explains why ReShift 3 seems to yield a H_2/CO ratio slightly below 1.0 according to the figure.

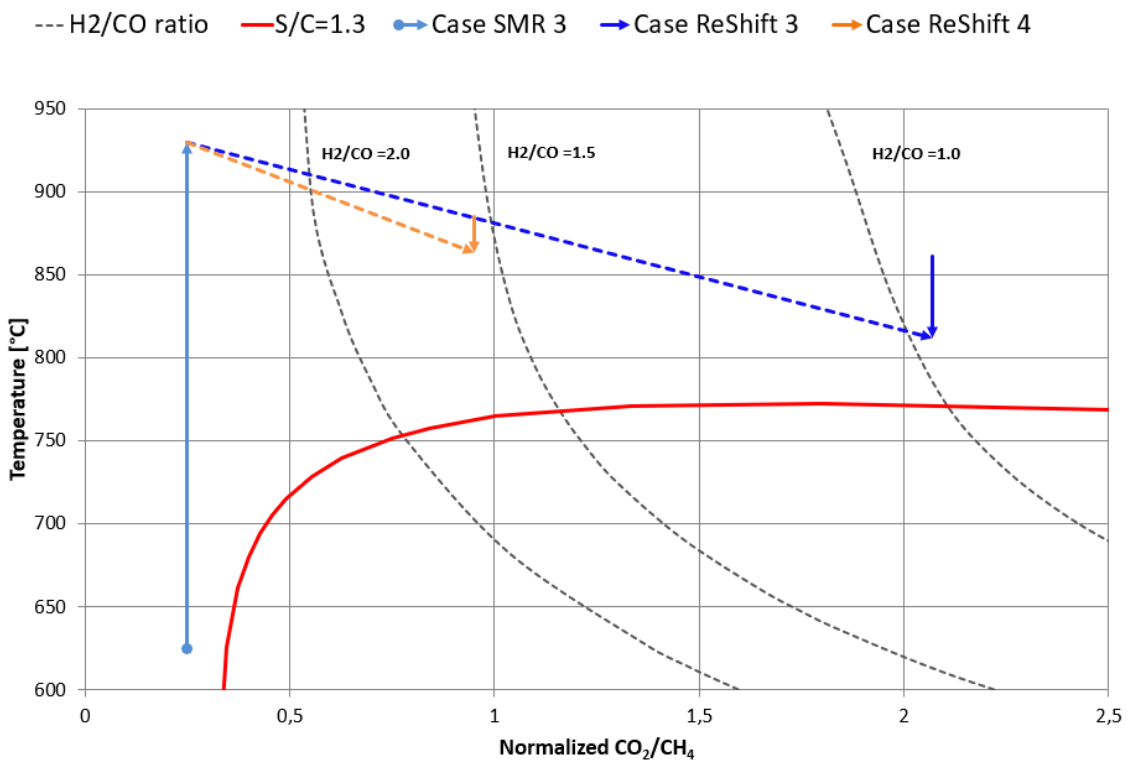

Figure 4.18. Carbon limit for S/C ratio 1.3 and a pressure of 27.1 barg. The dotted lines represent limits for different H_2/CO ratios, which are calculated at equilibrium. The light blue arrow represents the inlet and outlet conditions of the tubular reformer in case SMR 3. Both cases ReShift 3 and 4 illustrate how the APOC reactor lowers the H_2/CO ratio while circumventing the carbon limit, by adding different amounts of CO_2 to the APOC reactor.

Figure 4.19 shows the distribution of natural gas, CO_2 and product flows for the selected SMR and ReShift cases. For the SMR cases, increasing the CO_2 addition to the tubular reformer reduces the required natural gas feed when the reformer duty is kept constant. This is seen most clearly for SMR 1, which has the highest CO_2 flow to the tubular reformer and the lowest natural gas feed. However, as discussed previously, this case is not considered feasible due to the large pressure drop.

A particularly relevant comparison can be made between SMR 3, ReShift 3 and ReShift 4, since these cases have the same CO_2 addition to the tubular reformer and S/C ratio. Compared to SMR 3, both ReShift cases produce significantly more CO, showing that the APOC reactor shifts the product distribution towards more CO-rich syngas. ReShift 3 increases CO production by approximately 71.0% relative to SMR 3, while ReShift 4 increases it by approximately 34.7%. At the same time, the H_2 production decreases, resulting in a lower H_2/CO ratio.

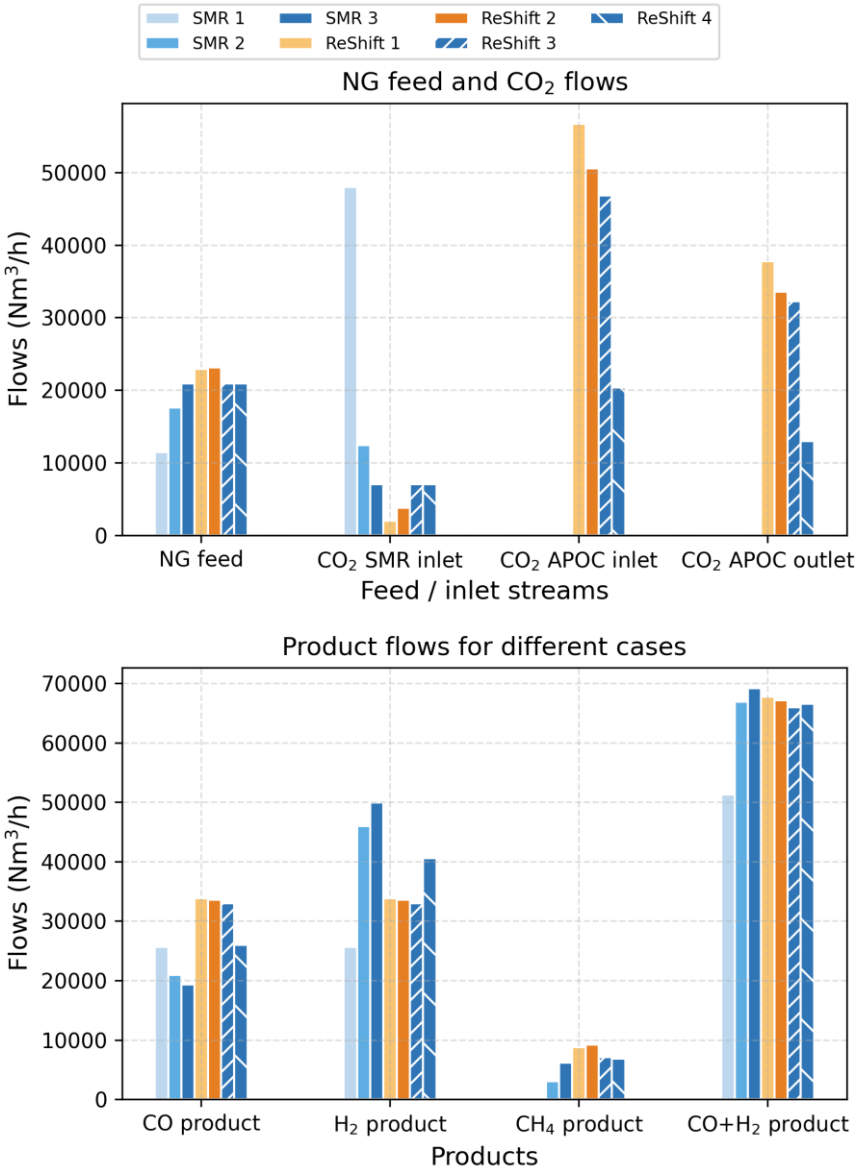

Figure 4.19. Component flows for seven different cases. Upper diagram shows natural gas feed flow (NG feed), CO_2 inlet flow to the tubular reformer (SMR) and CO_2 inlet flow to the APOC reactor. Lower diagram shows CO, H_2, CH_4 and $CO+H_2$ product flows for each case.

The ReShift cases are also associated with larger CO_2 flows through the process, particularly due to the recycling loop around the APOC reactor. For ReShift 3, the CO_2 recycling flow is more than twice as large as in ReShift 4. The larger recycling flow contributes to higher CO production, but it also increases the total process flow through compressors, heat exchangers, and reactors.

Overall, the flow comparison shows that ReShift enables significantly higher CO production than conventional SMR, but this comes at the expense of larger internal CO_2 circulation and a

more complex process. The most attractive operating conditions should therefore be selected based not only on CO production, but also on feasibility and the associated recycling burden.

Figure 4.20 shows the duty contributions for the selected cases, including the change in duty in E211 (relative to the base case), the duty in E231, the recycling compressor duties, and the total duty. Here, the total duty is taken as the sum of the burner duty in the tubular reformer (calculated from the heating value of the fuel), the duty in E231 and the recycling compressor work. The recycling compressors correspond to K231 in the SMR cases, and K221 and K222 in the ReShift cases, as shown in Figure 3.1 and 3.2, respectively. Furthermore, the burner duty is assumed to include all duties of the unit operations upstream of the tubular reformer, as they are included in the waste heat section.

It should be noted that the reformer duty corresponds to thermal energy supplied through fuel combustion, while compressor and E231 duties represent electrical energy consumption. Furthermore, heat exchanger E211 utilizes waste heat recovered from the flue gas. Although all energy contributions are expressed in MW, they differ in energy quality and exergy value, which should be acknowledged.

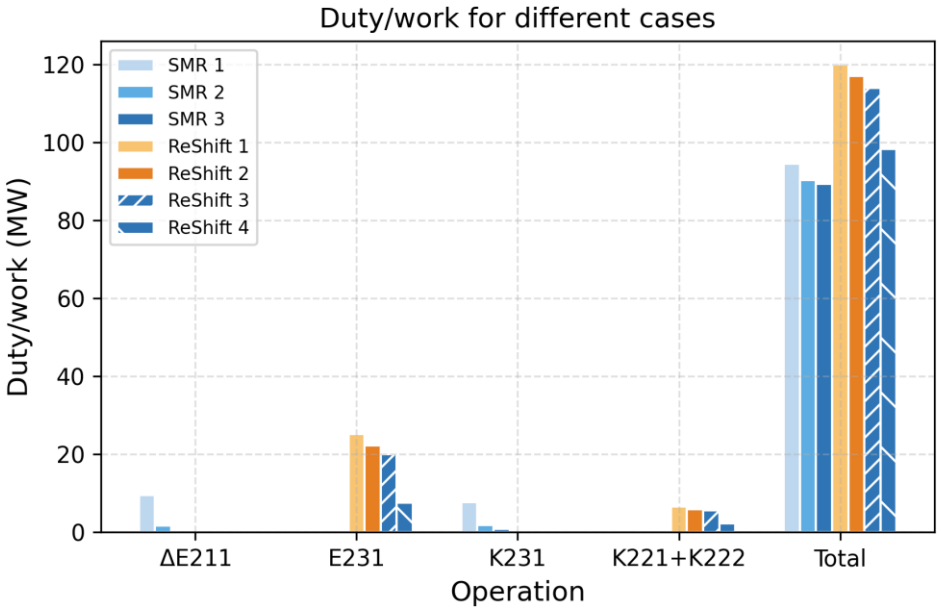

Figure 4.20. Delta duty of E211 (relative to base case), duty of E231 and compressor work in K231 (SMR) or K221+K222 (ReShift) for the selected cases. Total duty and work are also presented, which includes burner duty in the tubular reformer, E231 duty and recycle compressor work.

The burner duty remains almost constant for all cases, at approximately 87-89 MW. The differences in total duty are therefore mainly caused by the duty in E231 and the recycling compressor work. Among the SMR cases, SMR 3 has the lowest total duty, while SMR 1 has

the highest due to the significantly larger compressor duty associated with the high CO_2 flow to the tubular reformer.

All ReShift cases show higher total duty than the SMR cases. This increase is caused by the additional duties required for the large CO_2 recycling flow. ReShift 1 requires the highest total duty, while ReShift 4 requires the lowest among the ReShift cases. Comparing SMR 3 and ReShift 3, which have the same operating conditions in the tubular reformer, the total duty increases by approximately 27.7% with ReShift. For ReShift 4, the corresponding increase is only about 10.0%. This shows that the increase in CO production achieved with ReShift comes at the expense of higher total duty.

This trade-off can be further evaluated by comparing the total duty required per Nm^3/h of produced CO (Table 4.8). ReShift 4 exhibits the highest value, 0.00378 $MW/Nm^3/h$, indicating a higher energy demand relative to the amount of CO produced. In contrast, ReShift 2 and 3 have slightly lower values, 0.00347 $MW/Nm^3/h$ and 0.00346 $MW/Nm^3/h$, respectively, demonstrating a more energy-efficient CO production. Therefore, ReShift 2 and 3 appear to be the most favorable alternatives when the objective is to maximize CO production.

Table 4.8. The total duty (MW) required per Nm^3/h of produced CO for the four ReShift cases.

Case	Total duty/CO production ($MW/Nm^3/h$)
ReShift 1	0.00354
ReShift 2	0.00347
ReShift 3	0.00346
ReShift 4	0.00378

The results also suggest that the tubular reformer should be utilized as much as possible before relying on the APOC section for further conversion. More conversion of CO_2 in the tubular reformer reduces the CO_2 recycle requirement in the ReShift section, thereby lowering both the preheating duty in E231 and the compressor work in K221 and K222. Since these contributions dominate the increase in total duty for the ReShift cases, this strategy limits the additional energy demand associated with ReShift. Thus, this suggests that the most energy-efficient process configuration is obtained when the tubular reformer is used as much as possible within the constraints of carbon-free operation, and the APOC section is then applied to achieve the remaining adjustment in syngas composition and CO production.

4.5. CO_2 emission analysis

In this section, the CO_2 emissions for the different cases presented in Section 4.4 are evaluated. The analysis is intended as a rough estimate of the net CO_2 emissions for each case, based on CO_2-equivalent emission factors for fuel and electricity in Denmark and Sweden, shown in Table 4.9. The fuel emission factor corresponds to natural gas in Sweden and pipeline gas in Denmark, which consists of both natural gas and biomethane (Naturvårdsverket, 2025;

Sørensen et al., 2023). Fuel related emissions are calculated from the fuel flow to the burner in the tubular reformer, which is assumed to cover all duties upstream of the tubular reformer and thus also the associated upstream CO_2 emissions. Electricity related emissions are estimated from the duty requirement of heat exchanger E231 and the compressor work required for the CO_2 recycle stream (K221 and K222 for the ReShift cases, and K231 for the SMR cases).

Net CO_2 emissions are defined as the total CO_2 emissions minus the amount of CO_2 consumed in the tubular reformer and the APOC reactor. Positive values indicate net CO_2 emissions, while negative values indicate net CO_2 consumption. Annual emissions are calculated, assuming 8400 operating hours per year, corresponding to continuous plant operation with 30 days downtime every second year.

Table 4.9. CO_2-equivalent emission factors in Denmark and Sweden for fuel and electricity. Danish emission actors taken from Sørensen Nilsson et al. (2023), and Swedish emission factors are taken from Naturvårdsverket (2025) for fuel and European environment agency (2025) for electricity.

Emission factors	Fuel emission factor (kg CO_2-equivalent/kWh)	Electricity emission factor (kg CO_2-equivalent/kWh)
Denmark (2025)	0.1510	0.0801
Sweden (2024)	0.2055	0.0070

The estimated CO_2 emissions for the investigated cases, calculated using Danish emission factors, are presented in Figure 4.21, with the corresponding numerical values for both Danish and Swedish emission factors presented in Appendix A.9, Table A.7 and Table A.8. As shown in the figure, fuel emissions are the main contributor to the total emissions in all cases, while electricity emissions are smaller. The ReShift cases generally have higher total emissions than the SMR cases, mainly due to the increased electricity demand associated with the CO_2 recycle stream. However, they also consume substantially more CO_2 in the APOC reactor and tubular reformer, resulting in lower net CO_2 emissions overall.

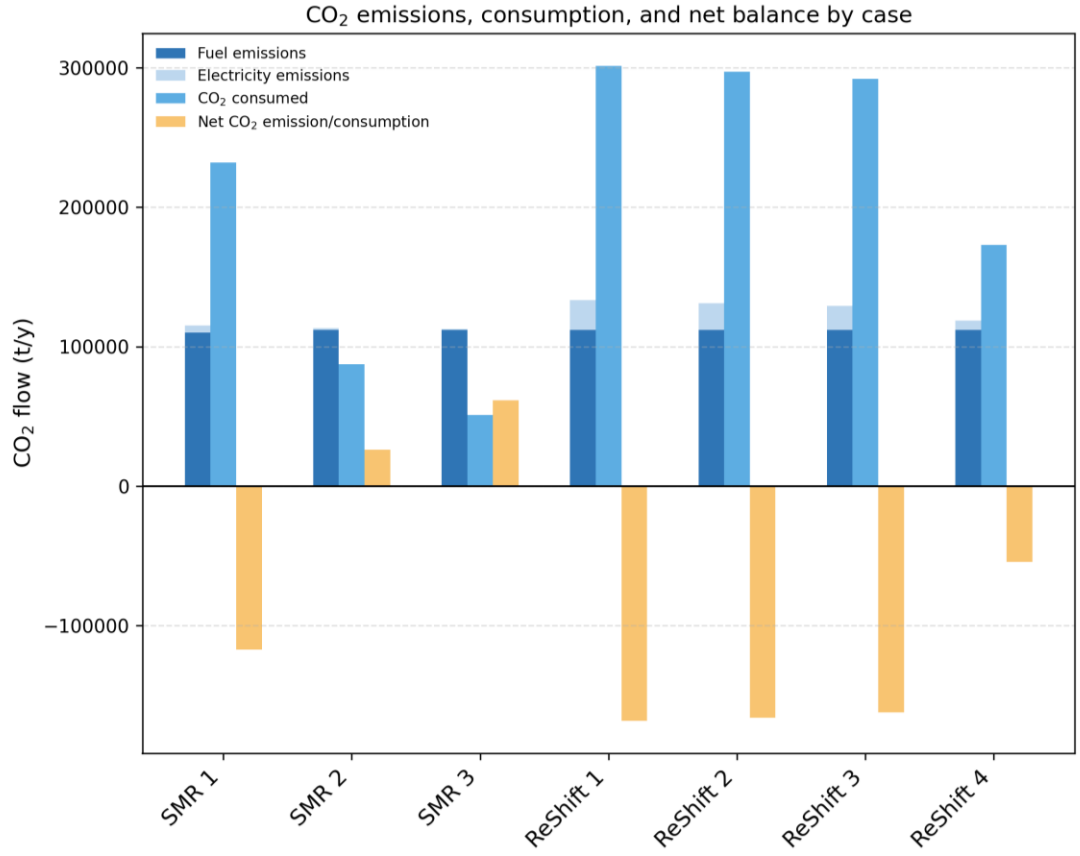

Figure 4.21. CO_2 emissions (t/year) calculated using Danish emission factors for fuel and electricity consumption. The poles illustrate the CO_2 emissions (from fuel and electricity), CO_2 consumption and net CO2 emission/consumption. Fuel emissions are calculated from the fuel flow to the burner and electricity emissions from the duty in E231 and work in the recycle compressors. Positive net values indicate net CO_2 emissions, while negative values indicate net CO_2 consumption.

Among the investigated cases, ReShift 1 gives the lowest net CO_2 emissions, corresponding to a net CO_2 consumption of 168,000 t/y with Danish emission factors and 147,000 t/y with Swedish emission factors. ReShift 2 and 3 show similar results, while ReShift 4 remains net CO_2 consuming to a smaller extent. For the SMR cases, only SMR 1 is net consuming due to the large CO_2 addition to the tubular reformer, whereas SMR 2 and SMR 3 are net CO_2 emitting.

Overall, the results show that the higher utility demand in the ReShift cases is more than offset by the increased CO_2 utilization. For the cases considered here, the amount of CO_2 consumed therefore has a greater impact on the net CO_2 balance than the increase in CO_2 emissions caused by the increased utility demand.

4.6. Economic analysis

The purpose of the economic analysis was to provide a preliminary estimate of the additional investment costs required for implementation of the ReShift™ technology compared to the reference SMR case. The analysis focused primarily on the revamp section and associated reactor components, as these represent the main additional process units introduced by the ReShift™ concept.

The economic evaluation included estimated costs for APOC reactor steel shell, refractory materials and installation, catalyst support materials, alumina balls, catalyst, as well as additional heat exchanger (E231) and compressors (K221 and K222). The costs of the heat exchangers used to cool the recycle stream (COOLER1 and COOLER2) were not included in this cost estimate due to limited available information and time constraints. The analysis was performed for ReShift 3 and ReShift 4, which were selected as the most relevant cases in comparison with the reference SMR process. These cases were evaluated at the same S/C ratio and CO_2 addition to the tubular reformer, but different CO_2 addition to the APOC reactor, and thus requiring different APOC reactor size.

Reactor sizing was calculated according to the simulated operating conditions and inlet flowrates for each case, and the cost estimations were based on these reactor dimensions.

The following assumptions were applied:

- APOC reactor dimensions were based on calculated catalyst bed diameters from GIPS simulations.
- Material costs for steel, refractory, catalyst support and alumina balls were estimated using a simple cost calculation from an internal Excel file (Appendix B.5).
- The costs for the electric heat exchanger and compressors were estimated using a cost calculation from an internal Excel file (Appendix B.5).
- The catalyst cost was estimated according to the calculation shown in Appendix A.6.
- Operating costs, including utilities, were not included in the present analysis.

A drawing of the APOC reactor, including its main components such as the steel shell, catalyst support, refractory and alumina balls can be found in Appendix A.10. The catalyst support is arranged in multiple layers at the bottom of the reactor, while the alumina balls are placed both below and above the catalyst bed to ensure proper flow distribution and support. The refractory is positioned along the inner reactor wall. With a reactor height of 3.0 m, the inner diameter of the catalyst bed was estimated to 2.6 m for ReShift 3 and 2.35 m for ReShift 4. The catalyst used in the APOC reactor had an estimated price of 15 EUR/L catalyst.

It should be noted that the represented cost estimations are intended for relative comparison between process configurations rather than for detailed economic evaluation. Consequently, the results should be interpreted as indicative, relative estimates.

Figure 4.22 shows a cost breakdown of the investment costs for ReShift 3 and 4. From this cost estimation, it can be concluded that the APOC reactor-related costs are expected to be significantly higher for ReShift 3 than for ReShift 4, due to the larger inlet flow requiring larger

equipment and more material. The additional costs for the heat exchanger and compressors are the largest contributions, with the total investment costs for the two cases being 20,885,000 EUR for ReShift 3 and 11,725,000 EUR for ReShift 4. These costs can be compared with the market value of the produced CO and H_2 to estimate the potential economic return from increased CO production and sales.

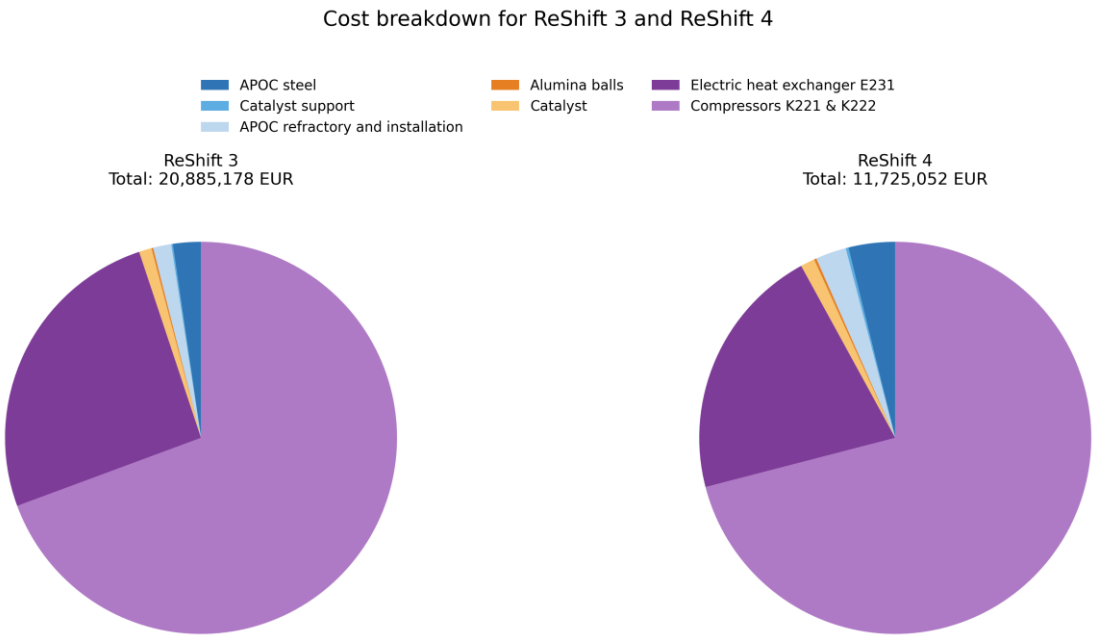

Figure 4.22. Cost estimation of the APOC reactor components, heat exchanger and compressors. The corresponding data can be found in Appendix A.11, Table A.9.

The estimated market value per Nm^3 is considerably higher for CO than for H_2, with H_2 in the range of 0.0986-0.2647 USD/Nm^3 and CO in the range of 0.4014-1.0166 USD/Nm^3 (IMARC Group, 2026). This suggests that, on a volumetric basis, increasing the CO fraction in the syngas could be economically attractive. However, the additional CO produced with ReShift™ is obtained at the expense of higher investment costs and increased duty demand. Therefore, the higher price of CO alone is not sufficient to conclude that the ReShift™ process is economically favorable. The overall benefit depends on whether the added value of the increased CO production and the modified syngas composition is large enough to offset the additional capital and operating costs. A complete economic analysis is therefore required to determine whether the ReShift™ concept is economically beneficial.

4.7. Simulation software discussion

To better understand the relevance of the simulation approach used in this work, it is useful to compare the GIPS simulations with simpler equilibrium-based calculations. This comparison helps show which of the observed results are mainly determined by thermodynamics and which require a more detailed reactor description.

For this study, equilibrium calculations would likely have been sufficient to capture the main trends, such as the effect of increasing CO_2 inlet flow on syngas composition and the S/C ratio. Equilibrium models are therefore useful in early-stage studies to identify general trends. However, such calculations would not be able to determine whether the predicted conversions and product compositions are achievable in the reformer under realistic operating conditions.

In this work, GIPS provides additional value because the reactor model includes kinetics and is based on an industrial catalyst. This gives a more realistic representation of the reforming process and therefore a better indication of which conversions and product compositions can be obtained under realistic operating conditions. In addition, the tubular reformer model predicts the risk of carbon formation along the reactor axis rather than only at the outlet. This is important since carbon formation may occur locally even if the outlet composition appears carbon safe. Overall, this means that while equilibrium calculations could likely have captured the general trends observed in this work, the GIPS simulation is more reliable for evaluating the feasibility of the process.

5. Conclusion

Based on the results presented in this study, ReShift^{TM} technology appears to be an effective revamp option when the objective is to increase CO production in the syngas, enhance CO_2 utilization and operate beyond the traditional carbon limits of conventional reforming. The results show that a H_2/CO ratio of 1 can be achieved at lower S/C ratios, which is not possible in industrial syngas manufacturing processes such as POX and ATR. However, this comes at the expense of higher total duty and increased investment cost due to the additional APOC reactor, heat exchangers and recycle compressors. Nevertheless, all investigated ReShift cases show significant net CO_2 consumption.

The sensitivity analysis further shows that external CO_2 addition has the largest influence on CO production, while CO_2 preheating mainly affects product distribution by increasing CO selectivity and yield. However, the increased duty requirement in E231 is disproportionally large compared to the increase in CO production, and larger preheat temperatures makes this difference even larger. The results additionally indicate that the extra duty and work associated with ReShift^{TM} can be reduced by maximizing the utilization of the tubular reformer, by adding CO_2 upstream of the reformer and thereby reducing the required load in the revamp section.

As illustrated by the decision diagram in Figure 5.1, no ReShift case is optimal with respect to all criteria. The preferred case depends on the priorities of the customer. Among the cases achieving a H_2/CO ratio of 1, ReShift 1 gives the highest CO production and CO_2 consumption, but also the highest duty. ReShift 2 has the lowest S/C ratio, while ReShift 3 has the lowest duty, and the lowest duty per CO production, indicating the most energy efficient CO production. ReShift 4 has the lowest duty among all ReShift cases but does not reach a H_2/CO ratio of 1.

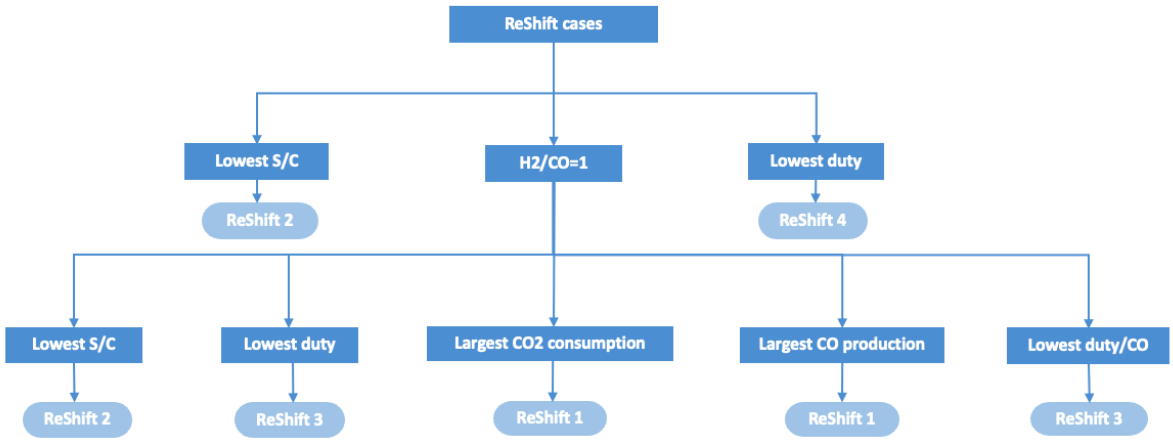

Figure 5.1. Decision diagram for the ReShift cases presented in Section 4.4, indicating the most suitable case depending on the prioritization of different criteria.

6. Future work

While the present study identifies and evaluates promising revamp options, several aspects remain open for further investigation. In particular, future work should focus on improving energy efficiency, economic feasibility, and overall process integration of the ReShift™ technology. Additional studies could also assess alternative process configurations and emerging technologies that may further enhance CO-rich syngas production performance.

Further improvement of the revamp case could include heat integration of the CO_2 stream (7014) with process gas from the APOC outlet. This could reduce the electricity demand required to heat the stream in E231 and thereby lower the total energy demand of the ReShift™ process. However, the additional costs for heat integration would likely represent a significant capital cost, and a more detailed techno-economic assessment would therefore be needed.

Another relevant area for further study is optimization of the tubular reformer by using a green field SMR process together with a unit based on Topsoe's eReact™ technology. This technology enables the production of syngas with H_2/CO ratios well suited for fuel synthesis by using renewable electric heating instead of natural gas combustion, together with green hydrogen and captured CO_2 (Topsoe, n.d.). In addition, eReact™ makes it possible to achieve reactor temperatures beyond those feasible in a conventional tubular reformer (Wismann et al., 2019). A greenfield SMR process based on renewable biomethane, derived from biowaste or other renewable sources, could also be considered. Such a configuration would be particularly relevant for reducing the overall carbon footprint of the process.

A further interesting study would be to compare the ReShift revamp case with an integrated CL process. This technology may simplify gas separation and enable operation at lower temperatures, which could offer both technical and economic advantages. It would therefore be relevant to investigate the downstream processing requirements after the APOC reactor in the ReShift™ technology. However, the current understanding of CL technologies for CO production remains limited, and further progress is needed to clarify the redox mechanisms, optimize reactor and process operation, and support scale-up of the technology.

7. References

1) Aasberg-Petersen, K., Christensen, T. S., Dybkjær, I., Sehested, J., Østberg, M., Coertzen, R. M., Keyser, M. J., & Steynberg, A. P. (2004). Synthesis gas production for FT synthesis. *Studies in Surface Science and Catalysis.* 152. pp. 258–405. https://doi.org/10.1016/S0167-2991(04)80461-0
2) Barin, I. (1989). *Thermochemical Data of Pure Substances.* VCH, Weinheim.
3) Bengaard, H.S., Nørskov, J.K., Sehested, J., Clausen, B.S., Nielsen, L.P., Molenbroek, A.M. & Rostrup-Nielsen, J.R. (2002). Steam reforming and graphite formation on Ni catalysts. *Journal of Catalysis*, 209(2), pp.365–384. https://doi.org/10.1006/jcat.2002.3579
4) Bown, R.M., Joyce, M., Zhang, Q., Reina T.R. & Duyar, M.S. (2021). Identifying commercial opportunities for the reverse water gas shift reaction. *Energy Technology.* https://doi.org/10.1002/ente.202100554
5) Chen, X., Chen, Y., Song, C., Ji, P., Wang, N., Wang, W., & Cui, L. (2020). Recent advances in supported metal catalysts and oxide catalysts for the reverse water–gas shift reaction. *Frontiers in Chemistry.* 8. https://doi.org/10.3389/fchem.2020.00709
6) Christensen, T.S. (1996). Adiabatic prereforming of hydrocarbons — an important step in syngas production. *Applied Catalysis A: General.* 138(2). pp.285-309. https://doi.org/10.1016/0926-860X(95)00302-9
7) Daza, Y. A., & Kuhn, J. N. (2016). CO_2 conversion by reverse water–gas shift catalysis: Comparison of catalysts, mechanisms and their consequences for CO_2 conversion to liquid fuels. *RSC Advances*. 6(55). pp.49675–49691. https://doi.org/10.1039/C6RA05414E
8) Dutta, N.N. & Patil, G.S. (1995). Developments in CO separation. *Gas Separation & Purification.* Vol.9. Elsevier. p.277-283. https://doi.org/10.1016/0950-4214(95)00011-Y
9) Dybkjær, I. (1995). Tubular reforming and autothermal reforming of natural gas – an overview of available processes. *Fuel Processing Technology.* 42(2-3). pp.85-107. https://doi.org/10.1016/0378-3820(94)00099-F
10) Ertl, G., Knözinger, H. & Weitkamp J. (1997). *Handbook of Heterogeneous Catalysis.* Vol.4. Wiley-VCH, Weinheim.
11) European Environment Agency. (2025). Greenhouse gas emission intensity of electricity generation in Europe. https://www.eea.europa.eu/en/analysis/indicators/greenhouse-gas-emission-intensity-of-1 (Accessed 18 May 2026).
12) Gangadharan, P., Kanchi, K.C. & Lou, H.H. (2012). Evaluation of the economic and environmental impact of combining dry reforming with steam reforming of methane. *Chemical Engineering Research and Design.* 90(11). pp.1956-1968. https://doi.org/10.1016/j.cherd.2012.04.008
13) García, I.D., Stankiewicz, A. & Nigar, H. (2021). Syngas production via microwave-assisted dry reforming of methane. Catalysis Today. 362. pp.72-80. https://doi.org/10.1016/j.cattod.2020.04.045

14) Ghoneim, S.A., El-Salamony, R.A. & El-Temtamy, S.A. (2016). Review on Innovative Catalytic Reforming of Natural Gas to Syngas. *World Journal of Engineering and Technology.* 4. pp. 116–139. https://doi.org/10.4236/wjet.2016.41011
15) Grossmann, K., Treiber, P. & Karl, J. (2016). Steam methane reforming at low S/C ratios for power-to-gas applications. *International Journal of Hydrogen Energy*. 41(40), pp. 17784–17792. https://doi.org/10.1016/j.ijhydene.2016.08.007
16) Holt, J., Herritsch, A., Watson M (2019). Modelling carbon formation using thermodynamic and kinetic methods in a steam methane reformer over nickel catalysts. Sydney, Australia: Chemeca 2019. 29/09/2019-02/10/2019.
17) Hulteberg, C., 2012. Sulphur-tolerant catalysts in small-scale hydrogen production: A review. *International Journal of Hydrogen Energy*, 37(5), pp.3978–3992. https://doi.org/10.1016/j.ijhydene.2011.12.001
18) IMARC Group (2026). Hydrogen Price Trend, Index and Forecast. https://www.imarcgroup.com/hydrogen-pricing-report. (Accessed 25 May 2026).
19) IMARC Group (2026). Carbon Monoxide Price Trend, Index and Forecast. https://www.imarcgroup.com/carbon-monoxide-price-trend. (Accessed 25 May 2026).
20) Jensen, C. & Duyar, M.S. (2021). Thermodynamic Analysis of Dry Reforming of Methane for Valorization of Landfill Gas and Natural Gas. *Energy Technology*. 9(7). https://doi.org/10.1002/ente.202100106
21) Johnson Matthey's (n.d.). *HyCOgen™ technology*. Johnson Matthey's. HyCOgen™ technology | Johnson Matthey (Accessed 2 Mars 2026)
22) Kang, K., Sampei, H. & Sekine, Y. (2025). CO2 conversion to CO by reverse water gas shift and dry reforming using chemical looping. *Sustainable Energy & Fuels.* 3. pp.1598-1628. https://doi.org/10.1039/d4su00395k
23) Kim, T., Song, Y., Kang, J., Kim, S.K. and Kim, S. (2022). A review of recent advances in hydrogen purification for selective removal of oxygen: Deoxo catalysts and reactor systems. *International Journal of Hydrogen Energy*, 47(59), pp.24817–24834. https://doi.org/10.1016/j.ijhydene.2022.05.221
24) Lei, K., Liu, L., Wang, H., Li, K., Liao, D., Sun, Z. & Sun, Z. (2025). Fluidization-enhanced chemical looping reverse water-gas shift enables a cross-order-of-magnitude increase in CO production. Chemical Engineering Journal. 525. p.169742. https://doi.org/10.1016/j.cej.2025.169742
25) Li, H., Liao, Z., Sun, J., Jiang, B., Wang, J. & Yang, Y. (2019). Modelling and simulation of two-bed PSA process for separating H2 from methane steam reforming. Chinese Journal of Chemical Engineering. Vol. 27, Issue 8. pp.1870-1878. https://doi.org/10.1016/j.cjche.2018.11.022
26) Lloyd, L. (2011). Handbook of Industrial Catalysts. *Springer.* doi: 10.1007/978-0-387-49962-8
27) Mortensen, P.M. & Dybkjær, I. (2015). Industrial scale experience on steam reforming of CO2- rich gas. *Applied Catalysis A: General*. 495. pp141–151. https://doi.org/10.1016/j.apcata.2015.02.022

28) Mortensen, P.M. & Rautenbach, M. (2020). Circumventing carbon formation in CO_2 reforming of methane by an adiabatic post conversion reactor. *Catalysis Today,* 369, pp.12–18. https://doi.org/10.1016/j.cattod.2020.07.024
29) Mortensen, P.M., Rautenbach, M. & Stensengdt, M. (2023). Lower your carbon footprint while boosting your CO output by using Topsoe's unique ReShift™ technology. *White paper, Haldor Topsoe A/S.* https://engage.topsoe.com/y1680101230_lp?ctid=y1680101230 (Accessed 20 January 2026).
30) Naturvårdsverket. (2025, December 12). Beräkna klimatpåverkan: Beräkna direkta utsläpp från förbränning. Beräkna direkta utsläpp från förbränning. (Accessed 18 May 2026).
31) Oh, T. & Lee, S. (2024). Optimization of steam-methane reforming process using PSA off gas. Internation Journal of Hydrogen Energy. Vol. 95. Elsevier, pp.902-915. https://doi.org/10.1016/j.ijhydene.2024.11.149
32) Ross, J.R.H. (2012). Heterogeneous Catalysis. *Fundamentals and Applications*. pp.171–217. https://doi.org/10.1016/B978-0-444-53363-0.10008-8
33) Rostrup-Nielsen, J. & J. Christiansen, L. (2011). *Concepts in Syngas Manufacture.* 10th Edition. Imperial College Press.
34) Rostrup-Nielsen, Sehested J. & K. Nørskov J. (2002). *Hydrogen and synthesis gas by steam- and CO_2 reforming.* Advances in Catalysis. Vol. 47. Elsevier, pp.65-139.
35) Rostrup-Nielsen, J.R. (1982). Criteria for carbon formation (steam reforming and methanation). In: Figueiredo, J.L. (ed) Progress in Catalyst Deactivation. Dordrecht: Martinus Nijhoff Publishers, pp. 127-149. https://doi.org/10.1007/978-94-009-7597-2_9
36) Rostrup-Nielsen, J.R. (1984). Sulfur-Passivated Nickel Catalysts for Carbon-Free Steam Reforming of Methane. *Journal of Catalysis.* 85(1). pp.31-43. https://doi.org/10.1016/0021-9517(84)90107-6
37) Rostrup-Nielsen, J.R. (1982). *Sulfur Poisoning.* In: Figueiredo, J.L. (ed.) Progress in Catalyst Deactivation. NATO Advanced Study Institutes Series, vol. 54. *Springer*, Dordrecht, pp.209-227. https://doi.org/10.1007/978-94-009-7597-2_11
38) Salahi, F., Zarei-Jelyani, Rahimpour H.R. & Rahimpour M.R. (2023). Dry reforming for syngas production. Advances in Synthesis Gas: Methods, Technologies and Applications. Vol.1: Syngas Production and Preparation. Elsevier, pp.97-118. https://doi.org/10.1016/B978-0-323-91871-8.00018-0
39) Samipour, S. Manshadi M.D. & Setoodeh P. (2020). CO_2 removal from biogas and syngas. Advances in Carbon Capture: Methods, Technologies and Applications. Elsevier. https://doi.org/10.1016/B978-0-12-819657-1.00020-7
40) Santos, M.F., Bresciani, A.E., Ferreira, N.L., Bassani, G.S. & Alves, R.M.B. (2023). Carbon dioxide conversion via reverse water-gas shift reaction: Reactor design. *Journal of Environmental Management*. 345, pp.118822. https://doi.org/10.1016/j.jenvman.2023.118822
41) Sehested, J., 2006. Four challenges for nickel steam-reforming catalysts. *Catalysis Today.* 111(1–2), pp.103–110. https://doi.org/10.1016/j.cattod.2005.10.002

42) Sharifnattaj, A., Ghaziasgar, S., Bahadori, Y. and Saidi, M. (2025). Recent progress in catalysts development of dry reforming of methane process: Review of active phases and supports of catalyst, *Molecular Catalysis*, 582, 115060. https://doi.org/10.1016/j.mcat.2025.115060
43) Shell (2023). *Shell and MAN Energy Solutions Strengthen Relationship with Pilot Plant for Development of RWGS Technology*. Shell Catalysts & Technologies. Shell and MAN Energy Solutions Strengthen Relationship with Pilot Plant for Development of RWGS Technology | Shell Global [Accessed 2026-03-02]
44) Singh, D., Sirini, P. and Lombardi, L. (2025). Review of reforming processes for the production of green hydrogen from landfill gas. *Energies*, 18(1), pp.15. https://doi.org/10.3390/en18010015
45) Sircar, S. (2002). Pressure Swing Adsorption. *Industrial & Engineering Chemistry Research*, 41, 6, pp. 1389–1392. https://doi.org/10.1021/ie0109758
46) Song, C., Liu, Q., Ji, N., Kansha, Y. and Tsutsumi, A. (2015). Optimization of steam methane reforming coupled with pressure swing adsorption hydrogen production process by heat integration. *Applied Energy*, 154, pp. 392–401. https://doi.org/10.1016/j.apenergy.2015.05.038
47) Song, X. & Guo, Z. (2006). Technologies for direct production of flexible H_2/CO synthesis gas. Energy Conversion and Management. Vol. 47. Elsevier, pp.560-569. https://doi.org/10.1016/j.enconman.2005.05.012
48) Speight, J.G. (2014). *Gasification of Unconventional Feedstocks.* Gulf Professional Publishing, pp.118-134. https://doi.org/10.1016/C2013-0-14152-9
49) Su, X., Yang, X., Zhao, B., & Huang, Y. (2017). Designing of highly selective and high-temperature endurable RWGS heterogeneous catalysts: recent advances and the future directions. *Journal of Energy Chemistry*, 26(5), pp.854–867. https://doi.org/10.1016/j.jechem.2017.07.006
50) Sørensen Nilsson, M., Høibye, L. & Enersen Maagaard, S. (2023). Emissionsfaktorer for el, fjernvarme og ledningsgas 2025-2075 (Version 1, Project No. 1020565). Emissionsfaktorer for el, fjernvarme og ledningsgas for 2025-2075 | Social- og Boligstyrelsen (Accessed 18 May 2026).
51) Topsoe (n.d.) eREACT™ Fuels: New technology essential for electrofuels production. https://www.topsoe.com/products/equipment/ereact-fuels-new-technology-essential-for-electrofuels-production (Accessed 19 May 2026).
52) Wismann S.T., Engbæk, J.S., Vendelbo, S.B., Bendixen, F.B., Eriksen, W.L., Aasberg-Petersen, K., Frandsen, C., Chorkendorff, I. & Mortensen, P.M. (2019). Electrified methane reforming: A compact approach to greener industrial hydrogen production. Science, 364(6442), pp.756-759. https://doi.org/10.1126/science.aaw8775
53) Zhang, C., Xiao, Z., Guo, X., Tan, X., Gu, J., Li, J., Li, G., Zou, J. & Wang, D. (2025). Investigating the role of advanced catalysts and technologies in enhancing CO_2 conversion via reverse water-gas shift reaction. *Chemical Engineering Journal*, 519, 165414. https://doi.org/10.1016/j.cej.2025.165414

Appendix A

A.1. Chemical equilibrium constants

Equilibrium function for the carbon forming reactions:

$$\ln\left(K_{eq,j}\right) = C_{1,j}\ln(T) + \frac{C_{2,j}}{T} + C_{3,j} + C_{4,j}T + C_{5,j}T^2 + C_{6,j}T^3 \qquad (A.1)$$

Table A.1. Coefficients in equilibrium constant function for the carbon forming reactions taken from Rostrup-Nielsen et al. (2011).

	CH4 = C+2H2	2CO = C+CO2	CO+H2 = C+ H2O
C_1	$5.291666*10^{0}$	$-3.635623*10^{0}$	$-3.319458*10^{0}$
C_2	$-7.610846*10^{3}$	$2.005364*10^{4}$	$1.503716*10^{4}$
C_3	$-2.449759*10^{1}$	$3.805679*10^{-1}$	$4.471772*10^{0}$
C_4	$-2.023153*10^{-3}$	$5.096533*10^{-3}$	$2.956910*10^{0-3}$
C_5	$-1.593520*10^{-7}$	$-1.161530*10^{-6}$	$-5.570931*10^{-7}$
C_6	$7.797205*10^{-11}$	$1.3366629*10^{-10}$	$5.783769*10^{-11}$

A.2. Tøttrup diagram with operating points in SMR analysis

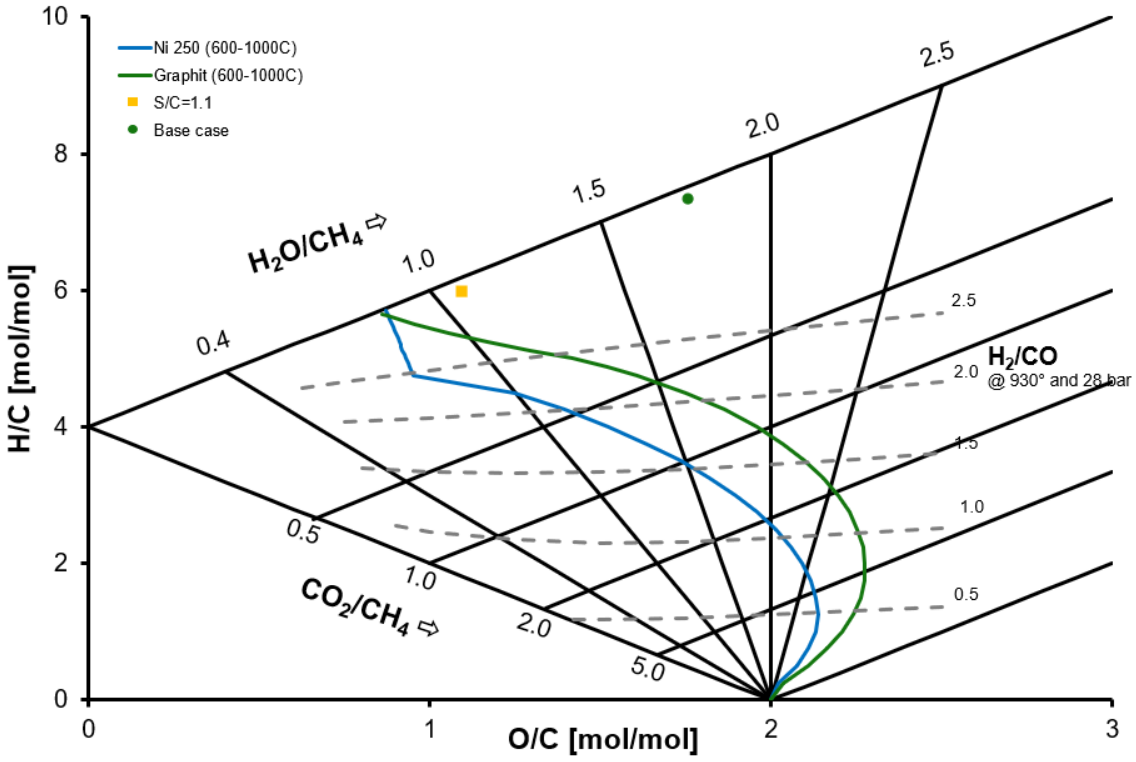

Figure A.1. Tøttrup diagram for the tubular reformer at a pressure of 28 barg and an outlet temperature of 930°C. Operation to the left of the carbon limit curves indicates a thermodynamic potential for carbon formation in the equilibrated gas. The dotted lines indicate the operating points corresponding to the respective H_2/CO ratios. Operating points are shown for a S/C ratio of 1.1 and for the base case with a S/C ratio of 1.76.

A.3. Data for carbon flow diagram

Table A.2. Flow rate of each carbon component in the streams shown in the carbon flow diagram in Figure 4.4.

Carbon component	2070 flow rate (Nm^3/h)	2075 flow rate (Nm^3/h)	2086 flow rate (Nm^3/h)	2090 flow rate (Nm^3/h)	3032 flow rate (Nm^3/h)	7001 flow rate (Nm^3/h)	5000 flow rate (Nm^3/h)
CO_2	1972	2646	17,095	9476	0	5671.8	5000
CO	49.5	16,059	16,052	22,926	22,931	0.961	0
CH_4	24,387	7701	7708	8458	8459	0	0

A.4. H_2/CO ratios at different CO_2 preheat temperatures

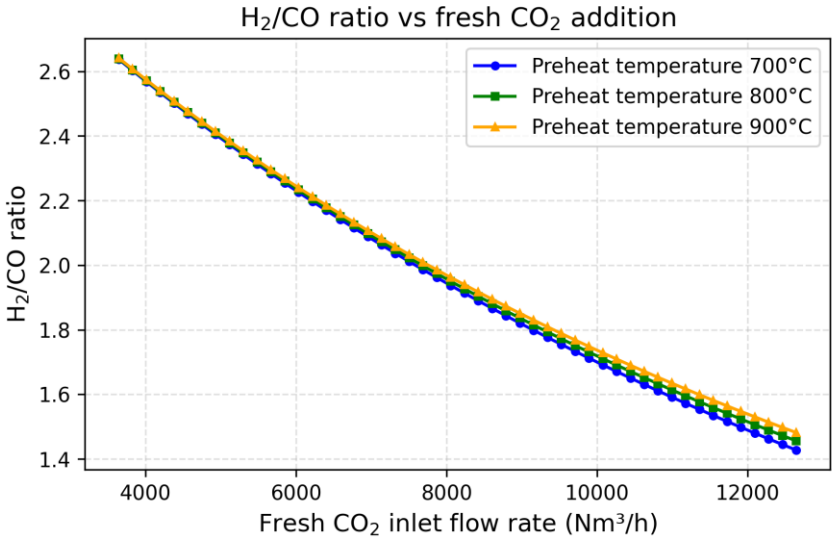

Figure A.2. H_2/CO ratios vs fresh CO_2 inlet flow rate, at three different preheat temperatures (700, 800 and 900°C).

A.5. Step change calculations

Table A.3 Step change in external CO_2 addition from 1000 Nm^3/h to 10,000 Nm^3/h at 700°C.

Variable	Before	After	Absolute change	Relative change
External CO_2 flow (Nm^3/h)	1000	10,000	9000	900%
Fresh CO_2 flow (Nm^3/h)	3647	12,647	9000	246.8%
CO production flow (Nm^3/h)	19,118	27,114	7996	41.8%
Heat duty 231 (MW)	1.42	7.66	6.24	439.4%

Table A.4. Step change in preheat temperature from 700°C to 900°C for external CO_2 addition of 5000 Nm^3/h corresponding to a fresh CO_2 flow of 7646.9 Nm^3/h.

Variable	Before	After	Absolute change	Relative change
CO_2 preheat temperature (°C)	700	900	200	28.5%
CO production flow (Nm^3/h)	22,659	23,195	536	2.4%
Heat duty E231 (MW)	3.85	5.68	1.83	47.5%

Table A.5. Step change in preheat temperature from 700°C to 900°C for external CO_2 addition of 10,000 Nm^3/h corresponding to a fresh CO_2 flow of 12,646.9 Nm^3/h.

Variable	Before	After	Absolute change	Relative change
CO_2 preheat temperature (°C)	700	900	200	28.5%
CO production flow (Nm^3/h)	27,114	28,116	1002	3.7%
Heat duty E231 (MW)	7.66	10.90	3.24	42.3%

A.6. Catalyst volume and catalyst price calculation

The catalyst volume is calculated by dividing the C_1 inlet flow to the APOC reactor by the C_1 space velocity, estimated at 5000 Nm^3/h C_1/ m^3 catalyst/h.

A rough estimate of the catalyst price is 20 EUR/kg, and the loaded density is approximately 0.75 kg/L, corresponding to a catalyst cost of 15 EUR/L catalyst.

A.7. Minimum S/C ratio

Table A.6. Minimum S/C ratio required to avoid carbon formation in the tubular reformer, the corresponding S/C ratio with a 10% margin, as well as the inlet CO_2 and natural gas feed flow rate to the tubular reformer. The tubular reformer is operated at fixed duty.

Minimum S/C	S/C with 10% margin	CO_2 inlet flow rate to the tubular reformer (Nm^3/h)	Natural gas feed flow rate (Nm^3/h)
0.89	0.979	2041	26,002
0.92	1.012	2871	25,146
0.97	1.067	3766	24,048
1.02	1.122	4747	23,058
1.09	1.199	5833	21,977
1.17	1.287	7038	20,935
1.28	1.408	8403	19,842
1.4	1.540	9923	18,853
1.52	1.672	11,588	17,992
1.65	1.815	13,419	17,207
1.78	1.958	15,395	16,512

A.8. Tøttrup diagram with operating points in third ReShift analysis

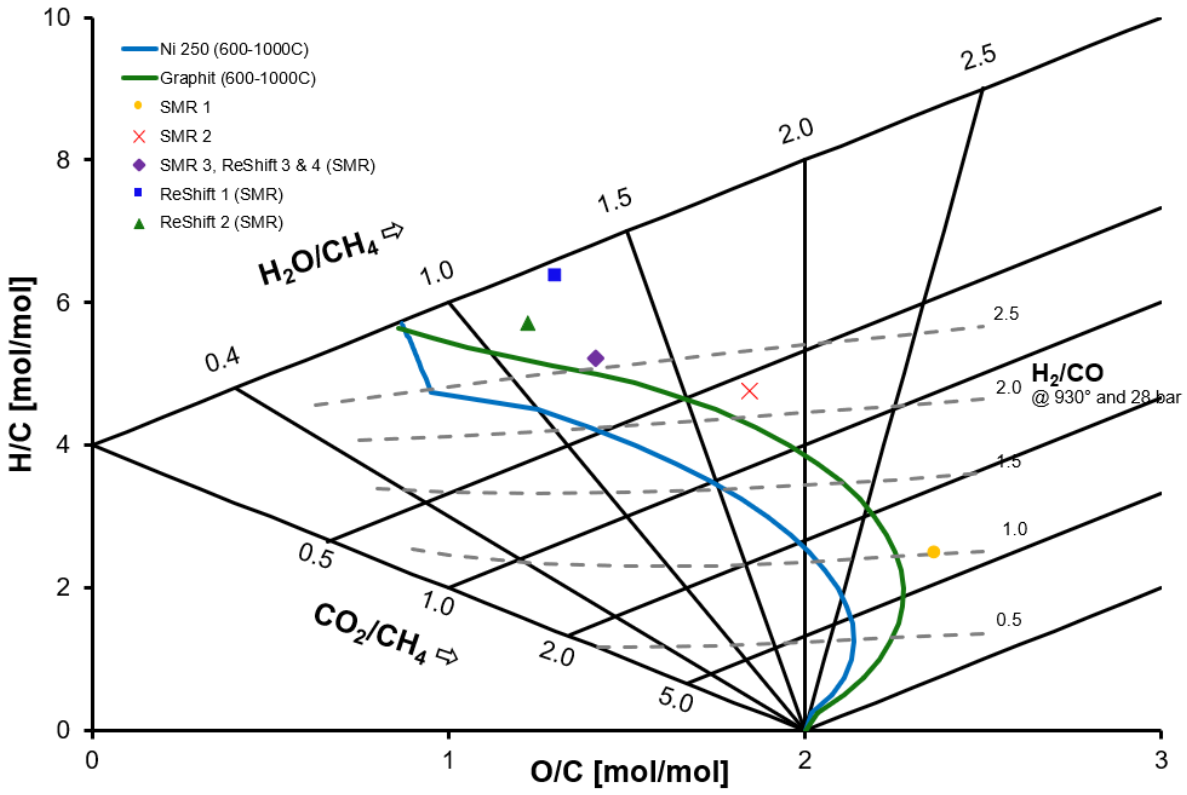

Figure A.3. Tøttrup diagram for the tubular reformer at a pressure of 28 barg and an outlet temperature of 930°C. Operation to the left of the carbon limit curves indicates a thermodynamic potential for carbon formation in the equilibrated gas. The dotted lines indicate the operating points corresponding to the respective H_2/CO ratios. Operating points are shown in the tubular reformer for the selected cases in Section 4.4.

A.9. Data for CO_2 emission analysis

Table A.7. CO2 emissions (t/year) calculated using Danish emission factors for fuel and electricity consumption. Presenting the CO2 emissions from fuel and electricity, CO2 consumption, and net CO2 emission/consumption. Fuel emissions are calculated from the fuel flow to the burner and electricity emissions from the duty in E231 and work in the recycle compressors. Positive net values indicate net CO2 emissions, while negative values indicate net CO2 consumption.

Case	Fuel emissions (t/y)	Electricity emissions (t/y)	Total emissions (t/y)	Consumed CO_2 (t/y)	Net CO_2 emission /consumption (t/y)
SMR 1	1.10E+05	5.18E+03	1.15E+05	2.32E+05	-1.17E+05
SMR 2	1.12E+05	1.19E+03	1.14E+05	8.75E+04	2.61E+04
SMR 3	1.12E+05	5.84E+02	1.13E+05	5.11E+04	6.17E+04
ReShift 1	1.12E+05	2.14E+04	1.33E+05	3.01E+05	-1.68E+05
ReShift 2	1.12E+05	1.90E+04	1.31E+05	2.97E+05	-1.66E+05
ReShift 3	1.12E+05	1.72E+04	1.29E+05	2.92E+05	-1.62E+05
ReShift 4	1.12E+05	6.66E+03	1.19E+05	1.73E+05	-5.41E+04

Table A.8. CO_2 emissions (t/year) calculated using Swedish emission factors for fuel and electricity consumption. Presenting the CO_2 emissions from fuel and electricity, CO_2 consumption, and net CO2 emission/consumption. Fuel emissions are calculated from the fuel flow to the burner and electricity emissions from the duty in E231 and work in the recycle compressors. Positive net values indicate net CO_2 emissions, while negative values indicate net CO_2 consumption.

Case	Fuel emissions (t/y)	Electricity emissions (t/y)	Total emissions (t/y)	Consumed CO_2 (t/y)	Net CO_2 emission /consumption (t/y)
SMR 1	1.50E+05	4.52E+02	1.50E+05	2.32E+05	-8.15E+04
SMR 2	1.53E+05	1.04E+02	1.53E+05	8.75E+04	6.56E+04
SMR 3	1.53E+05	5.11E+01	1.53E+05	5.11E+04	1.02E+05
ReShift 1	1.52E+05	1.87E+03	1.54E+05	3.01E+05	-1.47E+05
ReShift 2	1.53E+05	1.66E+03	1.54E+05	2.97E+05	-1.43E+05
ReShift 3	1.53E+05	1.51E+03	1.54E+05	2.92E+05	-1.37E+05
ReShift 4	1.53E+05	5.82E+02	1.53E+05	1.73E+05	-1.97E+04

A.10. APOC reactor

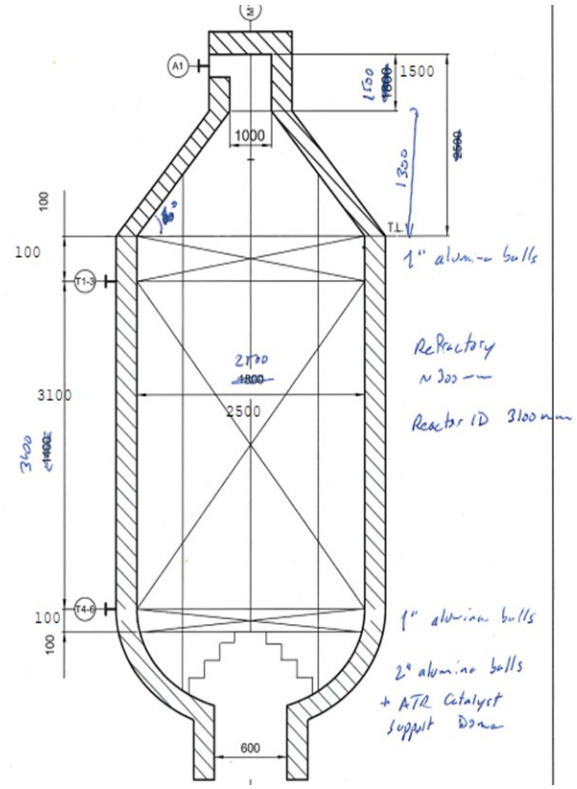

Figure A.4. Illustration of the APOC reactor with suggested dimensions.

A.11. Cost estimation

Table A.9. Cost estimation of the APOC reactor components, heat exchanger and compressor.

	Cost (EUR) ReShift 3	Cost (EUR) ReShift 4
APOC steel	482,000	451,000
Catalyst support	26,891 53,782 (with 1 spare set)	26,891 53,782 (with 1 spare set)
APOC refractory and installation	312,587	296,214
Alumina balls	30,263	23,096
Catalyst	216,829	137,394
Electric heat exchanger E231	5,331,435	2,470,357
Compressors	K221: 9,850,573 K222: 4,634,600	K221: 5,707,000 K222: 2,613,100
Total cost	20,885,178	11,725,052

Appendix B (Confidential)